Rotation Studies of Young very low Mass Stars and Brown Dwarfs

María Victoria Rodríguez-Ledesma
Max-Planck-Institut für Astronomie

Heidelberg 2009

Dissertation in Astronomy
submitted to the
Combined Faculties for the Natural Sciences and for Mathematics
of the Ruperto-Carola University of Heidelberg, Germany.
for the degree of
Doctor of Natural Sciences

presented by

Dipl.-Phys. María Victoria Rodríguez-Ledesma
born in Cap. Fed., Buenos Aires, Argentina

Oral examination: 06.07.2009

Rotation Studies of Young very low Mass Stars and Brown Dwarfs

Referees: **Prof. Dr. Reinhard Mundt**
Prof. Dr. Immo Appenzeller

Abstract

Rotation studies over as large a range of ages and masses as possible are important for constraining the angular momentum evolution of young stellar objects (YSO). Of particular interest are the very low mass (VLM) stars and brown dwarfs (BDs), because of the relatively small number of known rotational periods (P_{rot}) in that mass range. This thesis for the first time provides important information on rotational properties of a large sample of young VLM stars and BDs.

The extensive rotational period study of YSOs in the 1 Myr old Orion Nebula Cluster (ONC) presented here is based on a deep photometric monitoring campaign. As a result, 487 periodic variables (PVs) were found (377 of which are new) with estimated masses between 0.5-0.015 $M_{\odot}$, 124 of which are BD candidates. This is by far the most extensive and complete rotational period data set for young VLM stars and BDs to date. The dependence of the period distribution on mass and level of rotational modulation was investigated and a comparison with higher mass PVs in the ONC and with the PVs in the $\sim$2 Myr old open cluster NGC 2264 was carried out. Substellar objects were found to rotate on average faster than the VLM stars, a trend which was already seen for higher mass stars. In addition, the results presented here suggest a dependence of the P_{rot} on position within the ONC, with the objects located near the cluster center showing on average larger P_{rot}. This result can be explained by a possible age spread in the ONC with a somewhat younger central region.

An interesting correlation between P_{rot} and modulation amplitude was found in which PVs with larger amplitudes rotate on average slower than those with smaller amplitudes, which can in principle be explained by different magnetic field topologies.

In addition, 732 periodic variables in the ONC with known JHK colours were analysed in order to investigate whether rotation periods correlate with the presence of circumstellar accretion disks in particular at very small masses. A highly significant rotation-disk correlation was found among the low and very low mass periodic variables ($0.075 < M < 0.4\,M_{\odot}$), in which objects with NIR excess tend to rotate slower than objects without NIR excess. Interestingly, no correlation was found in the substellar regime. Possible reasons for the absense of such a correlation are discussed in detail.

Zusammenfassung

Rotationsuntersuchungen von jungen stellaren Objekten (JSO) über einen möglichst breiten Massen und Altersbereich sind sehr wichtig, um Einschränkungen über die Drehimpulsentwickung dieser Objekte zu erhalten. Von besonderem Interesse sind hierbei Sterne sehr geringer Masse (VLM-Sterne)und Braune Zwerge (BZ), da in diesem Massenbereich die Zahl der bekannten Rotationsperioden (P_{rot}) relativ klein ist. Diese Doktorarbeit liefert zum ersten Mal wichtige Informationen über die P_{rot}-Werte eine großen Stichprobe von VLM-Sternen und BZ.

Die hier beschriebene ausführliche Untersuchung der P_{rot}-Werte von JSO in dem 10^6 Jahre alten Orion Nebel Haufen (ONH) basiert auf tiefen photometrischen Beobachtungen. Es wurden 487 periodisch Veränderliche (PV) gefunden (377 davon sind neu) mit abgeschätzten Massen zwischen 0.5-0.015 $M_{\odot}$; 124 von ihnen sind BZ-Kandidaten. Dies ist der bei weitem größte und vollständigste P_{rot}-Datensatz bei jungen VLM-Sternen und BZ. Die Abhängigkeit der P_{rot}-Verteilung von der Masse und Modulationsamplitude wurde untersucht und ein Vergleich mit den massereichsten PV im ONH und den PV in dem offenen Sternhaufen NGC2264 ($\approx 2 \times 10^6$ Jahre) durchgeführt. Es wurde herausgefunden, dass BZ im Durchschnitt schneller rotieren als VLM-Sterne. Ein solcher Trend wurde bereits bei Sternen höherer Masse beobachtet. Darüberhinaus geben die hier vorgestellten Ergebnisse Hinweise für eine Abhängigkeit von P_{rot} von der Lage innerhalb des ONH, wobei Objekte, die in der Nähe des Haufenzentrums sind im Durchschnitt größere P_{rot}-Werte zeigen. Dieses Ergebnis kann durch eine Altersstreuung im ONH erklärt werden, mit einer etwas jüngeren Zentralregion.

Es wurde eine interessante Korrelation zwischen P_{rot} und der Modulationsamplitude gefunden, wobei PV mit größeren Amplituden im Durchschnitt langsamer rotieren als solche mit kleineren Amplituden. Dies kann in Prinzip durch verschiedene Topologien des Magnetfeldes erklärt werden.

Darüberhinaus wurden 732 PV im ONH mit bekannten JHK-Farben untersucht, ob ihre P_{rot}-Werte mit dem Vorhandensein einer zirkumstellaren Akkretionscheibe korreliert, insbesondere bei sehr kleinen Massen. Eine sehr signifikante Korrelation zwischen P_{rot} und dem Vorhandensein einer Scheibe wurde bei PV mit einer geringen bis sehr geringen Masse ($0.075 < M < 0.4\, M_{\odot}$) gefunden, wobei Objekte mit einem NIR-Exzess im Durchschnitt langsamer rotieren, als solche ohne NIR-Exzess. Interessanterweise wurde im substellaren Bereich keine solche Korrelation gefunden. Mögliche Erklärungen für das Fehlen einer solchen Korrelation werden detailiert diskutiert.

This thesis is dedicated
to the loving memory of my father:
Omar Rodriguez

Contents

Chapter 1

Introduction

1.1 Low mass pre-main sequence stars

Low mass ($< 3\,M_\odot$) pre-main-sequence stars were first recognised as a separate group by Joy (1945), who related these objects with obscured regions and nebulosity in the Taurus-Auriga dark cloud. Two years later, Ambartsumian (1947) studied the physical nature of the star T Tauri, which gave its name to the whole group of pre-main sequence stars nowadays known as T Tauri stars (TTSs). Detailed reviews of the physical characteristics of these objects are given by Appenzeller & Mundt (1989) and Bertout (1989).

Apart from being associated with regions of obscuration and molecular clouds, the youth of T Tauri stars is additionally evident from their high level of activity and excess emission, which are observed both in the spectral lines and continuum, and in the presence of strong Lithium absorption at 671 nm.

Many TTSs exhibit hydrogen lines and some metallic lines in emission as well as veiling of the optical continuum. These objects are called classical TTSs (CTTSs), while the TTSs which have a much lower level of activity are called weak-line TTSs (WTTSs). A commonly adopted division between CTTSs and WTTSs stars is based on the strength of the Hα emission. CTTSs show Hα in emission with equivalent widths $W_\lambda(H\alpha) > 10$ Å while WTTSs have $W_\lambda(H\alpha)$ below this value (Appenzeller & Mundt 1989). TTSs possess strong surface magnetic fields which result in large magnetic cool spots in their atmospheres as well as in chromospheric emission and which are probably of fundamental importance for all accretion and outflow processes. Most TTSs are surrounded by circumstellar disks and accretion onto the star is channelled by the magnetic field resulting in hot spots which are highly variable on short time scales (hours-days). The presence of a dusty circumstellar disk can be detected through an IR excess observable in many cases over a large wavelength range (1-100 μm). In addition to the optical and infrared emission, TTSs

have significant flux in the X-ray regime (e.g Flaccomio et al. 2003; Preibisch & Feigelson 2005). Both optical emission lines and X-rays are also present in late type main sequence objects and are a consequence of their strong magnetic field which can trap the hot coronal gas. However, the level of surface activity is usually much greater in TTSs than in main sequence objects.

A fundamental characteristic of TTSs is their temporal variability, which was one of the original defining features of TTSs. The fluctuations are observed both in spectral lines and continuum emission and span a large range of amplitudes, wavelengths, and time scales. These variations can be periodic or irregular. In WTTSs the variability pattern is usually simpler and is in most cases periodic with changes in amplitudes over weeks or months. However, the rotational periods of the stars are in almost all cases highly stable over many months or years (e.g. Grankin et al. 2008; Rodriguez-Ledesma et al. 2009a, and references therein). The temporal variability is due to cool spots in the atmospheres of TTSs. The presence of these cool spots suggests that magnetic field lines penetrate the stellar surface and inhibit local transportation of thermal energy (by convection processes) from the inner atmosphere. The large range of periodic brightness modulation observed is probably a combination of several reasons: different temperature ratios between the star and the spots, different filling factors (i.e. larger or smaller areas covered by spots), and/or different spot distribution patterns (Stahler & Palla 2005, and references therein). The often highly irregular variations of CTTSs cannot be explained, or only partially explained, by magnetically induced cool spots. The amplitude of the brightness modulation observed in CTTSs tend to be much larger than in WTTSs, reaching in some cases a few magnitudes in the I-band (e.g. Herbst et al. 2007, and references therein). Most of these objects show only erratic or irregular variations of their brightness over a large range of timescales from hours to years. However for a certain fraction of them, a periodic signal can usually be measured superimposed to short-term irregular variations. To explain the irregular variations of CTTSs a combination of cool and highly unstable hot spots is necessary, with the latter areas resulting from matter being magnetically channelled from the circumstellar disk onto the stellar surface producing high temperatures due to shock heating (see Sect. 1.2.1 and Fig. 1.3) .

Flaring activity is also detected in TTSs. The usually observed irregular variations are easier to detect at short wavelengths (i.e. U or B band) and are probably superimposed on the periodic signal of both CTTSs and WTTSs. The rise of brightness is usually drastic and occurs over short time scales. These effects may correlate with coronal activity (X-ray flares) in which the energy is released in magnetised regions in the corona (e.g. Getman et al. 2008a,b).

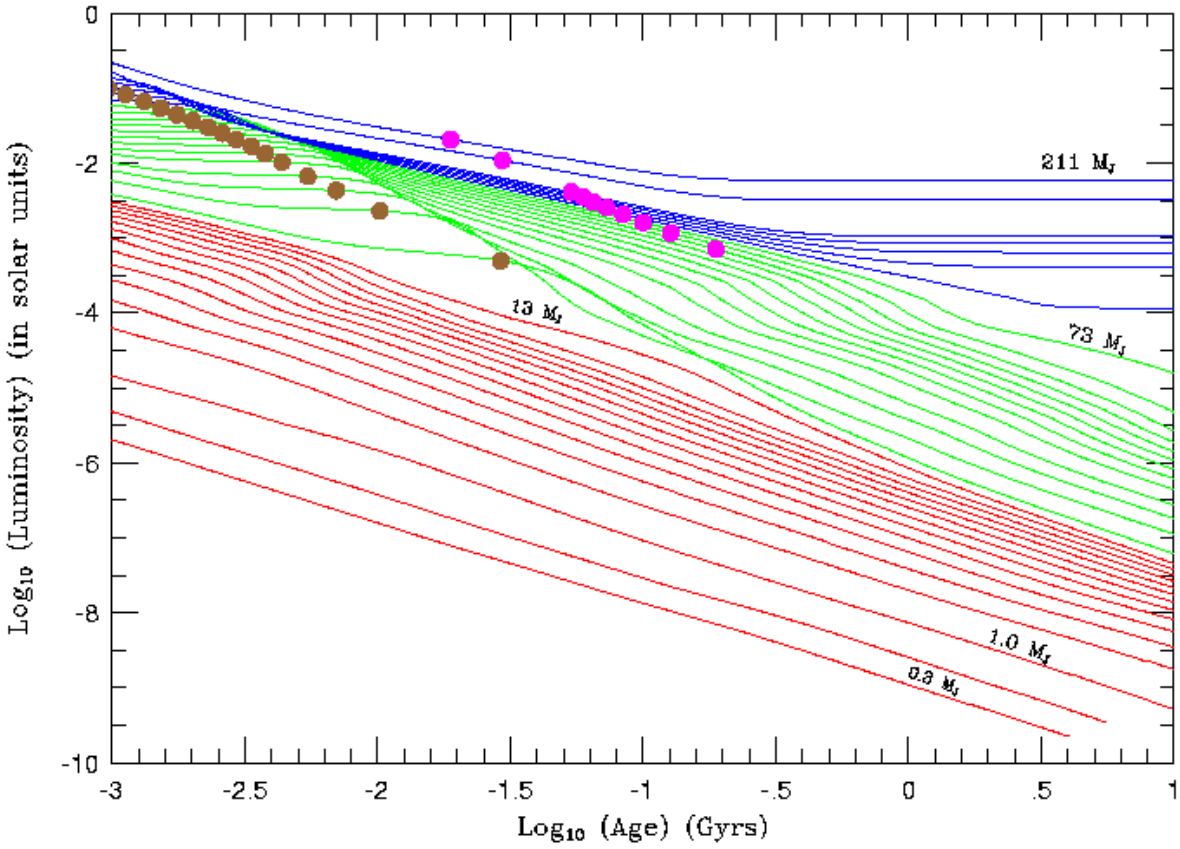

Figure 1.1 Evolution of the luminosity (in $L_\odot$) of red dwarf stars and substellar-mass objects versus age. The stars are shown in blue, brown dwarfs above 13 M_{Jup} are shown in green, and brown dwarfs/giant planets equal to or below 13 M_{Jup} are shown in red. For a given object, the gold dots mark when 50% of the deuterium has burned and the magenta dots mark when 50% of the lithium has burned (Figure from Burrows et al. (2001))

.

1.1.1 Pre-main sequence brown dwarfs

Brown dwarfs (BDs) are gas spheres which have a mass too small to achieve stable hydrogen burning. A 0.075 $M_\odot$ object defines the boundary between stellar and substellar objects. Fig. 1.1 shows the evolution of the luminosity for stars (blue), brown dwarfs (green), and

planets (red) (from Burrows et al. 2001). Blue tracks (stars) show a decreasing luminosity until they reach the zero-age main sequence (ZAMS). At that stage they mantain an approximately constant luminosity over very long time scales, which is not observed in the substellar objects. Both BDs and planets continuously decrease in luminosity with time, i.e. substellar objects always cool while they age. Fig. 1.1 also shows for a given mass at what time of the evolution about 50% of the deuterium and the lithium is burned (gold and magenta dots, respectively). It is worth noting that, according to these models, BDs with masses $\gtrsim 0.06\,\mathrm{M}_{\odot}$ are capable of burning lithium.

It is still not fully understood how brown dwarfs are formed. Several formation mechanisms have been proposed, including a *star-like formation* and a *planet-like formation* (e.g. Luhman et al. 2007; Whitworth & Stamatellos 2006). In the context of the angular momentum evolution studies, it makes a large difference whether brown dwarfs form like stars or like planets. To account for a regulation of the rotational rate (see following sections) all theoretical models require the presence of a circumstellar accretion disk. Any detection of circumstellar disks and/or signs of rotational braking in brown dwarfs should therefore support the star-like formation scenario.

1.2 The angular momentum problem

Stars are formed from gravitationally induced collapse of dense and cold molecular cloud cores. These molecular cloud cores contract by a factor of a million to end up in forming stars. Since the initial molecular cloud core has a small but finite angular velocity ω (at least on the order of the ω of the Milky Way) all protostellar cores should rotate at very high ω values if angular momentum is conserved.

Although recent observations and theory provide a more comprehensive picture of star formation, there are still many open questions, one of which pertains to the loss of angular momentum during the star formation process. As shown in the schematic plot in Fig. 1.2, the basic angular momentum problem of star formation is that molecular cloud cores have five to six orders of magnitude higher specific angular momentum (j=J$\diagup$M where J is the angular momentum and M the mass) than stars on the ZAMS. The angular momentum problem was first mentioned by Spitzer (1978) and described in detail by Bodenheimer (1995), who pointed out that a combination of several phenomena acting during different phases of star formation is required to solve the problem. Important processes include magnetic braking of the molecular cloud due to coupling between the collapsing core and the surrounding medium, angular momentum transfer and distribution in disks and orbital motions, as well as angular momentum loss by magnetically driven outflows and jets. At

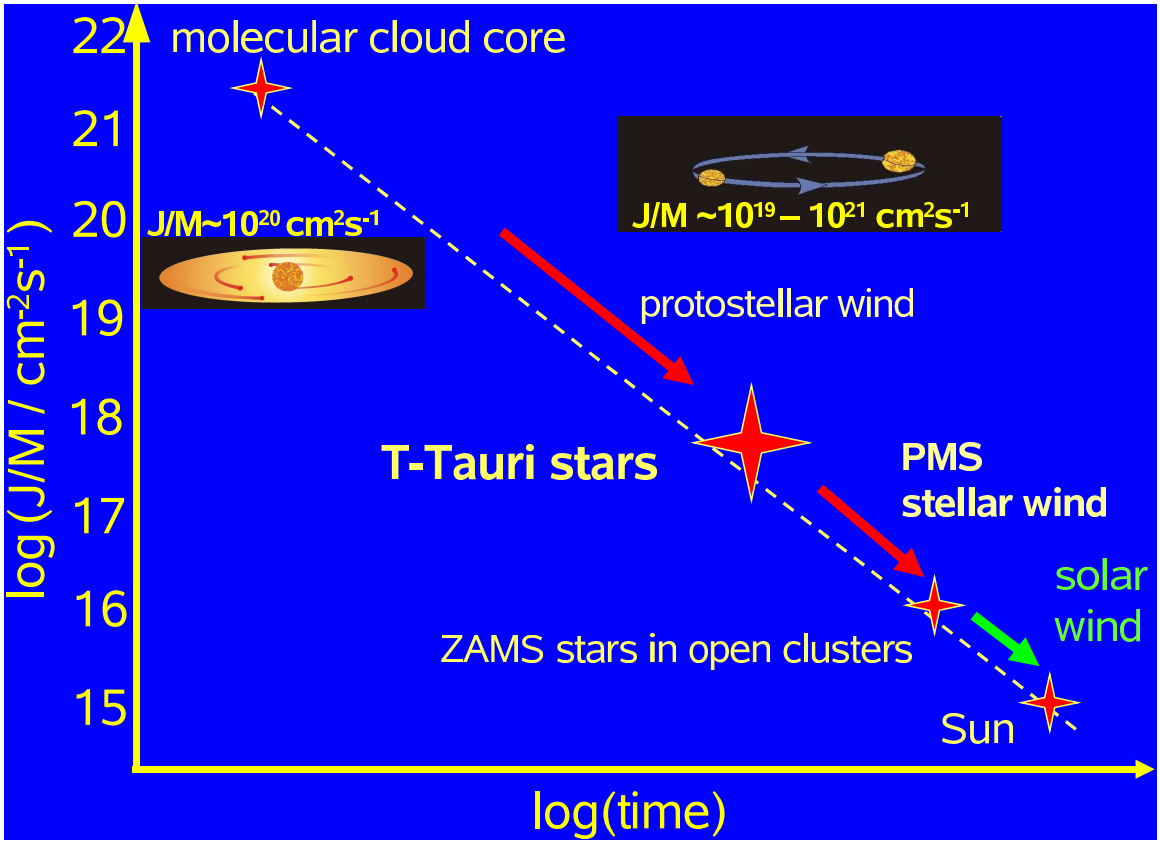

Figure 1.2 Schematic plot showing the evolution of the specific angular momentum during the star formation process. Note that a star on the ZAMS has a specific angular momentum J/M 5-6 orders of magnitude smaller than a molecular cloud core from which it was formed. At the stage when the objects become optically visible (TTS phase) it is possible to measure the rotational periods to study angular momentum evolution.

.

the stage when the objects become optically visible (TTS phase in Fig. 1.2) it is possible to measure the rotational periods and put constraints on the angular momentum problem.

1.2.1 The role of circumstellar accretion disks

Different theories, all of which require ongoing mass accretion from the disk to the star, are usually proposed to explain the removal of angular momentum during the accretion phase. One scenario includes massive stellar winds working in conjunction with magnetospheric accretion (Matt & Pudritz 2005). Another commonly used scenario to explain the

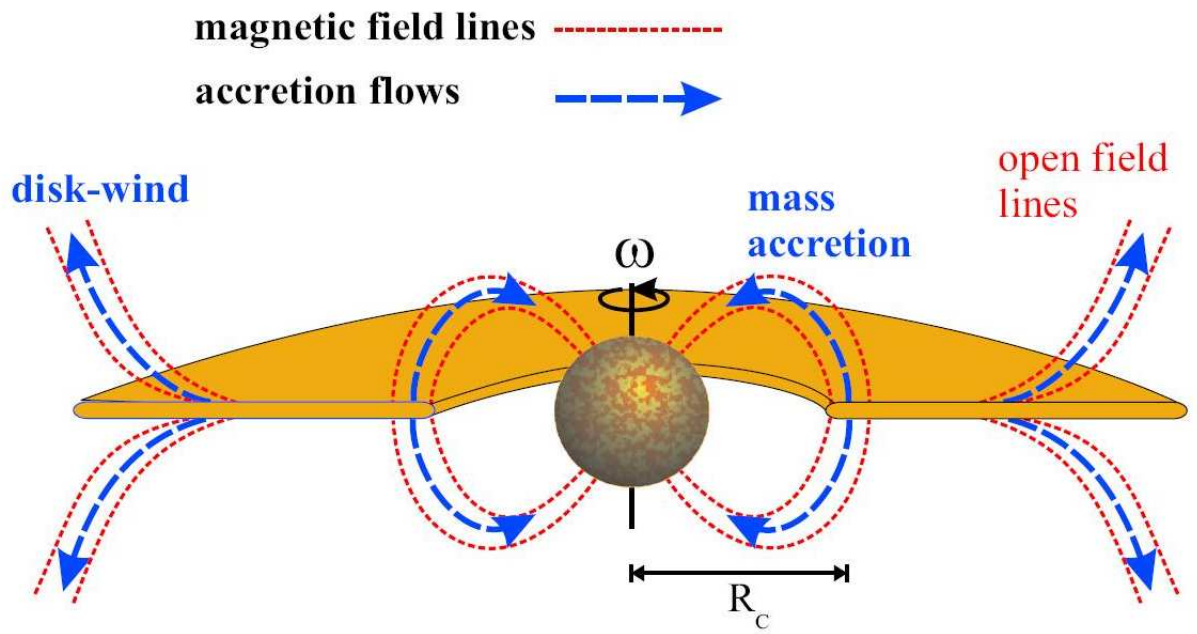

Figure 1.3 Schematic picture of the basic parameters in the disk-locking model proposed by Shu et al. (1994) in which the TTS is surrounded by a circumstellar disk. The magnetic field lines lock the star and the disk into co-rotation. The disk has an inner hole of a size defined by the truncation radius, which is slightly smaller than the co-rotation radius, R_c. Angular momentum is transported from the star to disk via magnetic torques and winds and also from the disk to the star via mass accretion. (Figure from Lamm 2003)

observational data is the disk-locking mechanism which was investigated by Camenzind (1990), Königl (1991), and Shu et al. (1994). The disk-locking model, which is based on the model of Ghosh & Lamb (1979) for accreting compact objects (i.e. neutron stars and white dwarfs), is capable to explain why disk accretion may result in a slow rotating TTS if the magnetic field is relatively strong (∼1000 gauss). A simple schematic of the disk-locking mechanism is shown in Fig 1.3 (Lamm 2003).

There is wide observational evidence that most low mass pre-main sequence stars and even substellar objects have circumstellar disks (e.g. Hillenbrand et al. 1998; Muench et al. 2001; Mohanty et al. 2003; Rebull et al. 2006; etc). Accretion features have also been observed in substellar objects (e.g. Mohanty et al. 2003).

For more than 15 years, several authors have been investigating possible correlations between rotation rates and the presence of circumstellar accretion disks (e.g. Edwards et al. 1993; Rebull 2001; Herbst et al. 2002; Lamm et al. 2005; Rebull et al. 2006; Cieza & Baliber 2007). While many of them found a rotation-disk correlation for solar and low mass

stars (e.g. Herbst et al. 2002; Lamm et al. 2005; Rebull et al. 2006; Cieza & Baliber 2007), others did not (e.g. Rebull 2001; Makidon et al. 2004; Nguyen et al. 2009). As stated by Cieza & Baliber (2007) the intrinsic dependence of rotation on mass and age, which were not taken into account in many of the previous works, could be one of the reasons why no rotation-disk correlation was found in some studies. Most of the studies mentioned above use NIR excess as a circumstellar disk indicator. However, NIR excess only probes the presence of circumstellar dust, but it does not probe ongoing accretion. Nevertheless, since remarkable correlation between mass accretion indicators such as Hα emission line widths and NIR excess has been reported in the literature (e.g. Sicilia-Aguilar et al. 2005, 2006) using a NIR excess as mass accretion indicator is a commonly used justifiable approach.

Although the details of how angular momentum is removed from the star/disk system are not clear, there is a general consensus that magnetically driven jets and outflows are largely responsible for this process.

1.3 The Orion Nebula Cluster

The Orion Nebula Cluster (ONC) is one of the most frequently observed star forming regions because of its proximity ($\approx 400\,\mathrm{pc}$), richness (> 3000 stars), and youth ($\approx 1\,\mathrm{Myr}$). The first major work on the ONC region was published by Parenago (1954b,a). He was the first to notice a group of stars lying above the main sequence (i.e. pre-main sequence objects). More recent works have reviewed different properties of the the ONC region (e.g. Goudis 1982; Genzel & Stutzki 1989; O'dell 2001; Muench et al. 2008). In addition, observed properties of the stars in the ONC region have provided important constraints on theories of star and cluster formation (e.g. Landin et al. 2006; Huff & Stahler 2006, 2007).

A comprehensive photometric and spectroscopic survey of the ONC was done by Hillenbrand (1997), in which nearly 1600 sources brighter than $\mathrm{I} \approx 17.5\,\mathrm{mag}$ were catalogued (about 300 of which were new detections). Additional photometric catalogues from Stassun et al. (1999) and Herbst et al. (2002) both provide information on the variability of the observed objects. NIR surveys have also been carried out in the ONC region (e.g. McCaughrean & Stauffer 1994; Hillenbrand et al. 1998; Hillenbrand & Carpenter 2000; Carpenter 2001; Muench et al. 2001; Lucas et al. 2005). Most of these surveys have concentrated on small regions (i.e. a few arcmin^2) centered on the Trapezium star Θ^1 Ori, particularly those which observed the very low mass and even substellar populations (e.g. Hillenbrand & Carpenter 2000; Muench et al. 2001; Lucas et al. 2005).

All surveys mentioned as well as several others have supplied enough data to constraint

properties of the stellar population of the ONC. One of the remaining controversial issues is its age. From the luminosity spread observed in the HR diagram (see Fig. 1.4), Hillenbrand (1997) suggested a mild age gradient, in which a somewhat younger population is located close to the ONC core while slightly older median ages can be derived for the outer regions ($\approx 2\,\mathrm{pc}$ away from the Trapezium stars). Additional evidence for an age spread in the ONC was provided by Palla et al. (2005), Palla et al. (2007) and Jeffries (2007). In the earlier work, the authors found a spread in the lithium depletion, which supported the observed luminosity spread and consequently age spread, and in the latter work, statistical distributions of stellar radii were derived, which was also interpreted as a possible age spread. Nevertheless, many sources of error as well as intrinsic effects may account for the observed spread (e.g. variability, non-accurate extinction corrections, emission from circumstellar disks, scattered light, etc.) and therefore additional work is needed in this matter.

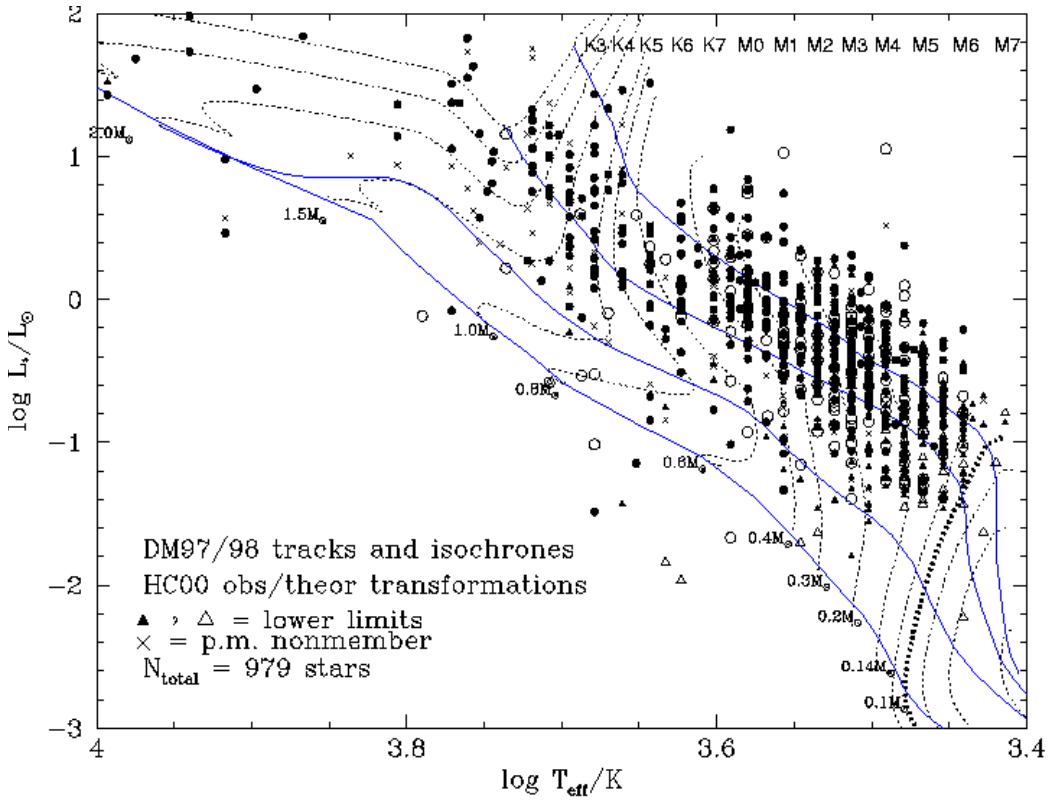

Figure 1.4 Hertzprung-Russel diagram for low mass objects in the ONC (Hillenbrand 1997). Isochrones and evolutionary tracks are from D'Antona & Mazzitelli (1997). Note that for example a $0.25\,\mathrm{M}_\odot$ object corresponds to a $\approx 0.4\,\mathrm{M}_\odot$ object if Baraffe et al. (1998) models are used.

Rotational data can also be used to constraint the age and age gradients in star forming regions. From a contracting PMS model, it is expected that the rotational period decreases with time ($P \approx t^{-2/3}$ if J is conserved). If angular momentum is effectively removed from the star-disk system, it is expected that this stage will last for a finite amount of time after which the star will spin up either conserving angular momentum or at a moderate rate if a certain amount of J loss not enough to keep the period constant occur. Older objects are therefore expected to rotate faster than younger ones (for objects having the same mass). Observations of clusters with different ages confirm this effect (e.g. Herbst et al. 2002; Lamm et al. 2004; Scholz & Eislöffel 2004, 2005). Therefore, any spread observed in rotational periods for objects of the same mass located in different regions provides an indirect indication of different median ages between the two regions.

1.3.1 Rotation studies

The ONC is an excellent target for rotation and variability studies since a large sample of young stellar and substellar objects can be photometrically monitored simultaneously with large imaging devices in order to derive rotational periods. Several rotation studies in the ONC have been performed in the past (e.g. Mandel & Herbst 1991; Attridge & Herbst 1992; Choi & Herbst 1996; Herbst et al. 2000, 2002). Most of these studies extend only up to $\approx 0.2\,M_\odot$[1]. Herbst et al. (2002) confirmed that the period distribution found for stars with masses higher than $\approx 0.4\,M_\odot$ ($0.25\,M_\odot$ if D'Antonna & Mazzitelli 1997 models are used) is bimodal with peaks around 2 and 8 days. These results have been interpreted in terms of disk-star interactions, under which objects rotating slowly are likely to be magnetically coupled to their disks and are prevented from spinning up by magnetic braking, while those objects exhibiting short periods are more likely to be released from their disks or at least the magnetic coupling is much weaker as mentioned in the previous section. The bimodal distribution was not seen in the period distribution of the lower mass stars ($M \leq 0.4\,M_\odot$) which were found to rotate faster on average. In Rodriguez-Ledesma et al. (2009a) the mentioned mass dependence is extended into the substellar regime.

The observed fraction of circumstellar disks around low mass stars and brown dwarfs in the ONC suggests that at this young age most objects are still surrounded by dusty disks. Lada et al. (2000) found that $\approx 50\%$ of objects in the Trapezium cluster have JHK excess, while their observations at $\approx 3\,\mu$m revealed a much higher disk fraction of about 85%. In addition, Muench et al. (2001) found that about 50% of their brown dwarf candidates in

[1]The estimated masses depend on the evolutionary models used, and among the several rotation studies different authors used different evolutionary models. In the work presented in this thesis, models from Baraffe et al. (1998) are used and all masses given within this thesis are based on this evolutionary model.

the Trapezium region show near infrared (NIR) excesses suggestive of a circumstellar disk.

Correlations between infrared excess (which results from a circumstellar disk) and rotational periods have been performed for higher mass objects in the ONC, suggesting that objects showing infrared excess rotate on average slower than their counterparts without infrared excess (e.g. Herbst et al. 2002; Rebull et al. 2006; Cieza & Baliber 2007). The same conclusion arises from studies of the Hα equivalent width and UV excess emission (e.g. Sicilia-Aguilar et al. 2005; Fallscheer & Herbst 2006). These results may indicate that magnetic coupling to the disks and magnetically driven outflows are important ingredients in the angular momentum regulation during these PMS phases. However, before the study presented here (Rodriguez-Ledesma et al. 2009a, 2009b) only a few very low mass stars and BDs in different star forming regions have measured rotational periods (e.g. Bailer-Jones & Mundt 2001; Joergens et al. 2003; Scholz & Eislöffel 2004; Mohanty & Basri 2003) and therefore no statistically significant analysis on a possible connection between rotation and NIR excess could be done so far in the substellar mass regime.

1.4 Outline of this work

The goal of this work is to fill the observational gap existing in rotation studies for the very low mass and, in particular, the substellar regime. The unique data set analysed within this thesis, which includes several hundred very low mass objects as well as about one hundred BD candidates, provide important constraints on the angular momentum evolution at these small masses. In summary, the aim of this thesis is to answer the following questions:

1. *Does the observed dependence of the period distribution on mass extend into the substellar regime?*

2. *Are the peak-to-peak amplitudes related to the rotational periods?*

3. *Is there evidence of distinct magnetic field topologies acting on slow and fast rotators at different masses?*

4. *Does the rotational data suggest an age spread in the ONC?*

5. *Do rotational periods correlate with disk indicators suggesting effective magnetic braking even in the substellar mass regime?*

6. *Are the peak-to-peak amplitudes related to the presence or absence of circumstellar disks?*

The thesis is structured as follows. First, I present in detail how the optical observations were carried out (Chapter 2). In Chapter 3, the astrometric and photometric analysis of the data are described. The time series analysis as well as the determination of irregular variables are presented in Chapter 4. The analysis of the period distributions and peak-to-peak (ptp) amplitudes and their dependence on mass and spatial location in the field are described in Chapter 5, where a comparison with rotational data from Lamm (2003) in NGC 2264 is also presented. To analyse the role of circumstellar accretion disks on rotational regulation and angular momentum loss the used NIR data set together with the method used to derived NIR excesses are presented in Chapter 6. Chapter 7 includes the rotation-disk connection analysis. There, the results as well as a brief discussion about the role of circumstellar disks as angular momentum regulators in the substellar regime are presented. Finally, a summary and conclusions on the major results of this work are presented in Chapter 8.

Chapter 2

Observations and data aquisition

2.1 Method: the photometric monitoring technique

Low mass pre-main sequence stars are known to be variable at all wavelengths (e.g. Appenzeller & Mundt 1989). Their variability level is very broad and can reach up to several magnitudes. The variability in low mass pre-main sequence objects is largely attributed to the brightness modulation due to magnetically induced cool spots in the stellar photosphere (e.g. Vrba et al. 1986, 1989; Bouvier & Bertout 1989; Bouvier et al. 1993; Herbst et al. 1994). The nowadays well established interpretation of their variable behavoiur was suggested for the first time by Hoffmeister (1965).

In the last phase of star formation, when PMS stars become optically visible, we can measure rotational periods and give observational constraints to the the angular momentum problem. Rotational period can be derived spectroscopically or photometrically. The former technique requires high resolution spectral observations and results in a measurement of the rotational velocity $v_{rot}\, sin\, i$ which is inclination dependent. A photometric monitoring technique can be used to derive the rotational periods of these young low mass objects from their brightness modulation (e.g. Rydgren & Vrba 1983; Vrba et al. 1986, 1989; Bouvier & Bertout 1989; Bouvier et al. 1993; Bailer-Jones & Mundt 1999, 2001; Herbst et al. 2000, 2001, 2002, from now on H2002). This technique is applicable over a broad mass range, from $\sim 2\, M_{\odot}$ down into the BD regime. The observed variations are largely due to the rotational brightness modulations by magnetically induced cool spots in the case of weak-line TTauri stars (WTTS), with the addition of an irregular component caused by accretion hot spots in the case of classical TTauri stars (CTTS) . In CTTS the irregular variations can add a strong noise to the periodic modulation, preventing the detection of the periodic signal. Due to this noise, the photometric monitoring technique is less efficient in finding rotational periods among the highly active CTTS than among the WTTS.

The rotation period measurements from this technique can be derived to an accuracy of about 1%, even for slow rotating stars. This accuracy, plus independence from inclination effects, provides a great advantage over $v_{rot}\, sin\, i$ measurements based on high resolution spectral observations.

2.2 Observations

The extensive rotational period study of young low mass objects in the 1 Myr old Orion Nebula Cluster (ONC) presented here is based on a deep I band photometric monitoring campaign using the Wide Field Imager (WFI) camera on the ESO/MPG 2.2m telescope on La Silla, Chile. Observations were carried out over 19 nights from 30 Nov. 2004 to 19 Dec. 2004. The WFI consists of eight 2K x 4K CCDs in a 4x2 mosaic. The pixel scale of $0\farcs238$ gives a field-of-view of 34 x 33 arcmin^2. All data were obtained through the ESO filter 851, with a central wavelength of 815.9 nm and a FWHM of 20.1 nm. In this wavelength range the contamination by nebular line emission is relatively small, while the signal from faint, red objects is relatively high. Fig. 2.1 shows the observed region in which the Trapezium stars were placed in near the center of the field and the eight CCDs are easily distinguished. The bright Trapezium stars may cause highly saturated images, with strong bleeding and light scattering. To minimize these effects, the brightest star Θ^1 Ori (RA(2000)= 05:35:16.3 and DEC(2000)= -05:23:16.3) was placed in the central gap near the center of the field. The central possition on the sky was fixed in all our frames. Special care was taking in the possitioning of the field since it is fundamental that all images are carried out at the same possition. We then provided an aligment star in our field which was used to check the possition of the field before the start of each observation. Nevertheless possitioning is never perfect and about 5% of the imaged area is lost due to the gaps and small diddering.

Hundred images were obtained in total. As shown in detail in Fig. 2.2, our time sampling is not evenly spread over the observing period. During the first six nights, 10 to 15 exposures per night were obtained, while during the rest of the campaign about five exposures per night were acquired. The exposure time of each image was 1130 seconds, which provides a three magnitudes deeper data set in I than the one obtained by H2002. The seeing during these observations varied between $0\farcs45$ and $1\farcs4$ although in most cases oscilated between $0\farcs9$ and $1\farcs0$. The airmass range in which the observations were carried out was of the order of 1.1-1.4.

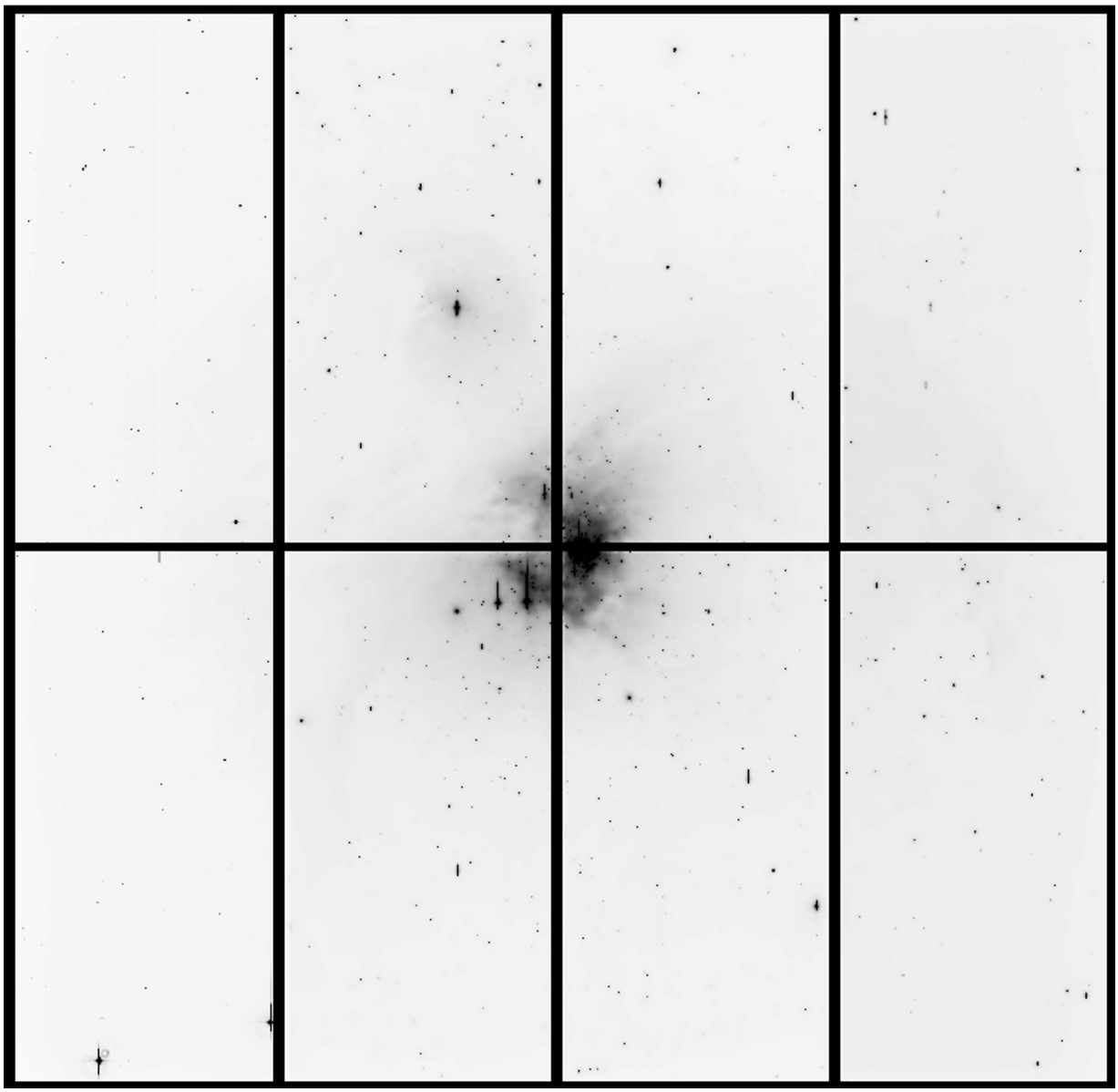

Figure 2.1 The observed field of the Orion Nebula Cluster (ONC). North is up and east is left. The WFI 4k x 2k mosaic, covering a field of 34 x 33 arcmin^2, is easily seen. The Trapezium cluster is in the middle of the field.

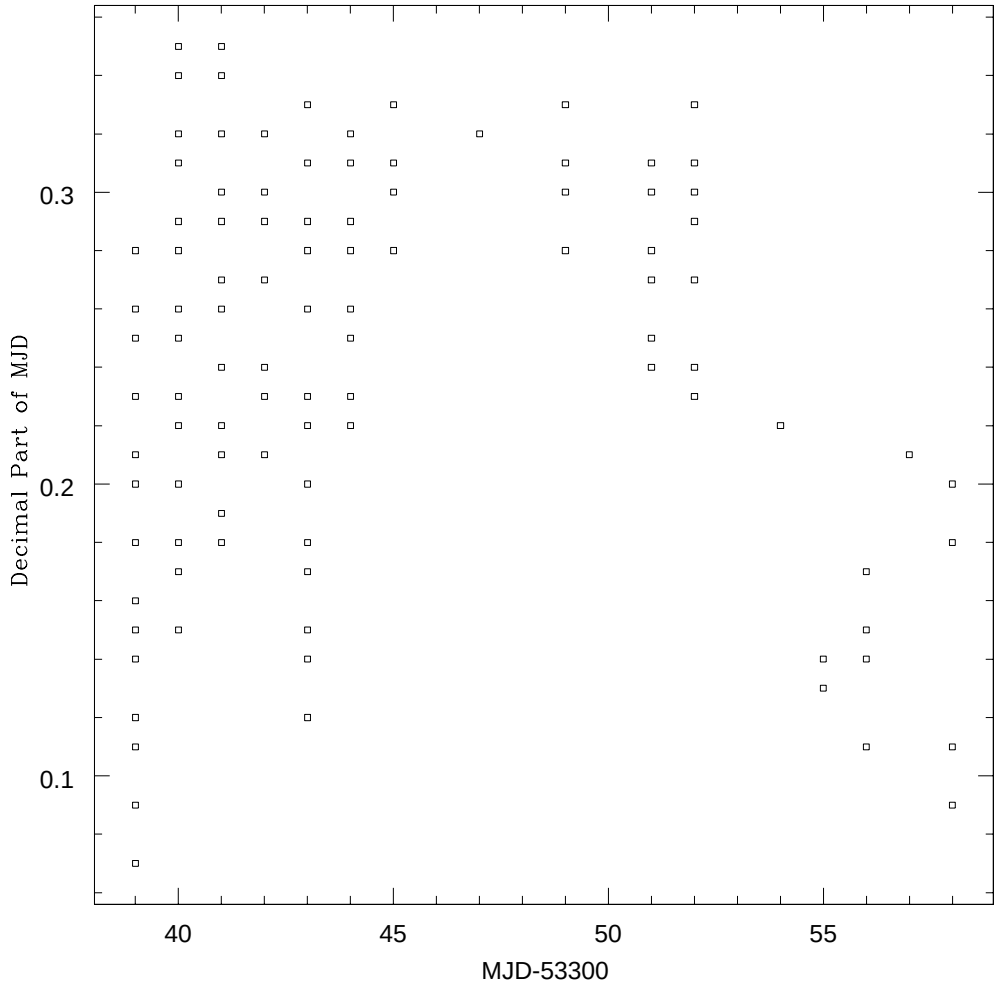

Figure 2.2 Time distribution of the observations, showing the decimal part of the night on the ordinate and the modified Julian day on the abscissa. Please note the dense sampling in the first six nights.

2.3 Data Analysis

Image processing was done using standard tasks in IRAF (Image Reduction and Analysis Facility distributed by the U.S National Optical Astronomy Observatory). Each step in the data reduction, astrometry, photometry, and time series analysis, was done separately for each of the eight CCDs, in order to account for the differences between them. A one-dimensional bias was subtracted using the overscan region, and a two-dimensional residual was removed using the zero integration time (bias) frames. For the flat-fielding

correction illumination-corrected dome flats were used, following the method described by Bailer-Jones & Mundt (2001) and summarised in the following. Averaged dome flats are sufficient to remove the small scale pixel-to-pixel variations but they do not correct the large scale variations which result from the different illuminations from the dome and the sky. Thus the global illumination of the combined dome flat was removed and replaced with the global illumination of the sky. The latter was obtained by making a low-order fit to a median-combination of several night sky images. Finally, each science frame was divided by the resulting corrected dome flat.

A catalogue source image (or "template" image) was created by adding all the aligned science images, in order to have an image with about ten times higher signal-to-noise ratio (S/N) than the individual ones. For the four inner CCDs a median filtered image was subtracted from the template images, in order to remove large scale nebular structures which helps considerably to reduce large gradients in the sky background. DAOFIND was used on the combined images to create the catalogue source list. In a visual inspection some faint stellar sources were added and as many as possible non-stellar sources were removed. Finally about 3300 objects were taken into account for the photometric analysis.

Chapter 3

Astrometry and photometry

3.1 Astrometry

The celestial coordinates of all the objects in the field were computed using the Guided Star Catalogue 2.3.2 as the reference coordinate list. The average rms in the plate solution fit was $0\farcs15$. The coordinates were checked for stars in different regions of each CCD. The highest positional differences reached $1\farcs1$, although these cases were very rare and the differences were normally not higher than $0\farcs4$. A cross-identification of our sources with H2002 and 2MASS was done. Since our study extends to much fainter sources, we have a considerably larger number of sources (about 1000) which are not included in any of these catalogues. In all tables given here we keep the numbering system by H2002 and extend it for the new objects found in this study by using numbers beginning at 20 000. In total our source list contains about 1600 new entries compared to H2002.

3.2 Photometry

Aperture photometry was used to obtain the instrumental magnitudes. Even in the central region of the ONC the stellar density is sufficiently low for this technique to be accurate enough. The S/N dependence on aperture size for objects located in regions with low and high nebular background were tested, which allows for an appropiate selection of aperture sizes used during the photometric analysis. Fig. 3.1 show the results of this test. The aperture was chosen to be nine pixels ($2\farcs1$) in diameter in the four inner CCDs and of ten pixels ($2\farcs4$) in the four corner ones. These values maximise the S/N and the somewhat smaller apertures for the four inner CCDs provide smaller contamination due to nebular background structures which are stronger in the center of our field. The sky was calculated as the median of an annulus with an inner diameter of 20 pixels ($4\farcs8$) and a width of

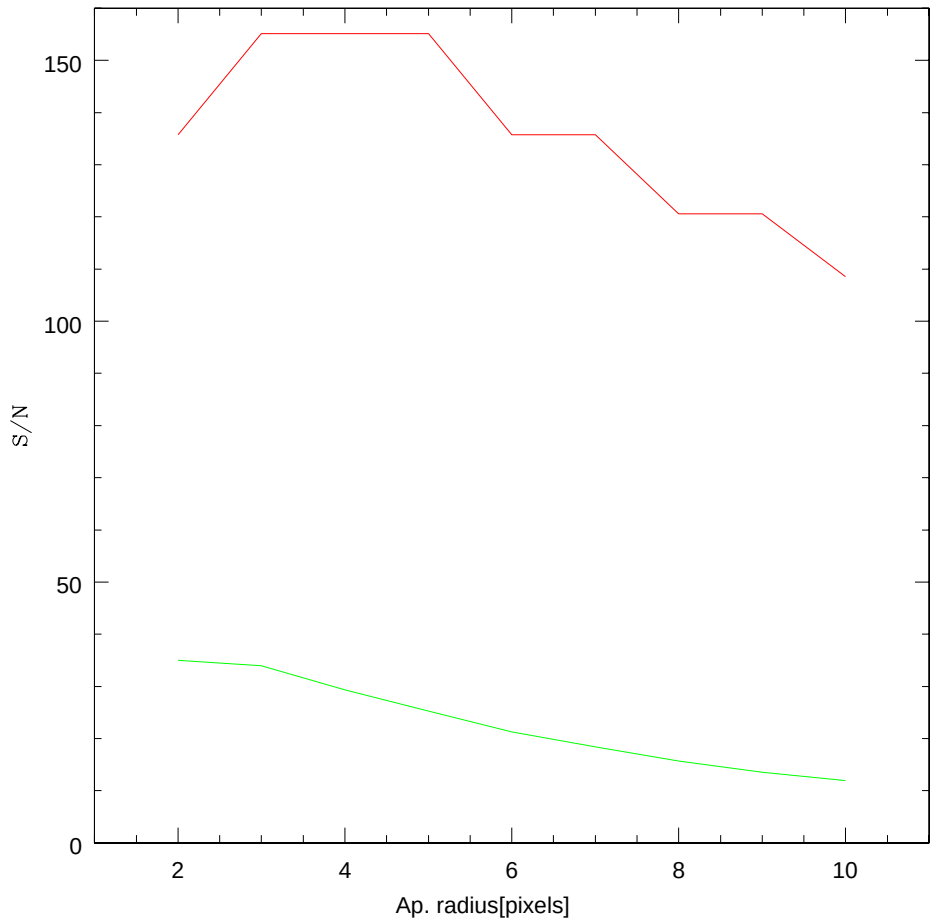

Figure 3.1 S/N dependence on aperture radius for a star located in a region with very low nebular background (top) and one located where the nebular bakground is very strong (bottom).

ten pixels (2.″4) centered on the source. Close companions (closer than $\sim$ 40 pixels, i.e. 9.″5) were removed from the source list, because of their non-reliable aperture photometry magnitude determination. Objects located close to the edges of the CCDs as well as those with high photometric errors (i.e. $>$ 0.5 mag) were also removed from our sample. In the end, accurate photometry of 2908 stars was performed with photometric errors ranging from 0.001 mag to 0.2 mag for the brighter and fainter limits, respectively. The instrumental magnitude system was placed roughly on the Cousins I filter system, following H2002. Since observations were performed in only one filter, a proper transformation to this system including a colour term was not possible. In Table 3.1 photometric results for all measured (2908) objects are summarised (full version is available electronically). The

magnitude range extends from 13 to 21 mag in I, i.e. three magnitudes deeper than H2002. The mean photometric errors of all monitored stars were calculated as:

$$\langle \delta \mathrm{m_{phot}} \rangle = \frac{1}{N_B} \sum_{j=1}^{N_B} \delta \mathrm{m_{phot}}, \tag{3.1}$$

where N_B indicates the number of images and δm_{phot} is the photometric error of a single measurement.

Fig. 3.2 shows $\langle \delta m_{phot} \rangle$ as a function of magnitude and the error curve, which was calculated as a two component fit to the median values of δm_{phot}. The medians were calculated in magnitude bins of 0.5 magnitudes. For objects brighter than 17, a linear fit was applied, while for objects fainter than 17, an exponential fit was used. Above 16.5 the mean photometric errors start to increase slightly, while above I=18 the increase of the mean photometric errors is rather strong. This introduces a bias, in the sense that it is more likely to measure somewhat higher amplitude modulations for the fainter objects in the sample.

3.3 Relative Photometry

Relative photometry of each individual chip was performed in order to obtain the light-curves of all the 2908 sources. This relative photometry is done with respect to carefully selected non-variable flux reference stars. The procedure adopted by Choi & Herbst (1996) was followed, in which the light-curves are calibrated using an average light-curve constructed from a set of non-variable reference stars. An initial sample of potential reference stars was formed using the following criteria:

1. Presence in all the images.
2. Photometric errors below 0.03 mag.
3. Sufficiently isolated from other sources.

The quality of all images was checked before determining the final reference star sample. For this purpose the approach described by Scholz & Eislöffel (2004) and summarised as follows was used:

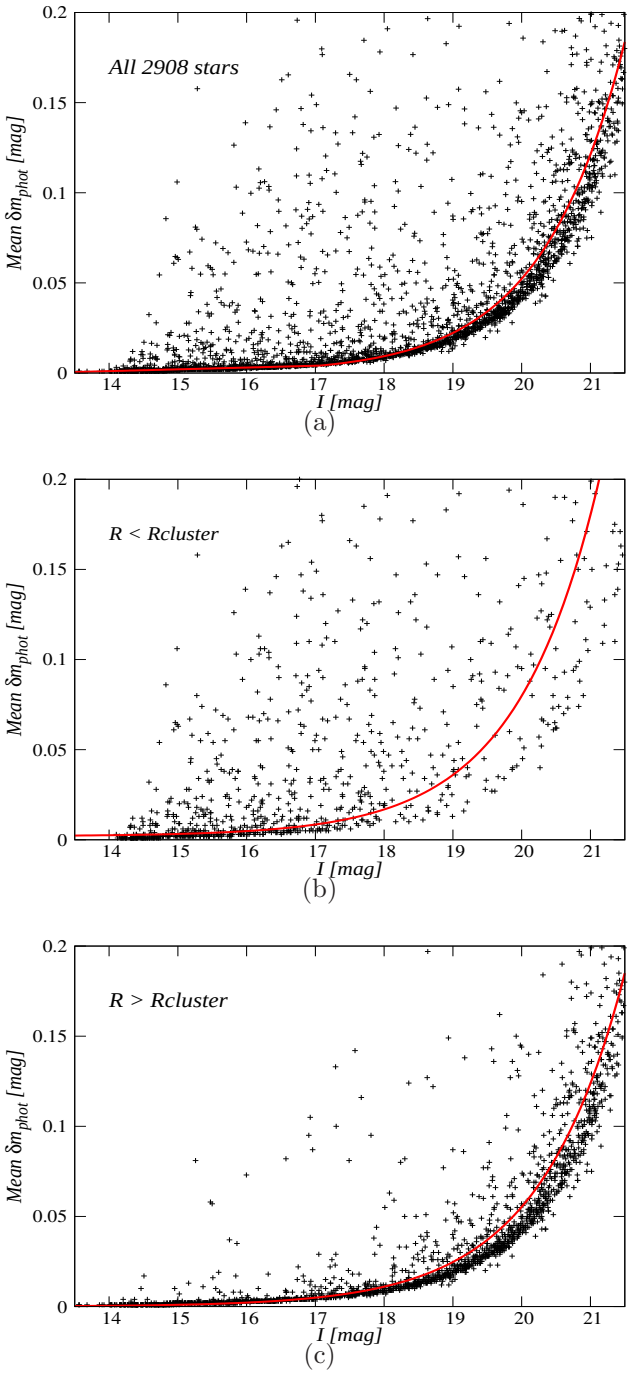

Figure 3.2 *a*) The mean photometric errors $\langle \delta m_{phot} \rangle$ of all the monitored stars as a function of I. The error curve, which was calculated as a two component fit function (linear for the bright regime, and exponential for the faint regime), is also shown. *b*) As in *a*) but for the stars located inside the so-called cluster radius (see Chapter 5) while in *c*) objects located outside the same radius are shown. In *b*) and *c*) the error curves correspond to exponential fit functions. The high dispersion in the photometric errors measured for objects located inside the cluster radius (where the nebular background is very strong) is evident from panel *b*).

1. Compute the average instrumental magnitude $\bar{\mathrm{m}}_{\mathrm{i}}$ for each potential reference star and subtract it from every value of the time series.

$$\bar{m}_i = \frac{1}{N_B} \sum_{j=1}^{N_B} m_i(j), \tag{3.2}$$

and

$$\mathrm{m}_{\mathrm{i}}^{0} = m_i(j) - \bar{m}_i, \tag{3.3}$$

in which the i= 1...N_{R} suffix indicate the number of the reference star while j=1...N_{B} indicate the image number.

2. Calculate the average and standard deviation of the previous differences for every individual image.

$$\bar{\mathrm{m}}_{\mathrm{j}}^{0} = \frac{1}{N_R} \sum_{i=1}^{N_R} \mathrm{m}_{\mathrm{i}}^{0}, \tag{3.4}$$

and

$$\sigma_j = \sqrt{\frac{1}{(N_R - 1)} \sum_{i=1}^{N_R} (\mathrm{m}_{\mathrm{i}}^{0} - \bar{\mathrm{m}}_{\mathrm{j}}^{0})^2}, \tag{3.5}$$

3. Reject the so-called "bad" images in the time series, which are the images with high standard deviation.

Once a few bad images were removed (i.e. three to five depending on the CCD), potential reference stars showing indications for variability were rejected by examining the standard deviation of each light-curve with respect to the average light-curve of all other stars. This procedure was iterated a few times, and about 30 stars relatively evenly distributed around the field were finally chosen on each CCD. Since most of the objects in the field are young and presumably variable, using many reference stars not only increases the precision in the relative photometry, but also strongly minimises the effect of very low level variations that any of the selected reference stars could still have. For this reference star sample the individual standard deviation σ_i in the light-curves was typically below 0.007 mag, where σ_i is defined as:

$$\sigma_i = \sqrt{\frac{1}{(N_B - 1)} \sum_{j=1}^{N_B} (\mathrm{m}_{\mathrm{j}} - \bar{\mathrm{m}}_{\mathrm{i}})^2}, \tag{3.6}$$

in which again the i= 1...$N_{\rm R}$ suffix indicates the number of the reference star, while j=1...$N_{\rm B}$ indicates the image number.
For the final relative photometry the averaged reference light-curve of the reference stars in each of the eight CCDs was subtracted from all 2908 stars. The light-curves of three periodic variables and a flux reference star are shown in Fig. 3.3 to illustrate the sampling of the data, and the variability level of the periodic variables compared to a reference star.

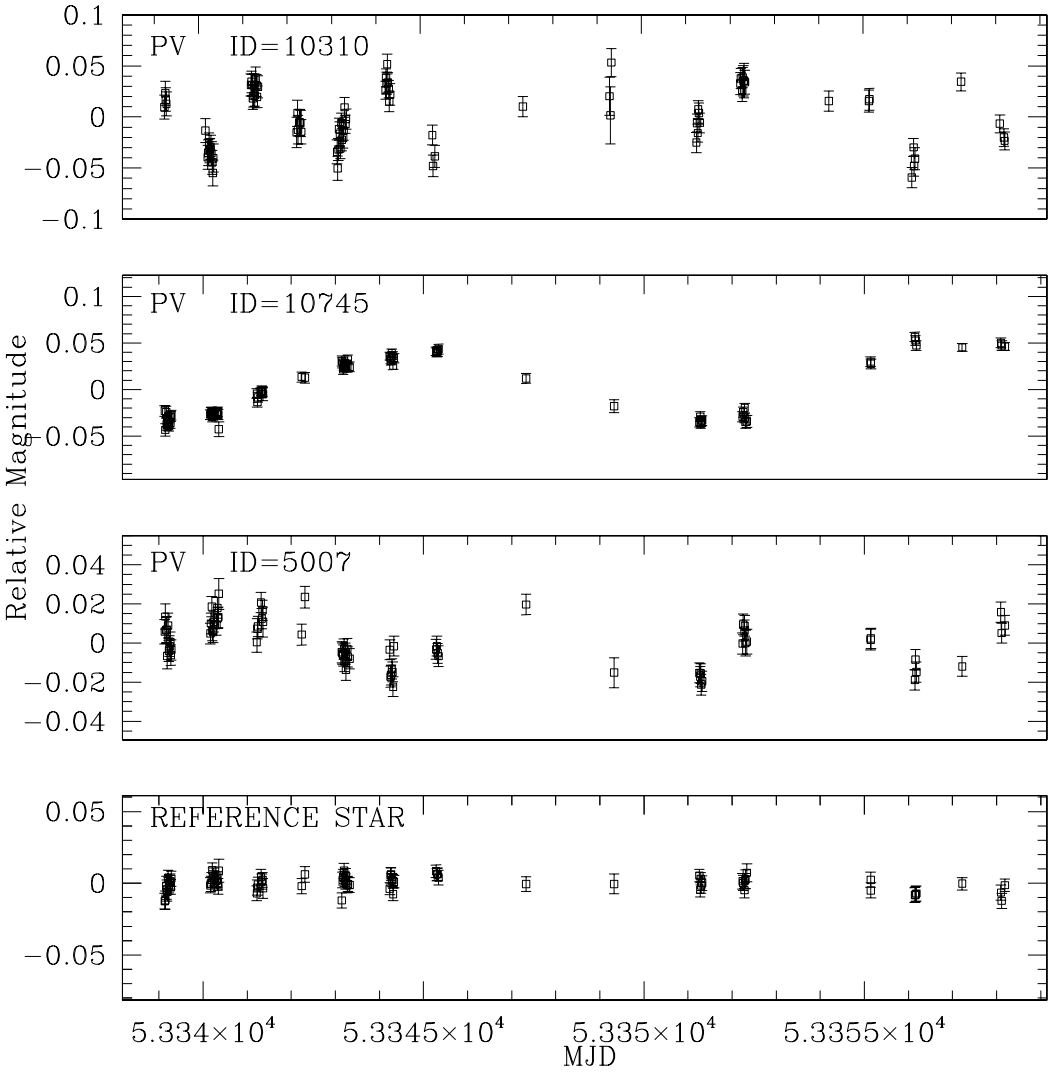

Figure 3.3 Examples of light curves of three periodic variable stars and a reference star.

Table 3.1 Sample of the photometric catalogue. The complete catalogue is available electronically at the CDS.

ID[a]	RA(2000)	DEC(2000)	I[b][mag]	I_{err}[c][mag]	N [d]	CCD[e]	VarFlag[f]	2MASS-ID[g]
1	5:34:28.21	-5:26:39.51	15.535	0.002	80	e	PV	05342821-0526397
89	5:34:47.65	-5:37:24.91	20.885	0.141	53	f	IV	05344765-0537250
3049	5:35:36.49	-5:20:8.96	16.431	0.004	74	b	IV	05353650-0520094
3051	5:34:26.78	-5:19:41.19	16.642	0.004	87	d	PV	05342678-0519414
3056	5:35:10.18	-5:21:0.29	16.758	0.013	85	c	PV	
5050	5:35:10.07	-5:17:6.52	18.389	0.019	85	c	PV	05351007-0517068
10667	5:35:28.51	-5:25:4.12	16.253	0.009	90	g	IV	
10668	5:35:28.56	-5:33:4.25	18.611	0.016	90	g	PV	05352856-0533043
10669	5:35:28.65	-5:22:24.89	17.863	0.080	74	b	NonV	05352865-0522253
10670	5:35:28.88	-5:29:14.40	17.847	0.017	90	g	PV	05352889-0529144
11102	5:36:20.46	-5:29:47.99	19.894	0.037	77	h	NonV	
11111	5:36:21.20	-5:29:12.61	17.889	0.008	81	h	NonV	05362123-0529128
11112	5:36:21.25	-5:18:26.71	18.168	0.010	82	a	NonV	05362126-0518266
20245	5:35:12.84	-5:21:4.92	18.535	0.103	85	c	PV	05351285-0521051
20442	5:35:34.14	-5:27:26.98	19.078	0.039	90	g	NonV	05353415-0527271
20443	5:35:34.90	-5:27:16.76	20.833	0.258	90	g	NonV	

[a]Identification numbers from Hillenbrand (1997) for numbers below 10000; from H2002 for numbers between 10000 and 11115, and from this study for identification numbers above 20000.

[b]I magnitude.

[c]Photometric I magnitude error.

[d]Number of data points considered in the time series analysis.

[e]CCD identification. Each CCD of the mosaic is named from *a* to *h*, starting from the upper left corner and going clockwise to the bottom left corner.

[f]The variability flag column catalogues all objects from their variation properties. The possibilities are: non-variable (NonV), irregular variable (IV), periodic variable (PV), possible periodic variable (PPV) and possible eclipsing system (PES).

[g]2MASS identification number.

Chapter 4

Time series analysis

4.1 Period determination

In order to get an as large as possible sample of young objects with known periods, all stars in the field were checked for periodic light modulations using the combination of two periodogram analysis techniques: the Scargle periodogram (Scargle 1982) and the CLEAN algorithm (Roberts et al. 1987). The Scargle periodogram analysis is particularly suited to a time series in which the sampling is not uniformly distributed. In order to decide whether there is a significant signal from a certain period in the power spectrum, the power at that period calculated by the Scargle algorithm has to be related to a False Alarm Probability (FAP), which is the probability that a peak with a power z would appear in a random data set. We derived $\mathrm{FAP_{Scargle}}$ for all monitored objects and only those with $\mathrm{FAP_{Scargle}}$ below 1% were considered in later steps of the analysis. The $\mathrm{FAP_{Scargle}}$ is given by

$$FAP_{\mathrm{Scargle}} = 1 - ([1 - \exp(-\mathrm{z})]^{\mathrm{N_i}}, \tag{4.1}$$

in which N_{i} is the number of independent frequencies and z the height of the peak. N_{i} is estimated as

$$N_{\mathrm{i}} = -6.3 + 1.2N + 0.00098N^2 \tag{4.2}$$

where N is the number of data points (Horne & Baliunas 1986). In the case of clumped data other authors (e.g. Scholz & Eislöffel 2004) preferred to used N_{i}=$N/2$ for their first estimation of $\mathrm{FAP_{Scargle}}$ although these two different approaches do not result in a significant change of $\mathrm{FAP_{Scargle}}$.

Because the data used in this study are not evenly spaced, but clumped, the values for

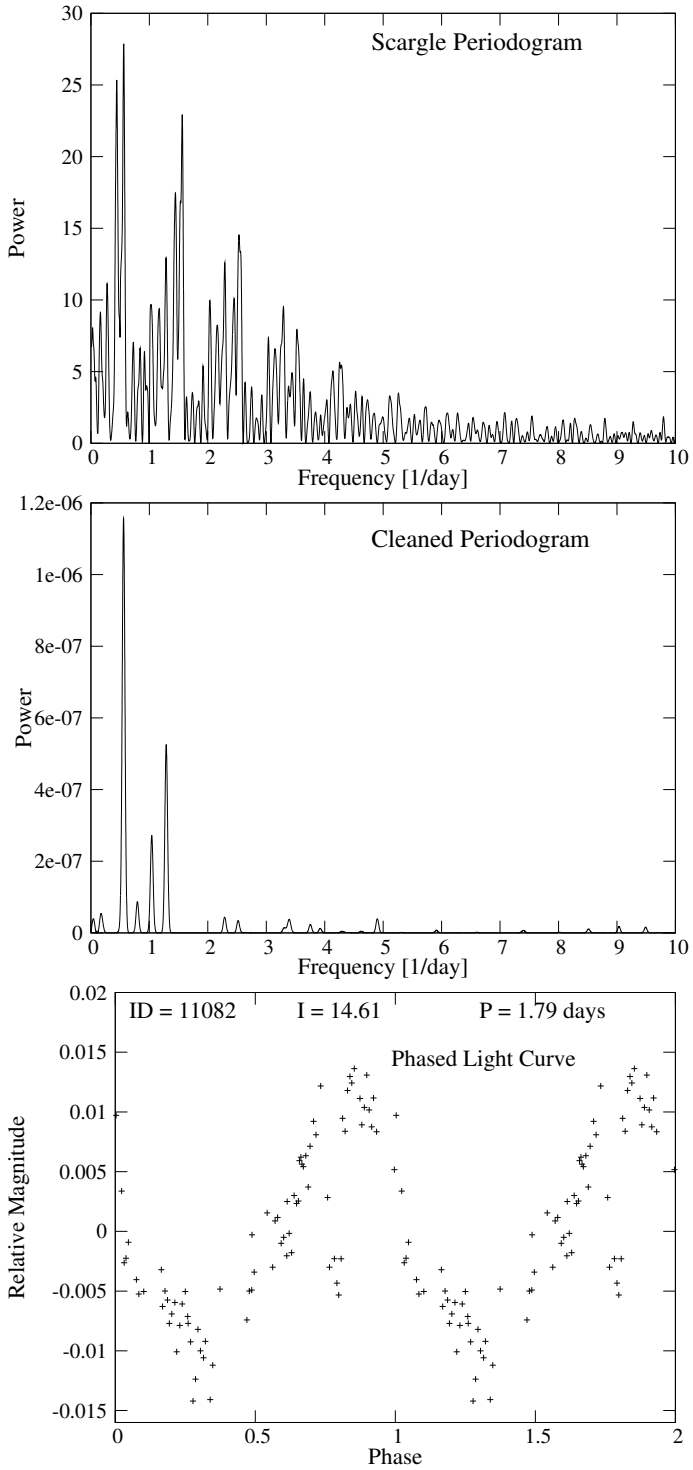

Figure 4.1 Example of a Scargle periodogram, a CLEAN periodogram and the phased light-curve of a periodic variable with P = 1.79 days found by both techniques.

$FAP_{Scargle}$ are considered as a first estimate in the analysis. Additional FAP determinations, also on the basis of Monte Carlo simulations were performed. As discussed more in detail below, the FAP_{sim} derived from the simulations are similar to those derived from Equ. 4.1.

Due to the windowing of the data, the Scargle periodograms are contaminated by false peaks or aliases which could result in spurious period detections. To overcome this problem the CLEAN algorithm by Roberts et al. (1987) was used to deconvolve the dirty spectrum and the window function, resulting in a clean periodogram in which false peaks due to sampling no longer appear, as shown in Fig. 4.1. The combination of these two techniques provides a reliable period detection as outlined in several rotational period and variability studies (e.g. Bailer-Jones & Mundt 1999, 2001; Lamm et al. 2004, 2005; Scholz & Eislöffel 2004).

Independent from the Scargle periodogram FAP calculation an additional test to control the significance of the periods found was performed, in which the statistical F-test and a derived FAP from it was used as proposed by Scholz & Eislöffel (2004). Its main idea is the following: if the detected period is not significant, the variance of the light-curve with a periodic light modulation and without it should not be significantly different. To perform this test every detected period was fitted with a sine wave and then subtracted from the original light-curve. The variance of both the original and the subtracted light-curves were compared as follows

$$F = \frac{\sigma^2}{\sigma^2_{\rm sub}}, \tag{4.3}$$

resulting in a measurement of the probability that the two variances are equivalent. Because FAP_{F-test} represents the probability that the period found is caused by variations in the photometric noise, it is completely independent of the previous periodogram analysis. The values of the FAP_{F-test} are larger than the $FAP_{Scargle}$ values for the lower S/N cases and smaller for the high S/N ones.

The final list of periodic variables only includes those objects which fulfil the following criteria:

- A significant peak was found by the Scargle Periodogram analysis with $FAP_{Scargle} < 1\%$.
- The CLEAN algorithm confirms the peak found by the Scargle Periodogram analysis.
- The $FAP_{F-test} < 5\%$.

- The light-curves and the phased light-curves show the found period clearly (final visual inspection).

In total 487 stars fulfil these criteria and are therefore adopted as periodic variables. They are listed in Table 4.1. A very small fraction of the adopted periodic variables have FAP values which are close to the limits given above (i.e. only 1% of them have $0.1\% < \mathrm{FAP}_{\mathrm{Scargle}} < 1\%$ and only 7% of the periodic variables have $5\% < \mathrm{FAP}_{\mathrm{Ftest}} < 1\%$).

In addition, a more reliable FAP calculation was done on the basis of Monte Carlo simulations similar to the approach by Kürster et al. (1997). 10 000 randomised data sets were obtained in which the observing times were kept as in the original data and the relative magnitudes were randomly redistributed. Scargle periodograms were derived for each data set and new $\mathrm{FAP}_{\mathrm{sim}}$ were calculated, which gives the fraction of data sets for which the power of the highest peak exceeds the power of the detected period. As it is a time-expensive simulation it was performed for a few objects, with slightly different sampling, magnitudes and variability level to get a reliable estimate of the power corresponding to a $\mathrm{FAP}_{\mathrm{sim}}$ of 1% and 0.1%. According to the simulations $\mathrm{FAP}_{\mathrm{sim}}$ of 1% and 0.1% corresponds to peak powers of about 10.5 and 12.6, respectively. For all periodic variables in the sample, the power of the peak corresponding to the found period is higher than 12 and in about 80% of them the powers exceed 20, this means all the final periodic variables have $\mathrm{FAP}_{\mathrm{sim}} < 1\%$ and 80% of them have even $\mathrm{FAP}_{\mathrm{sim}} < 0.0001\%$. I would like to emphasise that not only in these Monte Carlo simulations it is found that the $\mathrm{FAP}_{\mathrm{sim}}$ are similar (within a factor of about two) to the $\mathrm{FAP}_{\mathrm{Scargle}}$ derived from Equ. 4.1 . The same was found by Kürster et al. (1997); Scholz & Eislöffel (2004); Lamm (2003). These results provide additional strength to the used period searching procedure.

For comparison purposes I did a Monte Carlo simulation similar to the one proposed by H2002 for the same few objects used in the previous simulation. In this case, the decimal part of the observing days and the relative magnitudes were maintained while the integer part of the observing dates were randomly mixed. 10 000 randomised data sets delivered a FAP of 1% and 0.1% for powers of 8.8 and 10.7, respectively. If these simulations would provide realistic power and FAP values, which seems unlikely due to their arbitrary time sampling, then our above derived $\mathrm{FAP}_{\mathrm{sim}}$ would be even more conservative. That such type of simulation presumably does not provide realistic FAP estimates was already stated by Scholz & Eislöffel (2004).

Among the found periodic variables it is possible to distinguish between two different kind of variables. The first and much larger group includes objects with low-level variability (i.e. typical peak-to-peak amplitudes below 0.25 mag) which are relatively well-approximated by a sine wave. These variations are most probably caused by magnetic cool spots

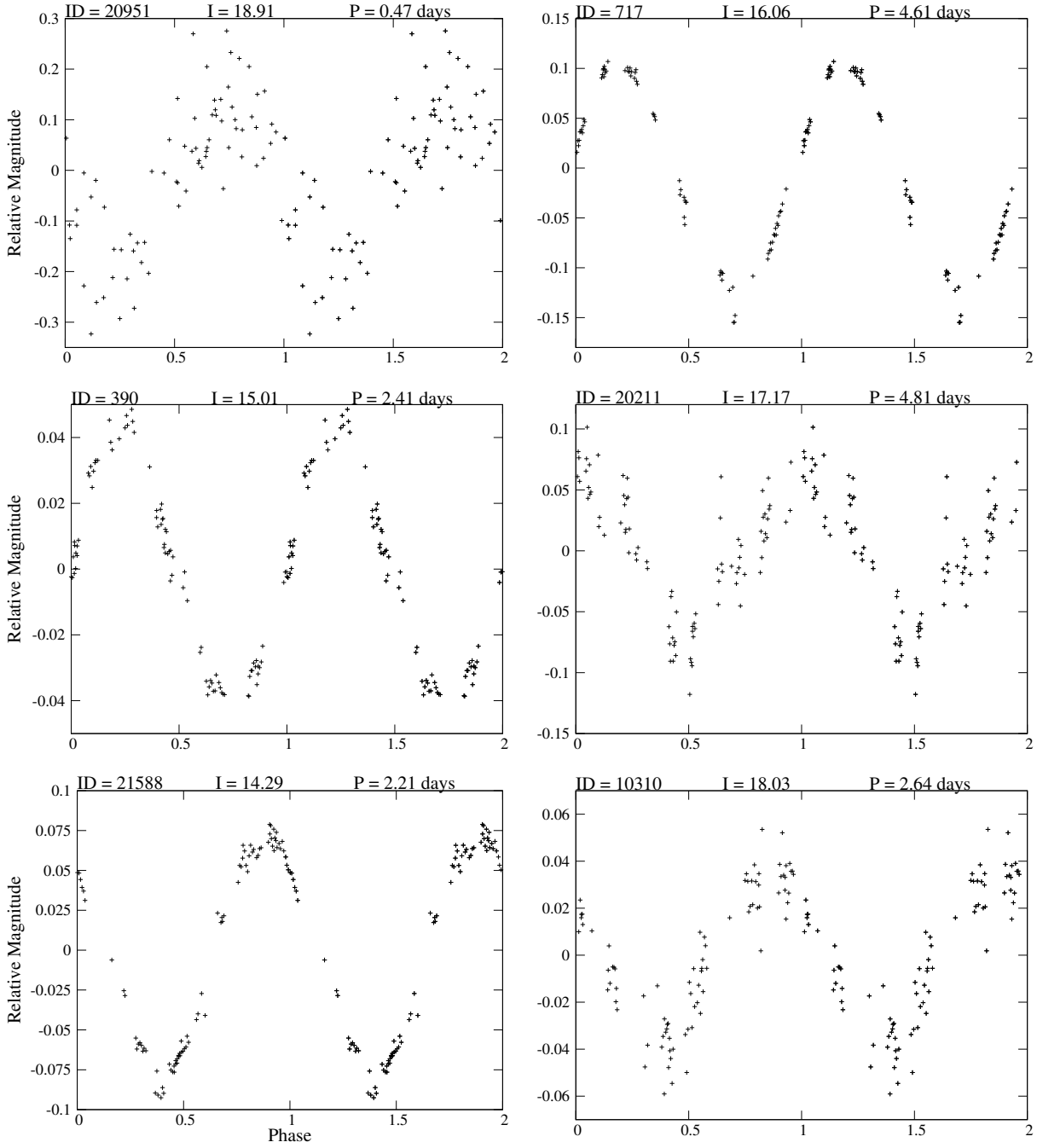

Figure 4.2 Phased light curves of six periodic variables which show mostly a quasi-sinusoidal low level light modulation. The ID number of the stars as well as the measured I magnitude and the detected period (in days) are shown for each of the objects.

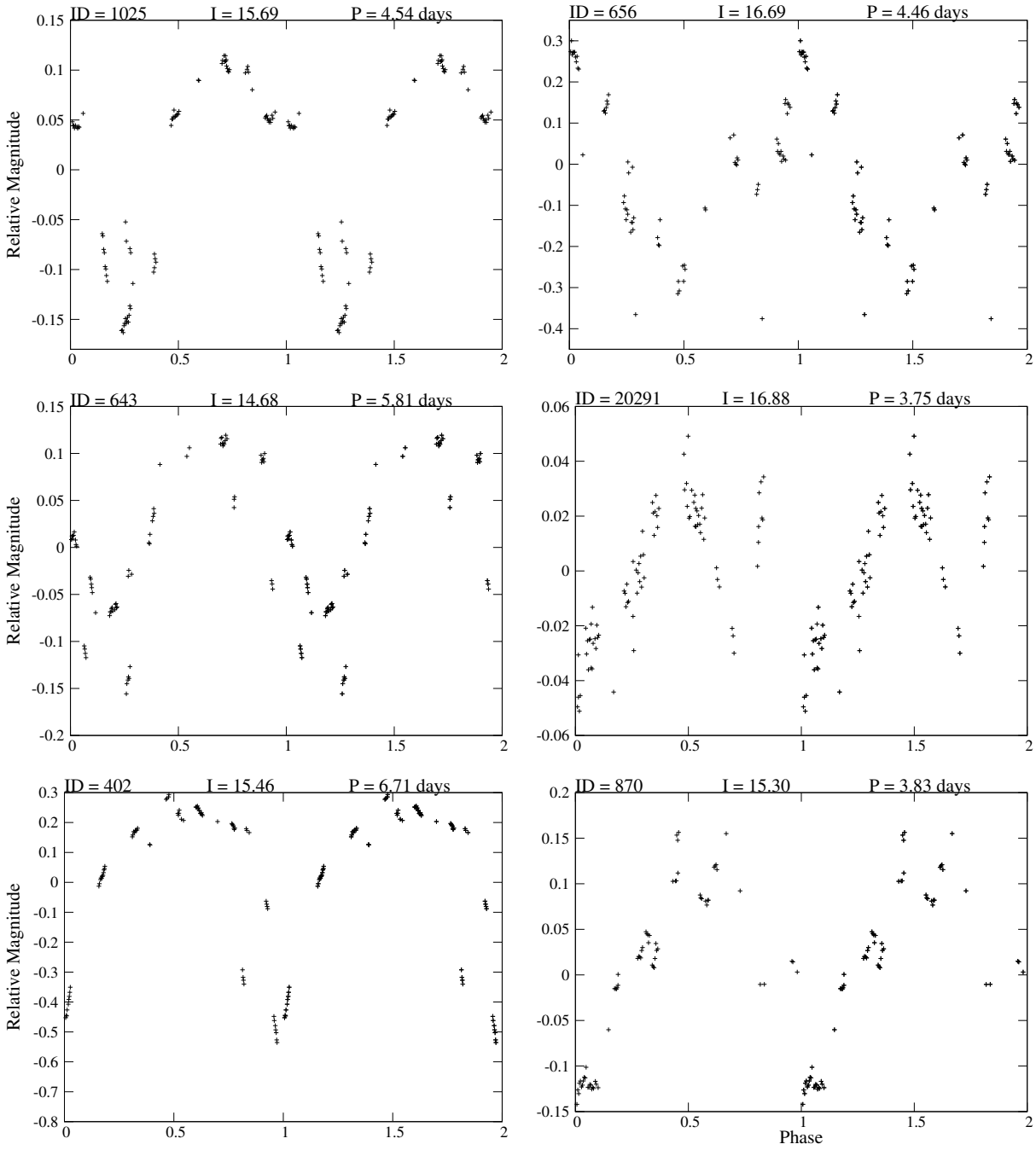

Figure 4.3 Phased light curves of six periodic variables showing irregular variations superimposed on their periodic light modulations, which is more typical for CTTSs. As in Fig. 4.2, ID, measured I and the period (in days) are shown.

co-rotating with the object. As an example, Fig. 4.2 shows six phased light curves of "well-behaved" periodic variables. The other group presents a superposition of short-term irregular variations ("noise") with a periodic light modulation as shown in Fig. 4.3. The irregular variations are often observed in CTTSs. These kind of objects are not very numerous among the 487 periodic variables. Only about 10% of the periodic variables outside the so-called cluster radius (see Chapter 5) belong to this group, while near the cluster center this number increases to about 15%. This increase probably results from a larger number of CTTSs in that region. I also classified 75 objects as possible periodic variables, as well as 7 objects as possible eclipsing systems. In the first case, the objects often show unusual phased light-curves and the false alarm probabilities give values close to the limits adopted above. Both the possible periodic and eclipsing objects are listed in Table 3.1 marked with 'PPV' and 'PES' in the Variability Flag column, respectively. They are not taken into account in any further analysis however.

4.2 Accuracy of the period determination

The uncertainties in the measured periods are determined mainly by the frequency resolution in the power spectrum, and the sampling error, i.e. the typical spacing between data points, which is mostly relevant for very short periods.

The "sensitivity" range of the period determination was investigated, i.e. the smallest and highest frequencies it is in principle possible to detect with acceptable accuracy. The Nyquist frequency $\nu_{max} = \frac{1}{2\Delta}$ (with Δ the distance between two data points) defines the upper frequency limit in a uniform sampling. The lower frequency limit is given by the total time interval of the sample. For non-regularly spaced data, the limits given above are only rough approximations. In order to get a more accurate determination of the period range over which rotational periods with an accuracy below ~ 2 % can be determined, a simulation was carried out following the procedure described in Scholz & Eislöffel (2004) and summarised in the following. Sine waves corresponding to periods between 0.1 days and 25 days were added to the light-curve of one of the non-variable flux reference stars. A S/N of 5 (i.e. ratio between the amplitude imposed and the noise of the light-curve) was assumed, corresponding to an imposed signal with an amplitude of 0.02 magnitudes. The Scargle periodogram was used in order to get the frequency of the highest peak in each case and the differences between the imposed and the measured period were compared. This procedure delivers information on the accuracy of the found periods. The results of the simulation are shown in Fig. 4.4, in which also a 2% period error is shown as a dotted line. The dependence of the accuracy of the recovered periods as a function of

period is a consequence of the irregular time sampling. These simulations were performed for several values of the S/N (2.5, 5 and 10), but any significantly different results were obtained between various simulations. Therefore, I conclude that the method is not highly dependent on the amplitude of the modulation, at least for S/N values higher than 2, which is in agreement with Scholz & Eislöffel (2004). Taking into account very high S/N (more than 10) will decrease only slightly the height of the higher peaks in Fig. 4.4, resulting in a slightly better accuracy in these regions. The simulation also shows that it is possible to detect periods even below the Nyquist limit, which in our case is $\sim$ 0.45 days, if the median time differences of the data points in the light-curve of the reference star used in the simulation are considered. This is consistent with Eyer & Bartholdi (1999) who proved that in time series with irregular spacing the Nyquist limit is only an upper limit for the P_{min}. The same was found by Scholz & Eislöffel (2004).

Finally, only periods below 17 days were considered, since longer periods may be affected by errors larger than 2% in the period determination. Only 12 of the periodic variables candidates had to be removed from the sample because of periods longer than 17 days. Fig. 4.4 also shows a zoom into the shorter periods. The simulation shows several peaks around 2 days as well as a high peak at 0.67 days which is directly related with the sampling of the data. Note that this test is only based on the Scargle periodogram technique, while as outlined before, only Scargle peaks which remain after running the CLEAN algorithm (which corrects for the non-uniformity in the time series) were taken into account in the period determination. This means that it should be possible to exclude spurious detections by means of the whole period analysis procedure. The 2% error curve in Fig. 4.4 was used as the estimated errors in the period determination. Note that these are upper limits and therefore the real errors are often much smaller.

4.3 Irregular variables

Many of the objects for which no significant period was detected nonetheless show relatively large brightness variations in their light curves. The peak-to-peak amplitudes for these objects are usually much higher than for the periodic ones, reaching up to 3 magnitudes. The χ^2 variability test was performed on all the 2908 monitored stars in which the time series data contain at least 30 data points. The χ^2 test gives the probability that the deviations in the light curves are due to the photometric errors and not due to an intrinsic variability of the object (e.g. Bailer-Jones & Mundt 1999), and it was computed as follows:

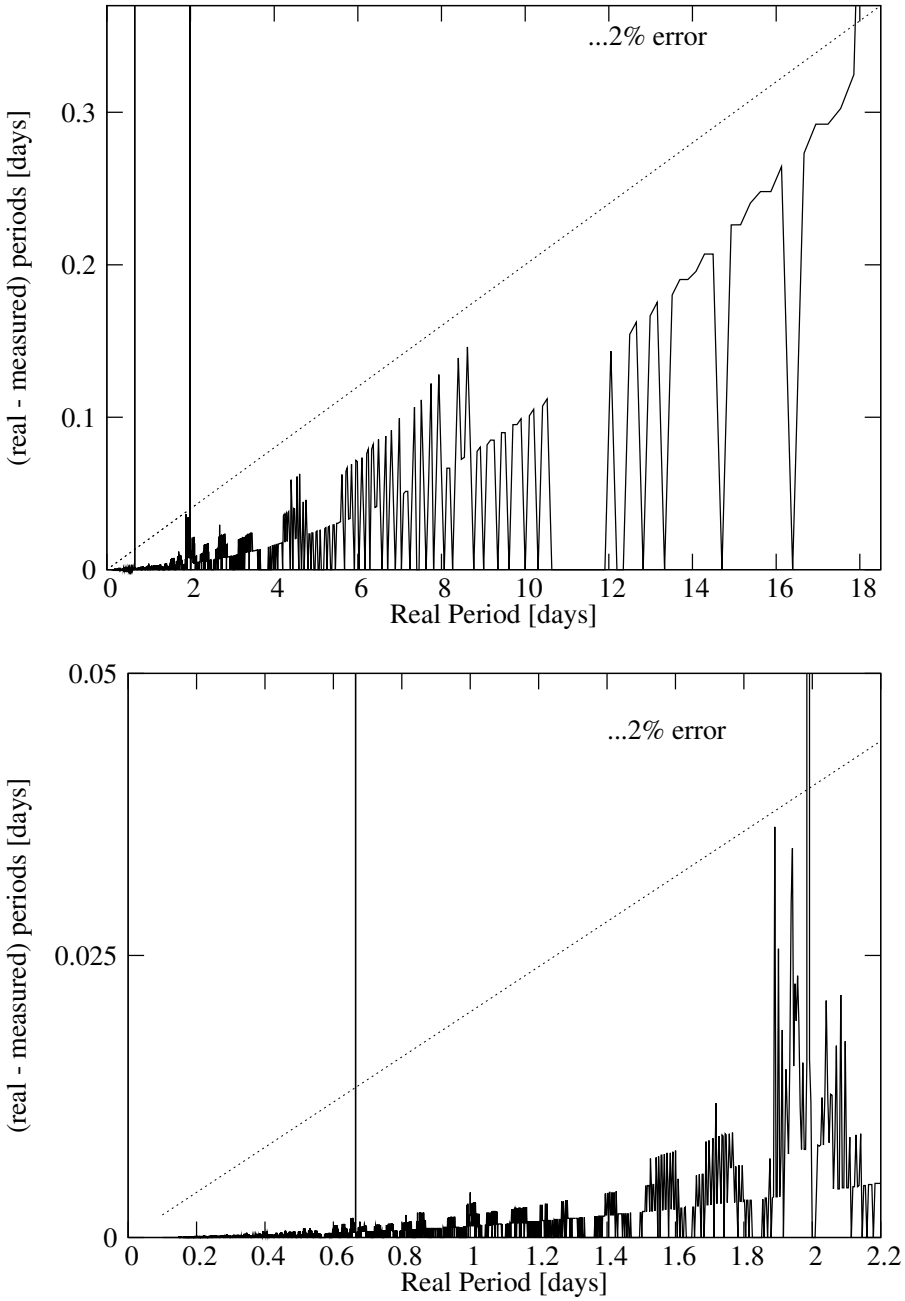

Figure 4.4 Results of a simulation showing the difference between measured and real period as a function of real period. This simulation reflects the sensitivity of the method used for searching for rotational periods (see text for details). The dotted line corresponds to a period error of 2%. The lower panel shows a zoom into the short period regime.

$$\chi^2 = \sum_{j=1}^{N_B} (\frac{m_{rel}(j)}{\delta m_{rel}(j)})^2 \tag{4.4}$$

with m_{rel} the (mean subtracted) relative magnitude and δm_{rel} the error of the *jth* star. N_B is again the number of data points in the light-curve.

The probability that the star is variable is given by Press et al. (1992)

$$p = 1 - Q(\chi^2|N_B) \tag{4.5}$$

where $Q(\chi^2|N_B)$ is the probability that a non-variable star with N_B time series measurements has a χ^2 value higher than the one given by Equ. 4.4. $Q(\chi^2|N_B)$ is described mathematically in the following Equ.,

$$Q(\chi^2|N_B) = \frac{\Gamma(\frac{N_B-1}{2}, \frac{\chi^2}{2})}{\Gamma(\frac{N_B-1}{2})} \tag{4.6}$$

where N_B*-1* instead of N_B has been used since the time series has been mean subtracted and therefore the degrees of freedom are reduced by 1.

As stated above, all the monitored stars in this analysis were included and since this test is also sensitive to periodic variations it was necessary to exclude from the resulting 1186 objects which are found to be variables by the χ^2 variability test the ones which are known to be periodic variables. 76% of the periodic variables (this number includes also the possible periodic variables) are variables by means of the χ^2 test. The reason why not all of the periodic variables are variables according to this test is that the periodogram analysis is sensitive to much lower amplitudes variations than the χ^2 test and therefore the low amplitude periodic variables are only detected by the time series analysis described above.

As a result, after removing the periodic and possible periodic variables from the sample, 808 objects were found to be irregular variables with a probability higher than 99.9%.

Table 4.1 Periodic variable catalogue. The complete catalogue is available electronically at the CDS.

ID	I[mag]	$FAP_{\mathrm{Scargle}}{}^{a}$	$FAP_{\mathrm{Ftest}}{}^{b}$	P^{c}[days]	$\mathrm{P_{err}}{}^{d}$[days]	$\mathrm{P_{H2002}}{}^{e}$[days]	$\mathrm{P_{adopt}}{}^{f}$[days]	PTP^{g}[mag]
1	15.535	1.13E-05	2.87E-02	0.710	0.014	...	0.710	0.019
11	15.139	6.34E-09	1.08E-07	1.740	0.035	1.730	1.740	0.030
87	16.194	6.34E-11	1.65E-12	3.100	0.062	3.110	3.100	0.020
1002	15.019	3.54E-09	3.07E-09	3.980	0.080	3.940	3.980	0.572
3001	15.533	1.84E-10	<1.00E-15	3.240	0.065	3.310	3.240	0.034
10054	20.031	1.86E-03	9.73E-02	0.830	0.017	...	0.830	0.258
10147	19.428	2.14E-06	9.43E-03	2.680	0.054	...	2.680	0.118
10310	18.209	1.13E-12	<1.00E-15	2.650	0.053	...	2.650	0.072
10327	19.120	1.18E-08	9.14E-09	2.580	0.052	2.590	2.580	1.240
10336	16.958	<1.00E-15	<1.00E-15	8.400	0.168	...	8.400	0.256
10349	18.237	1.85E-09	<1.00E-15	9.900	0.198	9.560	9.900	0.297
20033	15.456	1.25E-11	1.67E-14	1.260	0.025	...	1.260	0.090
20035	16.823	1.90E-08	2.54E-05	7.300	0.146	...	7.300	0.180
20124	17.871	3.60E-12	<1.00E-15	4.420	0.088	...	4.420	0.807
20297	19.436	6.86E-05	3.27E-02	3.920	0.078	...	3.920	0.433
20317	17.882	8.72E-11	1.50E-13	6.990	0.140	...	6.990	0.121
20347	19.013	1.38E-05	5.92E-02	1.200	0.024	...	1.200	0.134
20518	18.456	2.26E-12	<1.00E-15	4.110	0.082	...	4.110	0.915
20532	20.254	2.16E-04	4.06E-01	0.460	0.009	...	0.460	0.315

[a]False Alarm Probability computed from the Scargle time series analysis.
[b]False Alarm Probability computed from the Ftest
[c]Rotational period measured in this study.
[d]Error of the derived rotational period.
[e]Rotational period found by H2002.
[f]Final rotational period adopted.
[g]Peak-to-peak amplitude of the modulation.

Chapter 5

Properties of the periodic variables

5.1 Period distribution, overview

In the following, the period distribution of the already known and newly found periodic variables in the ONC and also their peak-to-peak amplitude distribution are investigated in detail. In addition, the results are compared with the ones by Lamm et al. 2004 in NGC 2264. In particular, the dependence of these two distributions on mass and position of the objects in the field are analysed. By including the H2002 results a more complete sample of periodic variables is used in all following analysis, and in particular a much broader range of masses is covered, ranging from about 1.5 $M_{\odot}$ (H2002) down into the BD regime with the faintest objects having a guesstimate mass of only $\sim 16\, M_{jup}$. As outlined in more detail below, 124 of the periodic variables from this study and 139 in the combined data-set (i.e. this study + H2002) are potential BDs, which is by far the largest rotational period sample of BDs and BD candidates.

New results are compared with the rotational data published by H2002. The result of this comparison is shown in Fig. 5.1. 110 of the periodic variables reported by H2002 are also found to be periodic in this study. From the 369 periodic variables found in H2002, 143 are brighter than 14.1 in I (which is the I mag of the brightest PV in this study due to the CCD saturation limit) and 14 are located in the gaps of our survey (since the positioning is not exactly the same in the two surveys). These results in 212 periodic variables that in principle can be recovered, although only 52% of them (i.e. 110 objects) are actually recovered in this study. The remaining 48% consist of 34% irregular variables, 5% possible periodic variables and 7% non-variables, which means that a small fraction of the non-recovered periodic variables are found to be non-variables in this study. Moreover, 74% of the recovered periodic variables were found to have periods which agree within the errors in both epochs. The high level of agreement implies that many of these objects have spot groups stable enough to be detectable by the used method over many years. This is quite

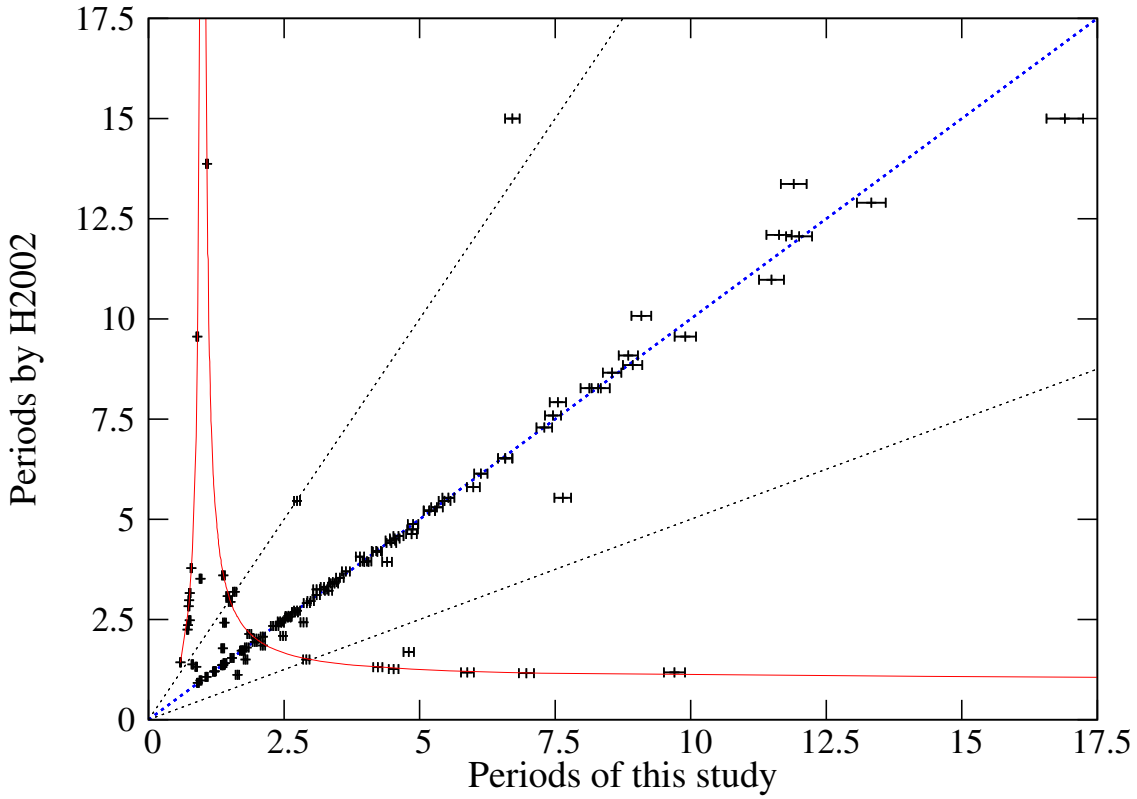

Figure 5.1 Comparison of the periods measured for the 110 stars common to this and H2002 study. Stars with the same periods found in both studies are located on the blue dashed line. They represent 74 % of the total. The beat periods and the harmonics curves are shown as red solid and black dotted lines, respectively. The error bars correspond to a 2% error in the period determination, which is an upper limit to the measured errors (see Fig. 4.4).

different to Scholz et al. (2009), who found that in the much older (40 Myr) cluster IC4665 only 10% of the rotational periods could be recovered after 1 year. This may suggests that the fraction of objects having detectable spot groups over many years is strongly decreasing with age.

Most of the periods that show no agreement can be understood as aliasing or harmonics. Aliasing or "beat" phenomena result from the one day sampling interval in data taken at the same longitude (H2002). This means that a periodic variation of period P will result in a beat period B:

$$\frac{1}{B} = \frac{1}{P_{\text{sampling}}} - \frac{1}{P} \qquad (P > P_{\text{sampling}}) \tag{5.1}$$

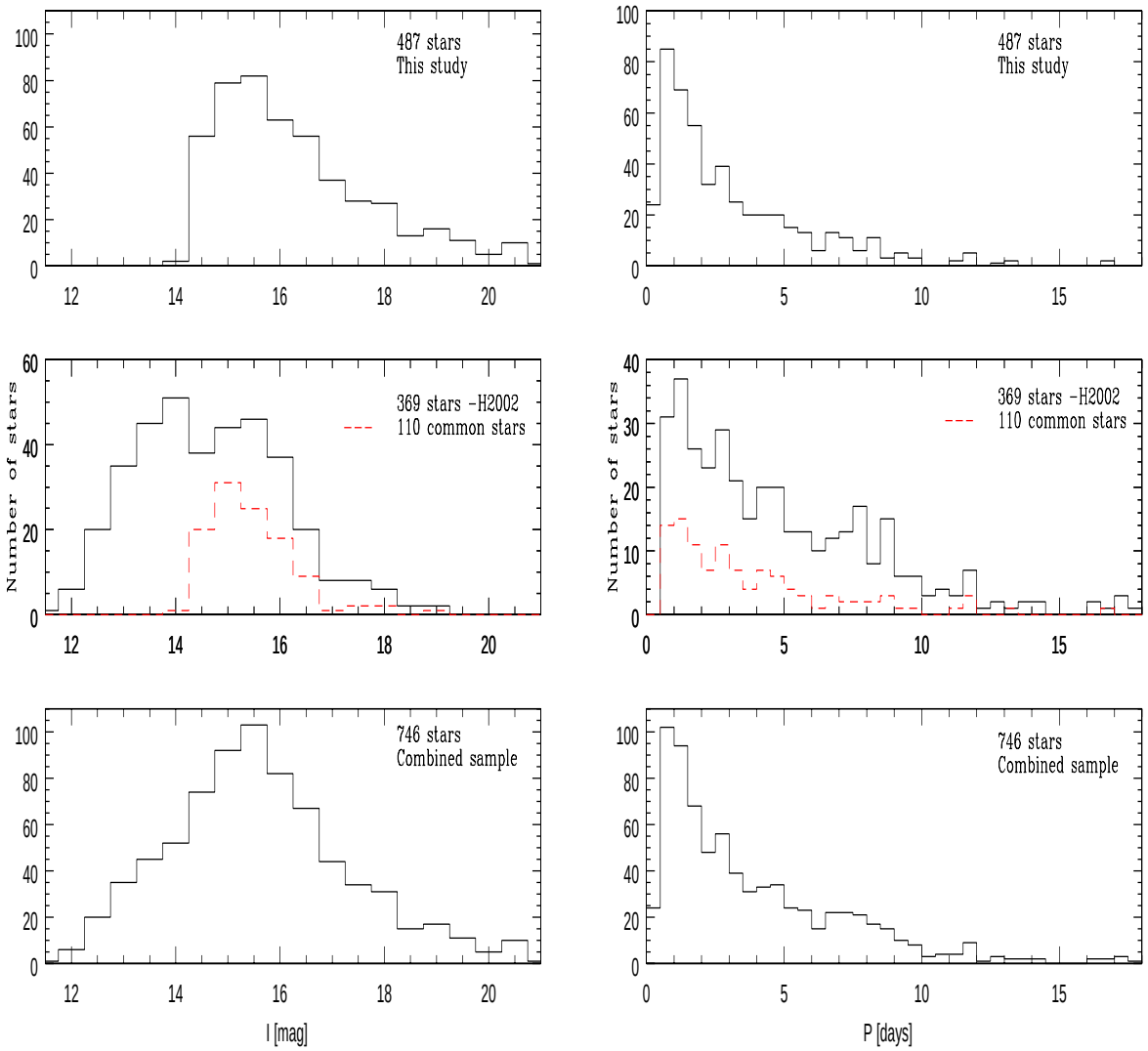

(a) Magnitude distribution of the periodic variables. (b) Period distribution of the periodic variables.

Figure 5.2 *a*) Magnitude and period distribution of the periodic variables. The top panel shows the magnitude distribution of the 487 periodic variable stars detected in this study. In the middle panel, the variables found by H2002 are displayed (solid line), where the dashed line indicates the 110 objects which are common for both studies. The bottom panel shows the distribution for the combined sample of 746 periodic variables. *b*) Same as *a*) but for the period distribution of the periodic variables.

$$\frac{1}{B} = \frac{1}{P} - \frac{1}{P_{\text{sampling}}} \qquad (P < P_{\text{sampling}}) \tag{5.2}$$

with $P_{sampling}$ equals 1 day in our case.

Only five possible beat periods were identified in this study as shown in Fig. 5.1, while in the H2002 sample there are 12 possible long beat periods. This result is as expected since the data sampling was taken into account by using the CLEAN algorithm (see Chapt. 4) and therefore the beat effect should be much smaller on our period determinations than on H2002 who did not take this effect into account.

In Fig. 5.1, about 3% of the 110 common periodic variables lay on two straight lines of slope 1/2 or 2. The effect in which a measured period is found to be a double or half of the true period is called harmonics. The beat periods and the harmonics curves are shown in Fig. 5.1 as solid and dotted lines, respectively.

Because of the more sophisticated time series analysis used here (e.g. combination of Scargle and CLEAN algorithms and several FAPs calculations) the period determination is regard as more reliable and therefore the periods measured in this study were used for the further analysis. Only for the five objects in which the measured periods seem to be (long) beat period of the true (short) ones, the periods determined by H2002 were adopted.

The magnitude as well as the period distribution of the periodic variables detected in this study and in the one by H2002 are shown in Fig. 5.2. In the top panels of Fig. 5.2*a* and 5.2*b*, the distribution of the 487 periodic variables from this study are shown. The middle panels show the distributions of all the periodic variables found by H2002 with the following discrimination: objects found to be periodic in both studies (dashed red lines) and the stars found to be periodic only in H2002 (solid line). Fig. 5.2*a)* clearly shows that the overlapping magnitudes mostly range from 14 to 17 magnitudes. The combined samples are shown in the two bottom panels of Fig. 5.2. Note that extinction corrected magnitudes are not considered for this analysis.

5.2 Period distribution and its dependence on mass

In order to estimate masses of the periodic variables in the ONC from evolutionary models, knowledge of the individual extinction values is necessary. This requires knowledge of the spectral type and at least one colour, which is difficult to measure for some wavelength bands (e.g. R-band) due to the strong nebular background. Since for most objects the

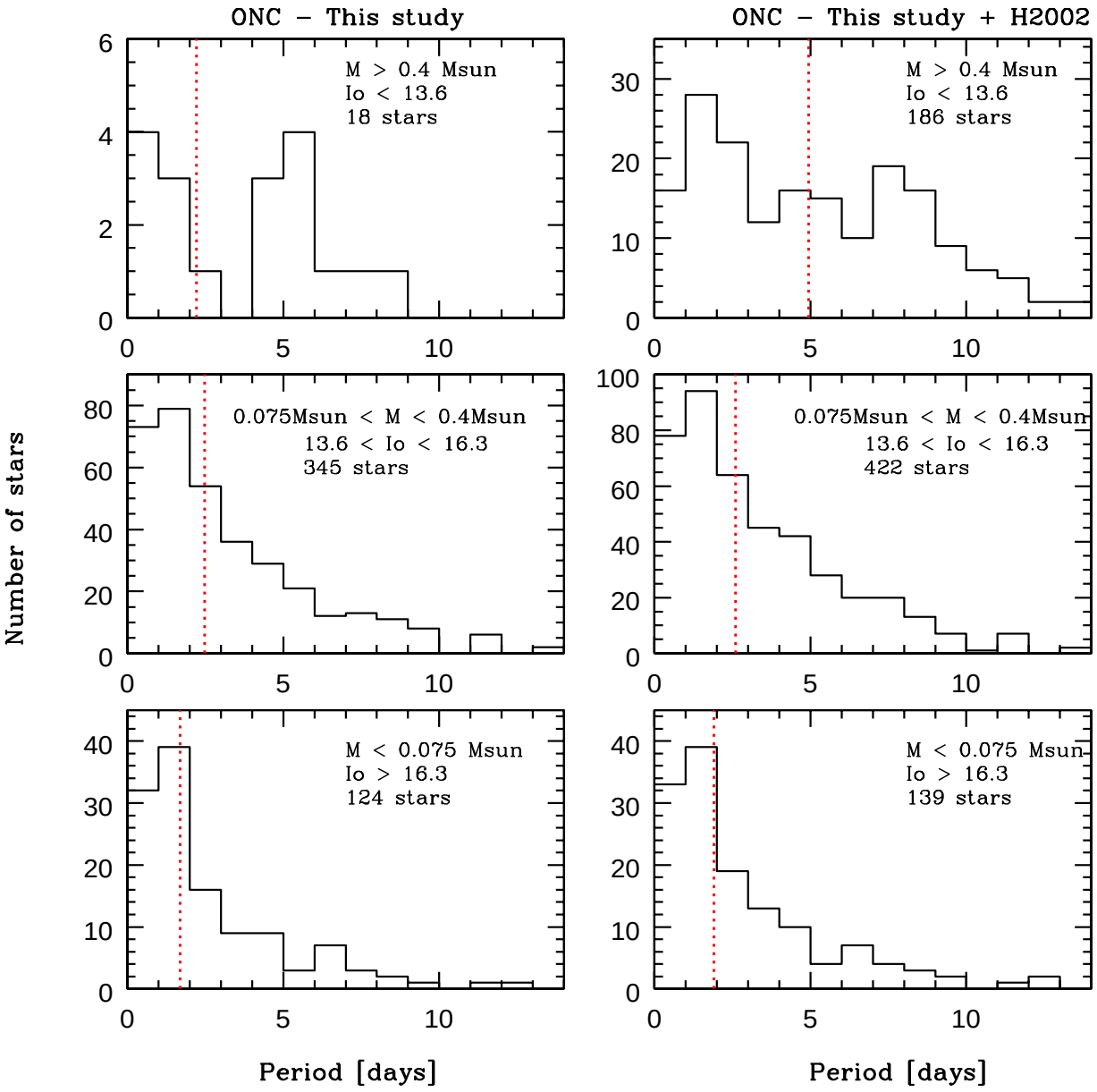

Figure 5.3 The left panels show the period distribution for the periodic variables in this study, while the right hand side shows the period distribution of the periodic variables in the combined data set (This study + H2002) for the whole region covered by the CCD image displayed in Fig. 2.1. The mass regime for each panel is indicated and is based on models by Baraffe et al. (1998) and Chabrier et al. (2000), assuming a constant $A_v = 1.4$ mag for all stars (see text for details). Only a few stars of this study have I magnitudes within the bright regime (top left panel), therefore a meaningful analysis can only be done in combination with the H2002 data (top right panel). The medians of the periods for each panel are shown as dashed lines.

Table 5.1 Number of variable objects found in the ONC ($\sim$ 1 Myr) by this study and in NGC 2264 ($\sim$ 2 Myr) by Lamm et al. 2004.

VarFlag[a]	ONC ($\sim$ 1 Myr)			NGC 2264 ($\sim$ 2 Myr)
	R<$R_{cluster}$	R>$R_{cluster}$	Total	Total
PV	196	291	487	405
IV	335	473	808	184
All Stars	847	2061	2908	10554

[a]As in Table 3.1, PV are periodic variables and IV irregular variables. All Stars include the total number of monitored stars independently on whether they are variables or not.

spectral types are unknown, individual extinction values cannot be determined.

For the sake of simplicity a uniform extinction for all stars in the field was assumed. Several authors (Jones & Walker 1988; Bautista et al. 1995; Hillenbrand 1997) have estimated the average visual extinction A_v within 1 pc of the Trapezium stars and derived values between 1.3 and 1.5 magnitudes. A constant value of $A_v = 1.4$ mag was then assumed, which corresponds to an A_I of 0.8 mag. I am aware that with this simplified assumption the intrinsic brightness (and therefore the mass) of some objects may be underestimated, particularly in the inner part of the field (because their true A_v can be much larger than 1.4 mag) as well as the intrinsic brightness of objects located where A_v are certainly much lower (e.g. at the eastern edge of the field Castets et al. (1990)) may be overestimated. I am also aware that local extinction (e.g. due to circumstellar disks) can vary strongly from object to object (see Chapt. 6 and 7) and in addition intrinsic brightness variations can mimic different masses than implied by the flux in the I-band[1]. Extinction-corrected magnitudes are denoted as I_0 from now on.

In order to investigate the dependence of the period distribution on mass, we selected the following three brightness bins:

- **A**: bright bin containing stars with $I_0 \leq 13.7$ mag, corresponding to $M \geq 0.4\,M_\odot$.
- **B**: intermediate bin with $13.7 < I_0 \leq 16.3$, corresponding to $0.4\,M_\odot < M \leq 0.075\,M_\odot$.
- **C**: faint bin in which all objects have $I_0 > 16.3$, corresponding to $M < 0.075\,M_\odot$.

[1]It is worth to note that mass estimations based on NIR colours may be more suitable since they are less affected by extinction and the amplitude of the variations are expected to be smaller. In contrast, they may provide larger fluxes for objects with circumstellar disks and therefore in many cases the masses may be overestimated. In Chapt. 6 independent mass estimates are presented based on J-band colours, which are probably more accurate than the I-band based mass estimates presented here.

This selection is not arbitrary. The limit for the brightest bin corresponds to the same limit used by H2002 to separate the high and low mass regime, in which the high mass regime showed a bimodal period distribution and the low mass did not. H2002 used Hillenbrand (1997) mass estimates based on D'Antonna and Mazzitelli (1994) models and the dividing line between the two populations corresponds to $0.25\,M_{\odot}$ with this model. In this study, however, models by Baraffe et al. (1998) are used to estimate masses from the measured magnitudes after assuming $A_{\rm v} = 1.4$ mag. The corresponding mass limit for the brightest bin when using Baraffe et al. (1998) models is $0.4\,M_{\odot}$. The middle mass bin corresponds to a mass range between $0.4\,M_{\odot}$ and $0.075\,M_{\odot}$, while the last bin is for substellar objects, i.e. $M < 0.075\,M_{\odot}$. This last mass bin contains 124 potential BDs (only this study) which is at least 10 times larger than the existing number known in any other cluster, e.g. σ Orionis (Scholz & Eislöffel 2004). Although, in this study, there are only a few objects in the brightest bin, this bin is useful when analysing the combined data of this study and of H2002.

The resulting period distributions for the periodic variables measured in this study and in the combined data (This study + H2002) are shown in Fig. 5.3, in the left and right columns, respectively. The median values for each set of data, plotted as vertical dashed lines, show the already known tendency to have faster rotators towards lower masses, which is expected from previous studies (e.g. H2002; Lamm et al. 2005), but has not yet been investigated for a large sample of objects in the BD mass regime. In order to give statistical significance to the mentioned tendency a K-S test was performed for the two data sets. Due to the small number of objects in the first mass bin in our sample, the K-S test was performed only for the intermediate and low mass bins, resulting in a 96% ($2\,\sigma$ level) probability that the two distributions are different. For the combined data, the K-S test confirmed the different distributions at a very high confidence level, $> 99.9\%$ for the high-intermediate mass-bins and at a $2\,\sigma$ level (95%) for the intermediate-low mass bins. These results indicates that the already known trend to have fast rotators towards lower masses extends also down into the substellar regime.

5.3 Spatial distribution of variable objects

The spatial distribution of the variable and non-variable objects in the ONC field was analysed. As a meaningful, although somewhat arbitrary spatial separation within the studied field, the half-mass radius of the cluster (also called cluster radius, Hillenbrand & Hartmann 1998) was used, which has a length of $6\farcm7$ from Θ^1 Ori, corresponding to about 1 pc distance from that star. The spatial distribution of the catalogued objects is shown

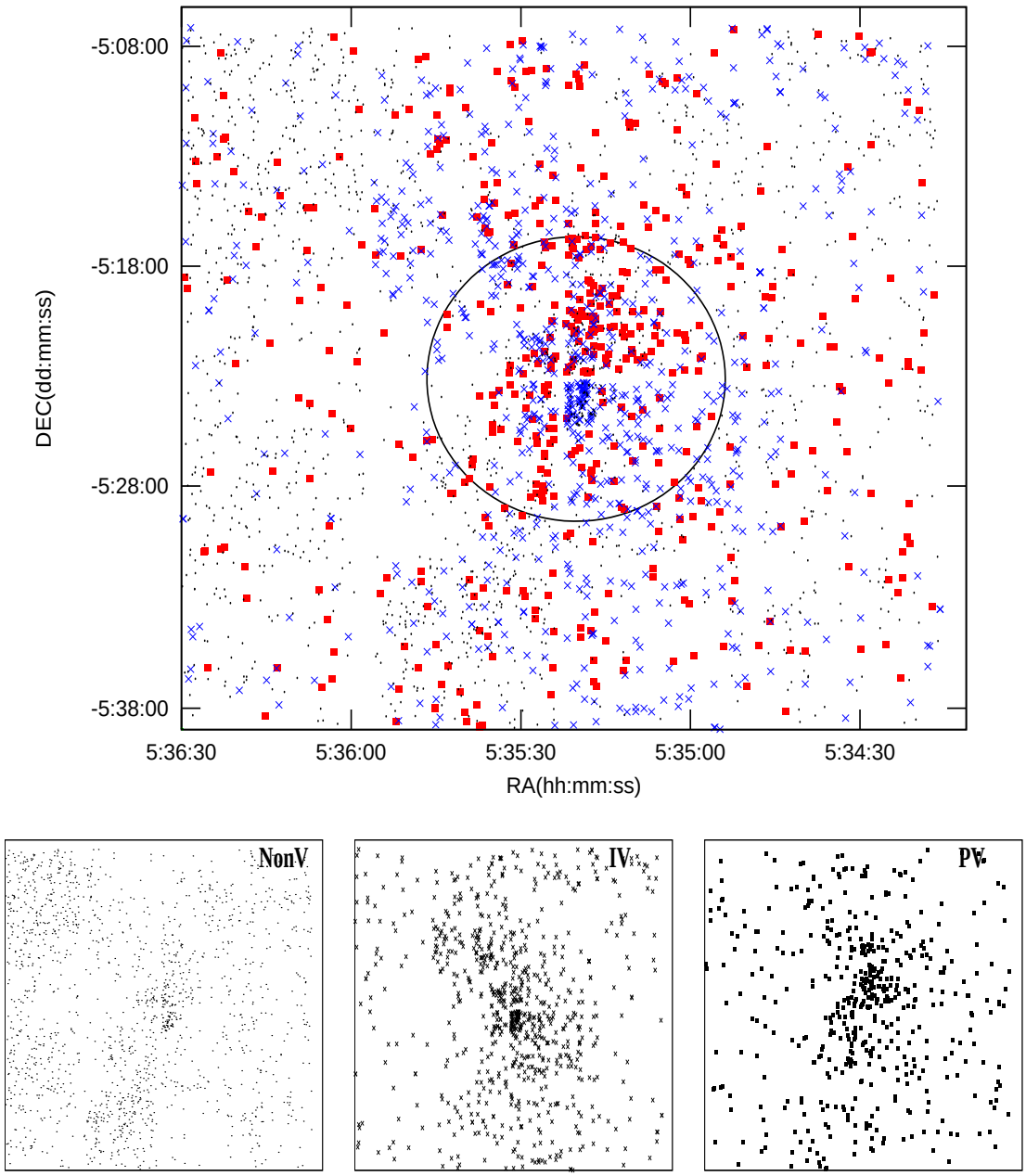

Figure 5.4 Spatial distribution of all variable and non-variable objects in our photometric catalogue, i.e. 487 periodic variables (squares), 808 irregular variables (crosses) and 1531 non-variables (dots). The circle in the center of the field in the top panel represents the cluster radius, and is used as a dividing criterion in the analysis of the properties of the periodic variables (see text). It is centered on Θ^1 Ori and has a radius of $6\farcm7$ (~ 1 pc). The top panel shows the spatial distribution of all objects, while the three lower panels show the corresponding distributions of the non-variable objects, the irregular objects and the periodic variables, from left to right. These lower panels illustrate the rather different spatial distributions between variables and non-variable objects.

in Fig. 5.4. The top panel shows the position of all stars observed. Periodic variables (487) are represented by squares, irregular variables (808) by crosses and non-variable objects (1531) by dots. The lower panels show the spatial distribution of non-variable, irregular, and periodic variable objects from left to right, respectively. It is clearly evident that the distribution of the non-variable objects is much smoother than the distribution of either the irregular or periodic variables. It is interesting that the irregular variables and the periodic ones are not located in exactly the same regions of the field, although an obvious clustering inside the cluster radius is evident in both cases. Most of the irregular variables are clumped in a small region south of Θ^1 Ori, while the periodic variables are mainly located north-west and south-east of that star. A K-S test resulted in a 99% probability that the distributions of the declination for irregular and periodic variables are different from one another and 43% for the right ascension values.

198 objects with periodic brightness modulations were found inside the cluster radius ($R_{cluster}$), and 291 outside of it. The number of irregular variables is 335 inside $R_{cluster}$ and 473 outside. Relative to all stars observed in each spatial region a higher fraction of irregular variables is found inside $R_{cluster}$ than outside it. Since this finding may be a consequence of the decreasing cluster membership probability toward the outer region, typical membership probabilities (Jones & Walker 1988) of 97% in the inner region and 70%[2] outside $R_{cluster}$ were taken into account. About 40% of the objects in the inner region are found to be irregular variables while a smaller fraction of $\sim$28% irregular variables is found outside $R_{cluster}$. Moreover, a higher fraction of periodic variables which show a superposition of short-term irregular variations is found inside $R_{cluster}$ than outside. Although these analysis may suggests a younger age for stars inside $R_{cluster}$ relative to the objects located outside it, the observed ratio between periodic variables (PVs) and irregular variables (IVs) is only marginally supporting this idea. Therefore no unambiguous conclusion can be derived from the number or ratio of IVs and/or PVs on a possible age spread in the ONC.

In addition, the fraction of irregular and periodic variables measured can be slightly biased towards the irregular variables. As stated by other authors (e.g. Lamm et al. 2004), the photometric method for measuring periodic brightness modulations is more efficient among the WTTs than for CTTSs, since irregular variations can add a strong noise to the periodic modulation, preventing the detection of the periodic signal. Due to this noise a certain fraction of periodic variables is definitely missing among the young highly active CTTSs.

[2]From $R = R_{cluster}$ towards the outer limits of our WFI field the membership probability varies from $\sim$90% to $\sim$60%.

5.4 Period distribution and its dependence on position and mass

A possible dependence of the period distribution on position in the field was investigated. Table 5.2 shows the number of periodic variables in the various mass intervals for the ONC and NGC 2264. In the case of the ONC, both this study and the combined data (This study + H2002) are considered and the two regions, i.e. inside and outside $R_{cluster}$, are taken into account.

The resulting period distributions for the periodic variables measured in this study are shown in Fig. 5.5, while the left and middle columns in Fig. 5.6 shows the combined data. In both figures the period distributions inside and outside $R_{cluster}$ are shown. The median values for each set of data are plotted as vertical dashed lines. A first look into Figs. 5.5 and 5.6 suggests different period distributions for stars located in the central and the outer region. For every mass bin, the median of the periods is always higher for objects inside $R_{cluster}$ than for objects outside $R_{cluster}$. The left and middle top panels in Fig. 5.6 furthermore illustrate that the distributions are smoother in the outer region than in the inner one for the highest mass-bin. A two-sided K-S test was performed to corroborate these differences on the combined data shown in Fig. 5.6. The result of the K-S test, which indicates the probability that the distributions come from the same population, is 0.07, 0.0001 and 0.13 for the top, middle, and lower panels, respectively. These numbers indicate that the differences in the top and bottom panels are not highly significant ($< 2\sigma$ level), while in the middle panels are statistically significant at a very high confidence level, $> 99.9\%$.

The same mass dependence found for the whole ONC field, in which towards lower masses the medians of the period distributions shift towards shorter periods, is seen in Figs. 5.5 and 5.6 for the two spatial regions considered. In addition the period distributions of the very low mass and substellar objects (second and third mass bin) are smoother than for the highest mass regime. These results suggest that the spatial position within a star forming region influences the period distribution as illustrated by Fig. 5.6. For example, it is interesting that in the inner region a bimodal distribution for stars with $M > 0.4\,M_{\odot}$ (two peaks around 2.5 and 8 days) is clearly seen, while for the outer region no such bimodal distribution is evident (maybe there are 2 peaks at 5 and 8 days in addition to a 1.5 day peak). In the middle left panel there might be a small bump around 8 days in addition to the 1.5 day peak (but this could result from more highly extincted more massive periodic variables). For the same mass bin, but in the outer region, the highest peak around 1.5 days is the most prominent and the period distribution declines more rapidly towards longer

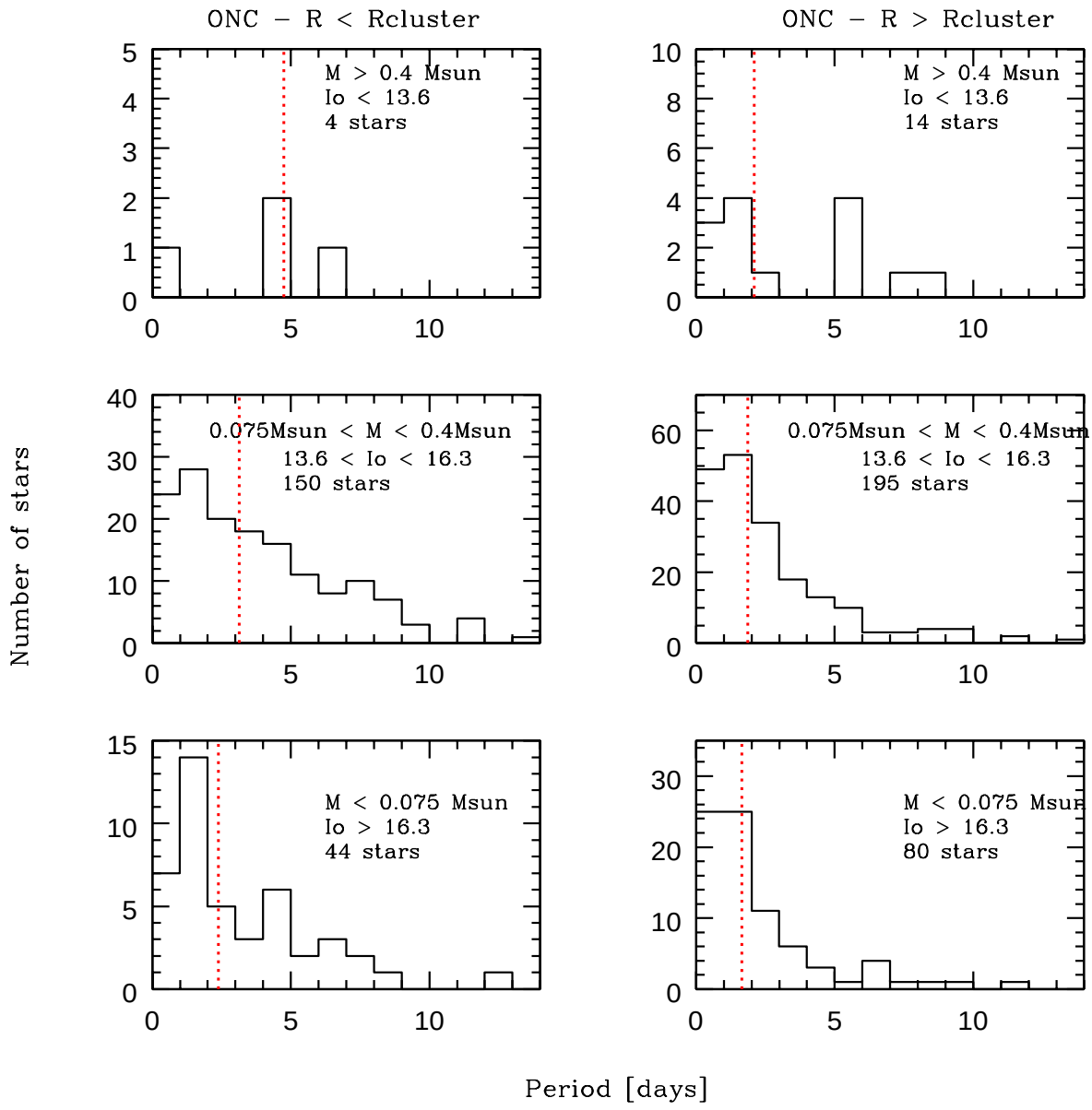

Figure 5.5 The left panels show the period distribution for the stars located inside the cluster radius (6.′7 i.e. ~ 1 pc), while the right hand side shows the period distribution of the stars outside this radius for stars from this study. The mass regime for each panel is indicated and is based on models by Baraffe et al. (1998), assuming a constant $A_v = 1.4$ mag for all stars (see text for details). In the bright regime (top panel) there are only a few stars from this study and a meaningful analysis can only be done in combination with the H2002 data (see Fig. 5.6). The medians of the periods for each panel are shown as dashed lines.

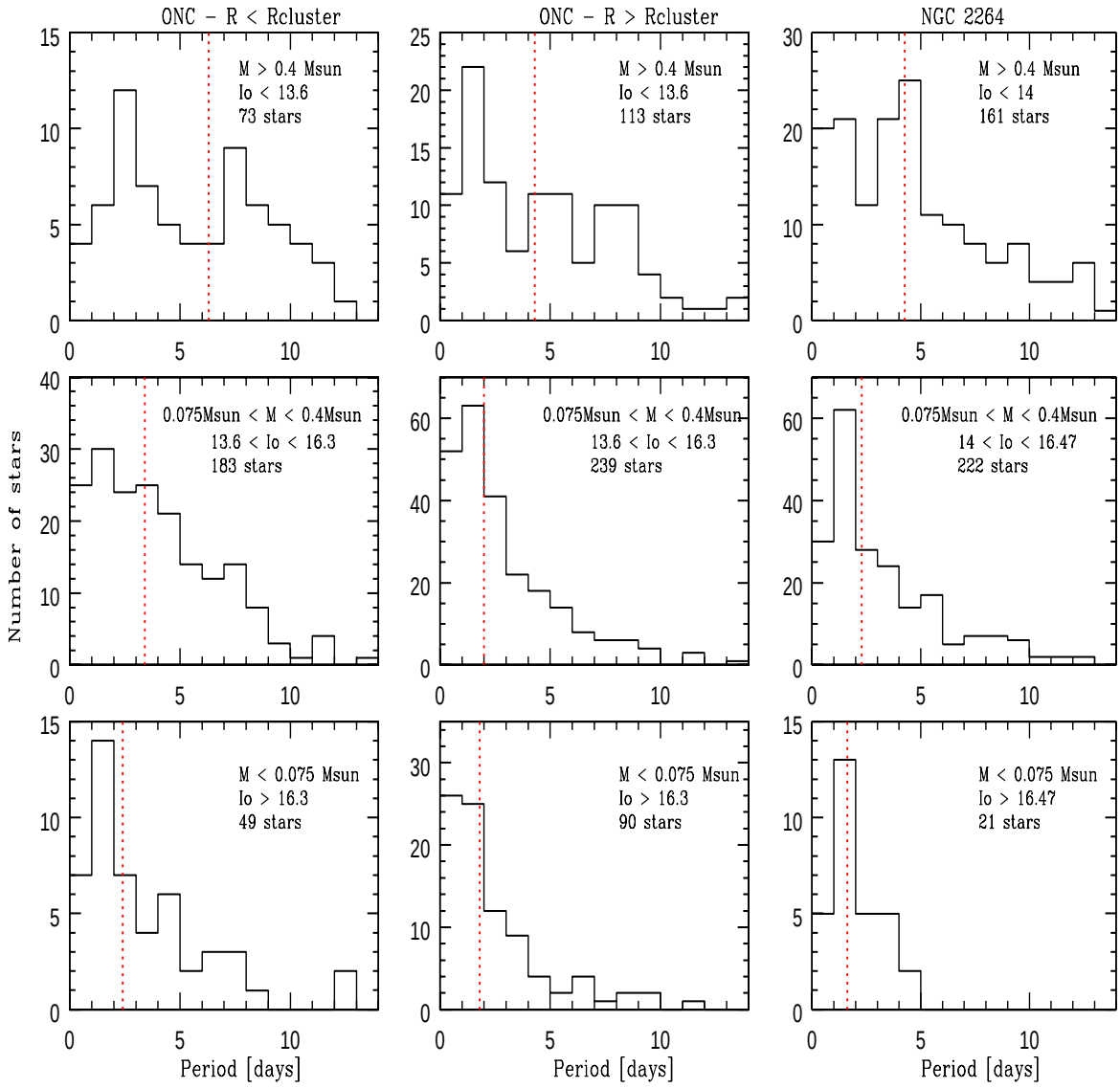

Figure 5.6 The same as Fig. 5.5, but for the combined ONC data of H2002 and this study in both left and middle columns, and for the periodic stars in NGC 2264 (Lamm et al. 2004) in the right column. The top left and middle panels consist mostly of H2002 data. The four lower panels in the ONC show the same trend as in Fig. 5.5, i.e. there is a clear difference in the distributions in and outside $R_{cluster}$ as well as a clear trend for shorter periods towards lower masses. The period distribution for the stars in NGC 2264 (Lamm et al. 2004) for which their measured I magnitudes were shifted to the corresponding ones at the distance of the ONC for a proper comparison are shown in the right column. As in the case of the ONC the mass estimations for each panel are based on models by Baraffe et al. (1998) and Chabrier et al. (2000) after assuming a constant $A_v = 0.18$ mag (Perez et al. 1987). The same trend found in the ONC in which the less massive objects have on average shorter periods is seen here. The median periods for each panel are indicated as dashed lines.

Table 5.2 Number of periodic variables in various mass intervals.

	ONC-This Study			ONC-Combined data			NGC 2264
Mass Bins[a]	$R < R_{cluster}$	$R > R_{cluster}$	Total	$R < R_{cluster}$	$R > R_{cluster}$	Total	
A	4	14	18	73	113	186	161
B	150	195	345	183	239	422	222
C	44	80	124	49	90	139	21

[a]As defined in the text: A, B and C corresponds to the highest, intermediate and substellar mass interval respectively.

periods. The same trend extends to the lowest mass bin (i.e. substellar bin). There, the highest peak is again around 1.5 days for $R < R_{cluster}$ and around 1 day for $R > R_{cluster}$.

The results presented here are possible affected by an observational bias in the mass estimations. As stated above, deriving masses assuming an average A_v leads to overestimating masses for stars in the outer regions and underestimated masses for stars in the more extincted inner region. This bias would result in a certain fraction of highly extincted higher mass objects, which are on average slower rotators, contaminating the lower mass bins in the inner region, while some of the low mass objects, which are on average fast rotators, would contaminate the higher mass bins in the outer region. To check whether the mentioned bias may affect significantly these results the following test was performed: an average extinction $A_v = 1$ was assumed in the outer region, an $A_v = 2$ was assumed in the inner one, and the masses of all objects have been recomputed. No significant differences were found between the new period distributions and the ones based on a constant $A_v = 1.4$. The median rotational periods were slightly different only in the highest mass bin. I then conclude that although this bias may be present it probably does not affect the results and conclusions derived from them.

In summary, on average objects situated outside $R_{cluster}$ tend to rotate faster than their inner counterparts. As observed in previous studies lower mass objects tend to rotate faster than their massive conterparts and for the first time this trend is shown to extends down into the substellar mass regime.

5.5 Comparison with NGC 2264 period distribution

Although not highly significant, the differences found in the rotational period distributions for objects located inside and outside $R_{cluster}$ might be attributed to an age spread in the

field. This means that objects inside $R_{cluster}$ rotate on average slower because they are somewhat younger and therefore have had less time to spin up. H2002 reached a similar conclusion for higher mass objects (i.e. above $0.4\,M_{\odot}$) when analysing the correlations that exist between rotational period and projected radius (Hillenbrand 1997), and also taking into account that the fraction of stars with disks is higher toward the center of the ONC (Hillenbrand 1997; Hillenbrand & Hartmann 1998).

The best way to test this hypothesis is to look at different young regions, such as NGC2264, which probably has twice the age of the ONC. Lamm et al. (2005) compared the ONC (H2002 data) and NGC2264, and found they could explain the different period distributions by different ages. They found that the median values of the period distributions in NGC 2264 are shifted towards shorter periods by a factor of ~ 1.5 relative to the ONC and they found this amount of spin-up consistent with expectation based on PMS contracting models and conservation of angular momentum.

Their conclusion was based on the ONC data from H2002 and therefore the very low mass regime as well as the substellar population were not studied. In addition, when re-evaluating the NGC 2264 data set during this study, models by Baraffe et al. (1998) were used, while Lamm et al. (2005) used models by D'Antona & Mazzitelli (1997) in the mass estimations, which results in a slightly larger number of VLM objects and BD candidates in NGC 2264 than reported by Lamm et al. (2005). This new mass estimates make a reasonable comparison between the ONC and NGC 2264 possible. The right column in Fig. 5.6 shows the period distribution of the periodic variables in NGC 2264 from Lamm et al. 2004 for the same three mass bins used in the analysis of the ONC (i.e. an average $A_{\rm v} = 0.18$ in NGC 2264 was considered (Perez et al. 1987). The median values of each distribution are shown as red dashed lines. It is evident that the trend towards shorter periods among lower masses is true in NGC 2264 even for the 21 substellar objects (bottom panel). The highest mass objects (top panel) show the previously reported bimodal period distribution, while both the VLMs and BDs (i.e. middle and bottom panels) show a smoother, unimodal period distribution with the highest peak at about 1.5 days in each case. The substellar objects in NGC 2264 were found to be entirely rapid rotators with periods below 5 days. Table 5.3 lists the median values of the period distributions for NGC 2264 and the ONC. The comparison of the medians between NGC 2264 and the periodic variables in the whole ONC field delivers a marginal difference, suggesting that objects in the ONC rotate on average slightly slower (by a factor of about 1.2) than the objects in NGC 2264. But the comparison with the periodic variables located inside $R_{cluster}$ results in a factor $\sim$1.5 faster rotators in NGC 2264 for all three mass bins. This is absolutely in agreement with the previous results by Lamm et al. (2005) and is consistent with the age ratio of the clusters. Moreover, when comparing NGC 2264 with objects outside $R_{cluster}$ in

Table 5.3 Median values of the rotational periods given in days for objects in the ONC (combined data) and NGC 2264.

Mass Bins[a]	ONC			NGC 2264
	$R<R_{cluster}$	$R>R_{cluster}$	Total	
A	6.2	4.3	4.9	4.2
B	3.4	2.0	2.6	2.3
C	2.4	1.8	1.9	1.6

[a]The same mass bins of Table 5.2, described also in the text.

the ONC, the median values are found to be almost identical for all three mass regimes. This result is a strong argument in favour of an age spread in the ONC, where the objects outside $R_{cluster}$ are on average older than their counterparts inside it. In addition, this comparison allows to give a rough estimate of the age difference, since the objects outside $R_{cluster}$ in the ONC rotate on average at the same rate as the ones in NGC 2264. These results apparently suggest that the outer region is about twice as old as the inner one[3].

5.6 Peak-to-peak amplitude distribution - high and low level variations

In the following it is discussed how the peak-to-peak (ptp) amplitude distribution of the periodic variables depends on mass and on their location with respect to $R_{cluster}$. For the determination of the ptp variation of the periodic variables the phased light-curve of each object was divided into 10 equally spaced phase bins as described by Lamm (2003). In each bin, the median of the relative magnitudes was calculated. The largest and smallest median values for each objects were used to compute the ptp amplitude as the difference between these two extreme median values.

Since H2002 did not report any ptp amplitudes, this analysis was performed only with the periodic variables measured in this study (487 objects). The small number of objects in the higher mass bin does not allow any meaningful analysis and therefore only the results

[3]Under the assumption of a 2 Myr old population in the outer region, the corresponding mass-intervals were recalculated to test whether this would have change the results based on a 1 Myr old region. Only 7 objects from the lower mass bin move to the intermediate one and 10 from the intermediate mass bin move to the higher mass bin with this new consideration. The new period distributions and their correspondent median values were found to be identical than the previously derived for a 1Myr old outer population, without affecting the whole mass-dependence analysis.

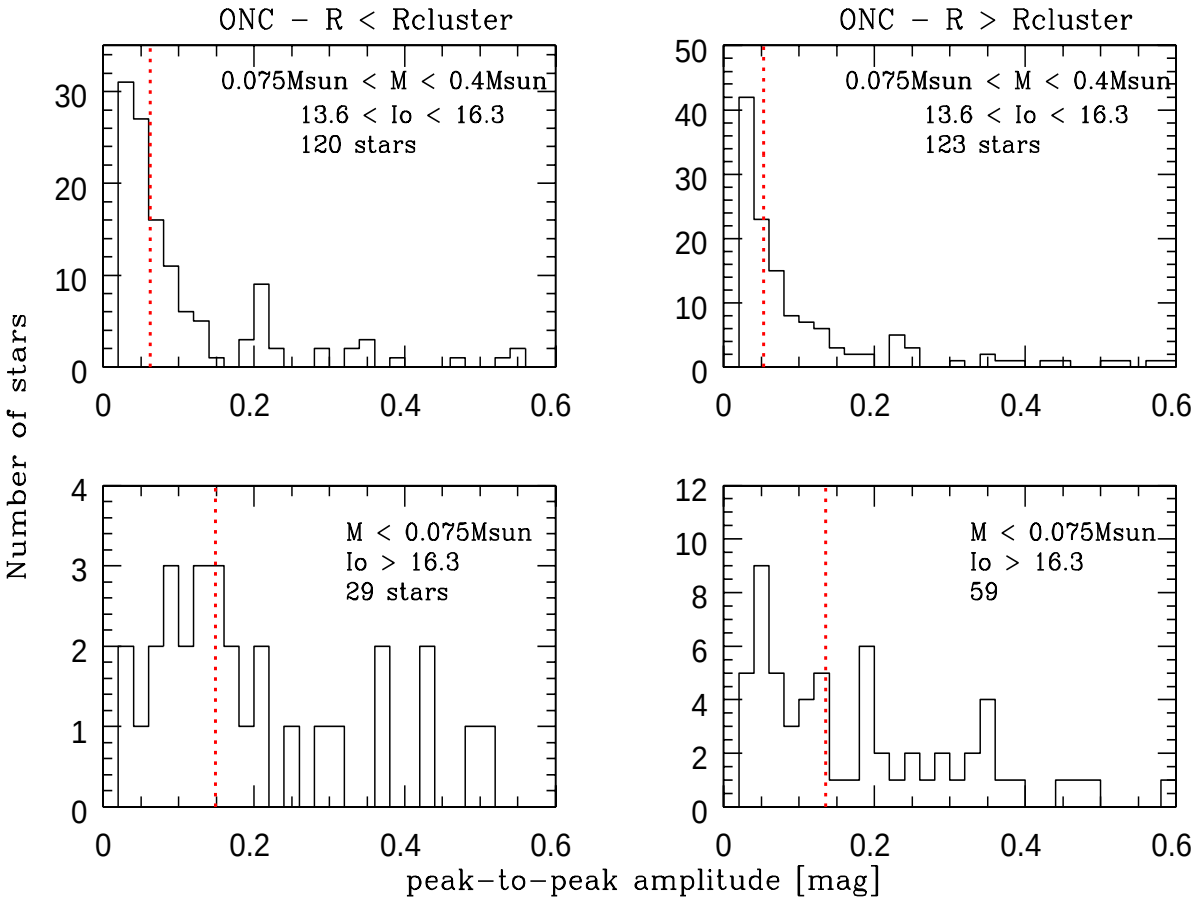

Figure 5.7 Peak-to-peak amplitude distribution of 331 periodic variables with $M < 0.4\,M_{\odot}$ and peak-to-peak amplitudes up to 0.5 mag and above a $1\,\sigma$ confidence limit. The left and right panels show the resulting amplitudes for stars inside and outside $R_{cluster}$, respectively. The top and lower panels show the distributions for $M_{\odot} < M \leq 0.075\,M_{\odot}$ and $M < 0.075\,M_{\odot}$, respectively. The medians of each distribution are shown as a vertical dotted line.

for stars with $I_0 > 13.6$ mag ($M < 0.4\,M_{\odot}$) were analysed.

In order to avoid any observational bias due to the higher photometric errors measured in objects located in the regions with strong nebular background, the sample was first restricted to objects with ptp amplitudes which are at least 2.5 times higher that the mean photometric error in the light-curve of each single star. For the remaining objects (470), those with ptp amplitudes located above the mean error curve (see Fig. 3.2*b*) plus 1 sigma rms were selected . Finally, 346 objects were used to perform the analysis of the ptp amplitude distribution.

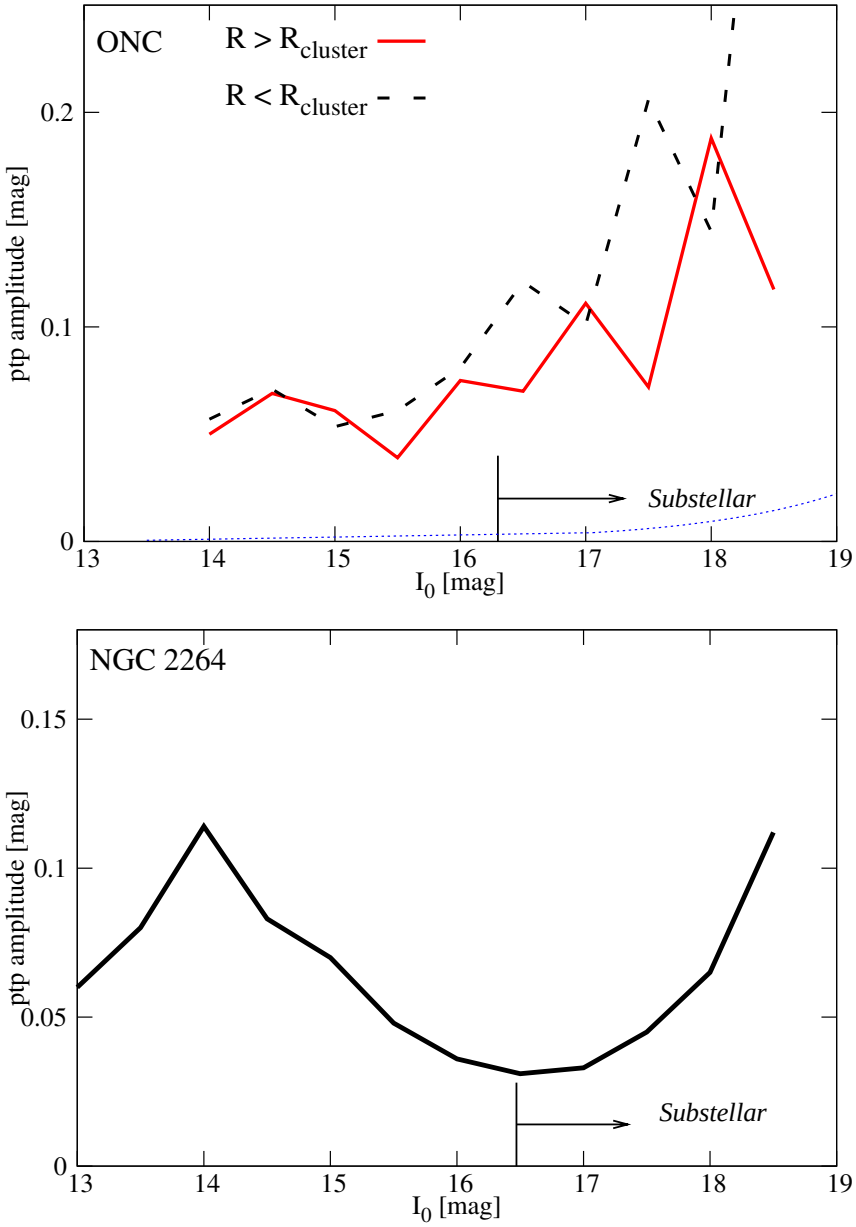

Figure 5.8 Median ptp amplitude (calculated in intervals of 0.5 mag) as a function of magnitude for 331 periodic objects in the ONC (top panel) with ptp variations which fulfil the criteria described in the text, as well as for 405 periodic variables in NGC 2264 (bottom panel). In the ONC the median ptp values are shown as dashed and solid lines for $R < R_{cluster}$ and $R > R_{cluster}$, respectively. We also indicate for comparison the error curve from Fig. 3.2 as dotted lines and the adopted substellar limit in the ONC and NGC 2264. To allow a proper comparison of NGC 2264 with the ONC, the magnitudes were shifted to the distance of ONC (450 pc). Note that the small difference in the substellar limit (from 16.3 mag for the ONC and 16.47 mag for NGC 2264) is due to the higher age of the objects in NGC 2264 and the different average extinction adopted for both fields.

.

Fig. 5.7 shows the ptp amplitude distribution for stars located inside and outside $R_{cluster}$ and considering only the middle and lowest mass bins previously defined in the period distribution analysis. This analysis is restricted to stars with ptp amplitudes < 0.5 mag (95.7% of the sample), while the 4.3% of objects with ptp variations ≥ 0.5 mag are regard as stars not having cool spots but hot spots (H2002).

The comparison of the ptp variations for objects in and outside $R_{cluster}$ exhibits a slight tendency for the objects inside $R_{cluster}$ to have higher ptp amplitudes than the stars located outside $R_{cluster}$. As for the period distribution a two-sided K-S test was performed resulting in a 23% and a 74% probability that the two distributions come from the same population for the middle and lowest mass regimes, respectively. Note that the size of the sample in the substellar regime is small.

Besides the small sample size, it is evident that in the substellar regime the ptp amplitudes are on average higher than for stars with masses between 0.4 $M_{\odot}$ and 0.075 $M_{\odot}$. The ptp amplitudes were found to have a tendency to increase towards lower masses (i.e. fainter I magnitudes), as can be seen in Fig. 5.8 where the median amplitude values were computed in bins of 0.5 magnitudes, and the error curve is shown as blue dotted lines for comparison. Again, objects inside and outside $R_{cluster}$ are discriminated. Objects with $I_0 > 16$ tend to have larger variations than stars with $I_0 < 16$ (i.e. more massive stars) in the cluster, independently of their location inside or outside $R_{cluster}$. This tendency is stronger for the faintest objects. Due to our conservative sample selection, the increasing ptp amplitudes of the faint objects are regard as an intrinsic phenomenon. The mean photometric error curve shows a clear increase above 16 mag but still is one order of magnitude smaller than the ptp amplitudes in all the plotted magnitude range. The typical mean photometric error of an $I_0 = 18$ mag periodic object is about 0.01 mag while the median ptp amplitude of an object with the same brightness is about 0.15 mag. In addition, it has to be pointed out that 32% of the lowest mass objects present low amplitude modulations below 0.1 mag (see Fig. 5.7). Since very low variations are indeed detected among the substellar candidates it is likely that an intrinsic physical phenomenon is at least in part responsable for the increasing ptp amplitudes of the faintest objects. The same analysis was done for the NGC 2264 data set published by Lamm et al. 2004 as shown in the bottom panel of Fig. 5.8. Quite in contrast to the ONC, the median ptp amplitude curve shows a maximum around 14 mag and a minimum at around 16.5 mag, which coincides with the substellar limit. The only similarity between the ONC and NGC 2264 is the increase in the ptp amplitudes at fainter magnitudes. I have no explanation for the differences shown in Fig. 5.8. Presumably the VLM objects in NGC 2264 develop smaller or more symmetrically distributed spots on their surface as was argued by Herbst et al. (2007). This probably requires different magnetic field topologies for objects belonging to the two clusters.

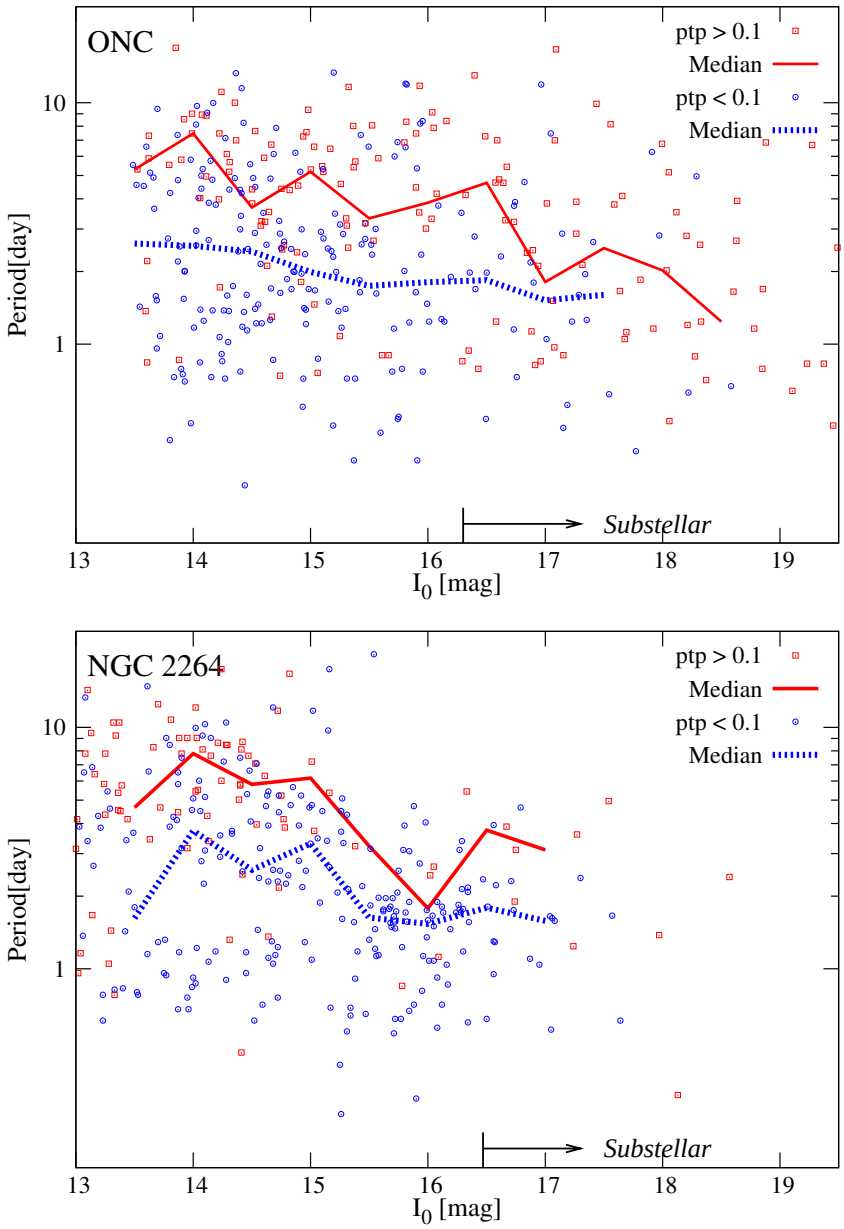

Figure 5.9 Period as a function of magnitude (mass) for two different variation amplitudes, namely for ptp amplitudes (ptp) below 0.1mag (blue open circles) and between 0.1 and 0.5 magnitudes (red open squares), respectively for the ONC (top) and NGC 2264 (bottom). The medians of the rotational periods are calculated within 0.5 magnitudes bins for both cases and are indicated as blue dashed and red solid lines for ptp amplitudes below 0.1mag and between 0.1 and 0.5 magnitudes, respectively. In the case of NGC 2264 the magnitudes were shifted to the distance of ONC (450 pc).

5.7 Rotational period and ptp amplitude correlation in the ONC and NGC 2264

The dependence of the period on the ptp amplitudes was analysed. For this purpose only objects showing ptp variations ≤ 0.5 mag were considered and divided into two subsamples, namely one with amplitudes ≤ 0.1 mag and the other with amplitudes from 0.1 to 0.5 mag. The top panel in Fig. 5.9 shows the rotational period as a function of magnitude for these two samples in the ONC. The medians for each sample were calculated in bins of 0.5 magnitudes and appear in Fig. 5.9 as a dashed (blue) and a solid (red) line for the objects with ptp amplitudes below 0.1 mag and above this value, respectively. It is evident from this figure that the stars with higher amplitudes have on average a significantly longer period. This is true for all masses, although the median rotation periods for both subgroups seem to approach each other in the very low mass regime.

Furthermore, the top panel of Fig. 5.9 is rather interesting with respect to the already discussed decrease in period with decreasing mass (see Fig. 5.6). This trend is only evident for the objects with ptp amplitudes between 0.1 and 0.5 mag. This decrease in periods towards lower masses is not so clear for the objects showing the lowest level variations (i.e. ptp amplitudes < 0.1 mag). In the latest group, independent of their I values (i.e. for all masses) all objects are on average fast rotators with a median period close to 2 days.

The bottom panel in Fig. 5.9 shows the same correlation for NGC 2264 (i.e. the I magnitudes have been shifted to the distance of the ONC, 450 pc). As in the ONC, objects with the smallest ptp amplitudes rotate on average faster than the highly variable objects. The differences between the two subgroups in NGC 2264 are roughly constant (and smaller than in the ONC) over the whole mass range, but due to the small number of objects fainter than 16 mag with ptp amplitudes above 0.1 mag it is difficult to perform a reliable statistical analysis.

It is rather intriguing that a correlation between rotational period and level of variability is found for periodic variables in two different clusters. Irwin et al. (2008) did not find such a correlation between rotational period and amplitude of the modulation in the 5 Myr old cluster NGC 2362. It is worth to note that their sample only extends down to about $0.1\,M_{\odot}$ with a high fraction of objects even more massive than $0.4\,M_{\odot}$.

This finding can probably be explained by differences in the spot coverage and/or differences in the magnetic field topologies. Recent studies of TTSs magnetic field structures (Jardine et al. 2006), argue that a variety of field topologies, from dipole to complex configurations, are required to explain the whole range of X-ray emission

measurements for COUP stars. In the complex field configurations, the coronal gas is confined within compact loops and covers a large fraction of the surface. These multipolar fields produce small and almost uniformly distributed spots which result, on average, in a low level periodic variability. In addition, this kind of magnetic configuration hardly allows for any magnetic braking through coupling with the disk and therefore these objects are more likely to be fast rotators. On the other hand, an extended dipolar field, more likely produces big spot groups near the magnetic poles which could result in a high level periodic variability if the magnetic and rotational axis are inclined. In the latter scenario, due to the slower decline in magnetic field strength with distance from the star, the magnetic coupling to the disk is much stronger, and therefore these objects are more likely to be slow rotators.

Chapter 6

Searching for circumstellar disks

6.1 Overview

In the previous chapters, I presented the whole rotational period analysis performed for a large sample of very low mass periodic variables in the ONC, and I reported rotational period and amplitude dependence on mass and location in the ONC field. As outlined in the Introduction, to understand the rotation properties of these YSOs it is necessary to investigate which are the possible mechanisms involved in the angular momentum and correspondingly rotational period regulation. Although the details on how angular momentum is removed from the star/disk system are not fully understood, circumstellar accretion disks are known to be somehow responsables for this process.

In this Chapter, I present the data set used in order to investigate a possible rotation-disk correlation in our sample of periodic variables. Independent mass estimates based on J-colours are also presented, as well as the method used to derive NIR excesses used as circumstellar accretion disk indicators. The rotation-disk correlation investigation is presented in detail in Chapt.7.

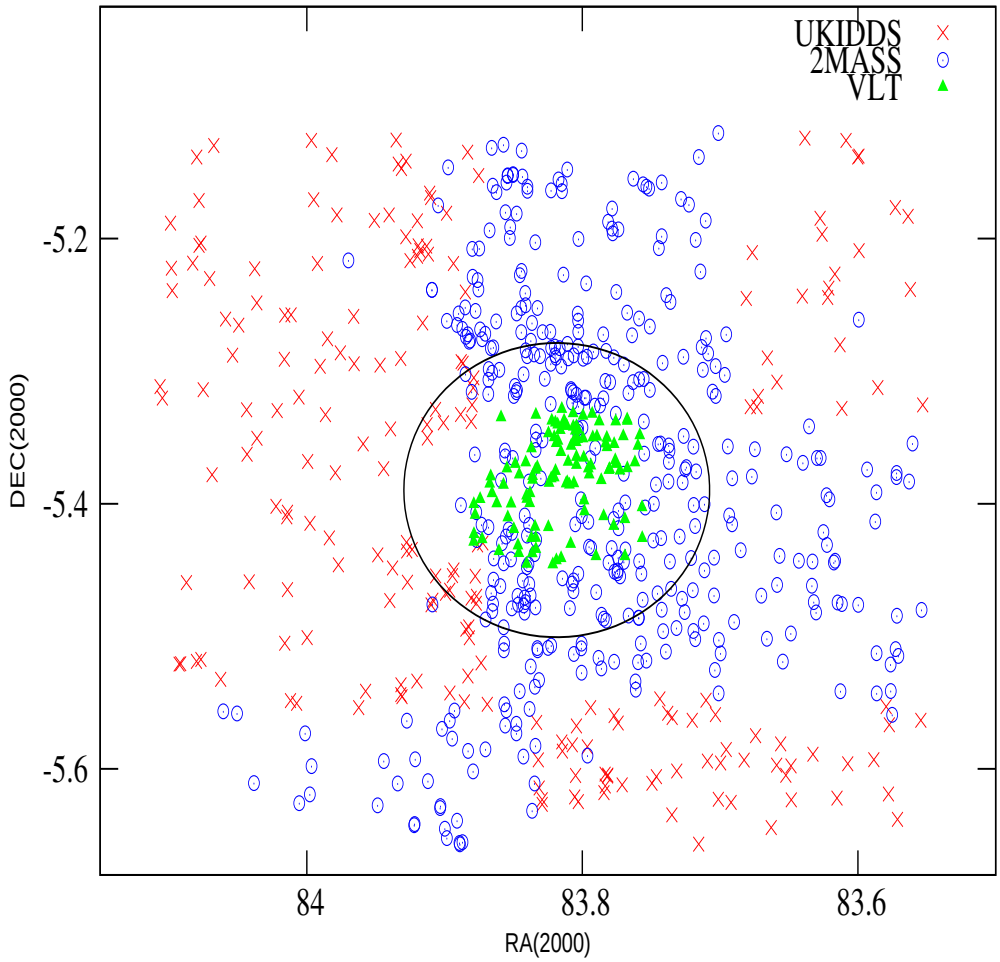

Figure 6.1 Spatial distribution of all 732 periodic variables with near infrared counterparts. Green triangles are 113 objects with VLT JHK measurements, red crosses are the 210 periodic variables with UKIDDS JHK measurements and blue open circles are the 409 periodic variables with 2MASS measurements. The circle centered on Θ^1 Ori with a radius of $\sim 6\farcm7$ represents the cluster radius.

6.2 Near infrared data

6.2.1 J, H, K data

For this study JHK data from three different sources: UKIDDS, VLT (McCaughrean et al. 2009, in prep.), and 2MASS were used. Ideally I would have used only UKIDDS since it provides much deeper and accurate JHK data than 2MASS, but unfortunately only less than 50% of the ONC WFI field (33 x 34 arcmin^2, center approximately at the position of

Θ^1 Ori) is covered in all three bands by the UKIDDS survey. In particular the inner most part of the ONC is not covered (for details see Fig. 6.1. I therefore used for a fraction of the inner ONC region deep VLT-ISAAC data (MacCaughrean et al. 2009 in prep.) covering approximately the central 7 x 7 arcmin^2. For those regions in our WFI field which were neither covered by UKIDDS nor by the VLT data 2MASS data were used. The cross-identification between the periodic variables and these near infrared catalogues was done by looking for positional matches within a $2\farcs0$ search radius. Finally 732 out of the 746 known periodic variables have an infrared counterpart for which data in J, H and K are available.
Many objects have JHK data in more than one of the used catalogues. Due to their higher accuracy higher priority was given to the UKIDDS and VLT data than to the 2MASS data (see Sect. 6.2.2 for details).
The basis of the VLT catalogue are VLT-ISAAC images although the catalogue is supplemented and calibrated with data from a large number of other surveys which have been transformed to the 2MASS system resulting in a homogeneous catalogue. To allow a proper comparison the UKIDDS magnitudes were transformed into the 2MASS system using the relations described in (Hewett et al. 2006). The magnitude distribution of the periodic variables in I and JHK are shown in Fig. 6.2 with separate distributions for the three infrared data sets used in this paper. As summarised in Table 6.1, 210, 113 and 409 JHK measurements were finally used, from UKIDDS, VLT and 2MASS, respectively. Most objects in the innermost part of the ONC for which 2MASS data had to be used are bright objects from H2002, 95% of which have J magnitudes brighter than 14 mag.

6.2.2 Photometric errors and completeness

As will be outlined in Sect. 6.4 IR excess determinations in this study are based on J-H and H-K colours. Therefore the accuracy of these colour determinations are briefly discussed.

There are bassically two sources of errors: photometric errors of the individual J, H and K measurements and errors resulting from variability of the periodic variables in combination with the non-simultaneous data acquisition in the used NIR bands. The second error source is irrelevant for the 2MASS data, which are practically taken simultaneously. This means that only for the UKIDDS and VLT-ISAAC data one has to investigate the relevance of this effect. As outlined in Sect. 5.6 (see there Fig. 5.7) the peak-to-peak (ptp) amplitudes in the I band for periodic variables of 0.075-0.4 $M_\odot$ have a median value of about 0.06 mag and for 85% of them the ptp values were below 0.2 mag. Since the ptp amplitudes are expected to be significantly lower in the NIR than in the I band and since it is rare to observe the periodic variables in minimum in one band and in maximum in the other band

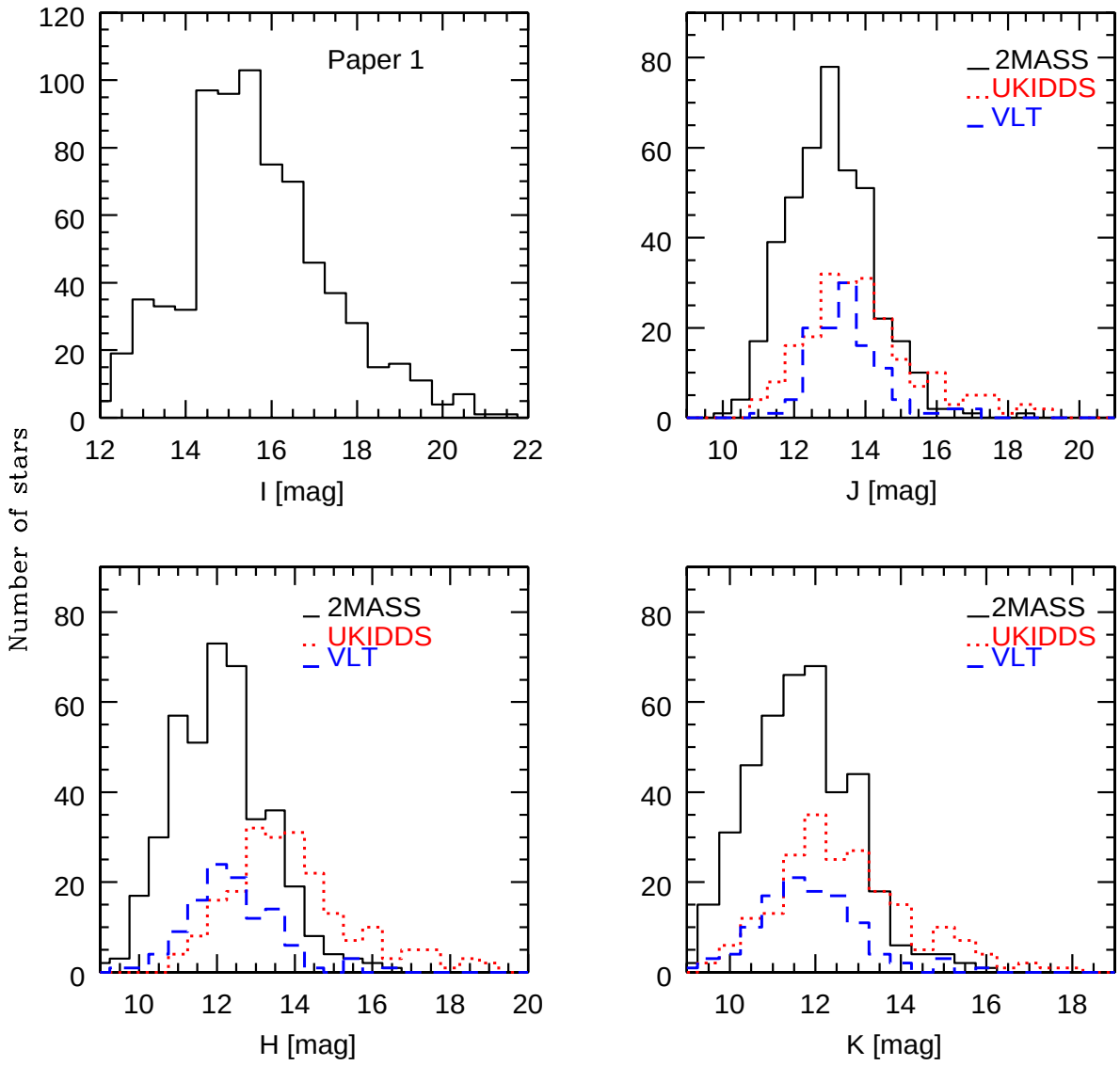

Figure 6.2 Histograms showing the magnitude distribution of the periodic variables in all four bands used in this study. The three different NIR data sets are discriminated.

the J-H and H-K colours calculated from the UKIDDS and VLT data are expected to have median errors due to variability of at most 0.05 mag.

The expected mean photometric errors depend on the survey/catalogue used. UKIDDS data is very deep and accurate with typical photometric errors for a J=14 , H=13.5 and/or K=13 mag object of ≈ 0.002 mag and typical errors of ≈ 0.01 mag for 2 mag fainter objects. As stated above, observations in the three bands are not taken simultaneously. Nevertheless, as already discussed we do not expect variability to cause errors larger than 0.05 mag.

The 2MASS data have photometric errors which are on average one order of magnitude higher than those from UKIDDS for the same magnitude. Most of our 2MASS counterparts are objects located in regions of our WFI field that are not covered by neither UKIDDS nor VLT (see Fig. 6.1).

The VLT catalogue reaches 5σ point source limiting magnitudes at approximately 22, 21, and 20 for J,H, and K, respectively. This is about 2 mag fainter that UKIDDS and therefore typical photometric errors are expected to be ≈ 5 times smaller than those of UKIDDS for the same magnitude. As already mentioned, the VLT data are not taken simultaneously. However, each data point is the average of several observations separated over timescales of hours to years and therefore "variability errors" will be smoothed out to some degree.

From the typical photometric errors uncertainties in the J-H and H-K colours calculation are expected to be about 1% for the VLT data and between 3% and 10% for the 2MASS data for $K = 12$ mag and $K = 14$ mag objects, respectively. Those colours derived from UKIDDS data are affected by both photometric and variability errors. The J-H and H-K colour errors are expected to be clearly smaller than 5% and 7% for a $K = 13$ and 15 mag object, respectively. This means that in principle it is possible to detect excesses from the intrinsic J-H and H-K colours which are larger than about 1-5% for objects with masses $\gtrapprox 0.1\,M_\odot$ and 7-10% for the less massive objects in our sample. A rough estimate of the amount of NIR excess under typical stellar + disk system parameters (e.g. Meyer et al. 1997; Hillenbrand et al. 1998) results in H and K band excesses which are expected to be of about 20%. Although the amount of NIR excess is highly dependent on the different stellar + disk parameters, as will be discuss in Sect. 7.5 the estimated errors in the colours should not affect significantly our disk detectability.

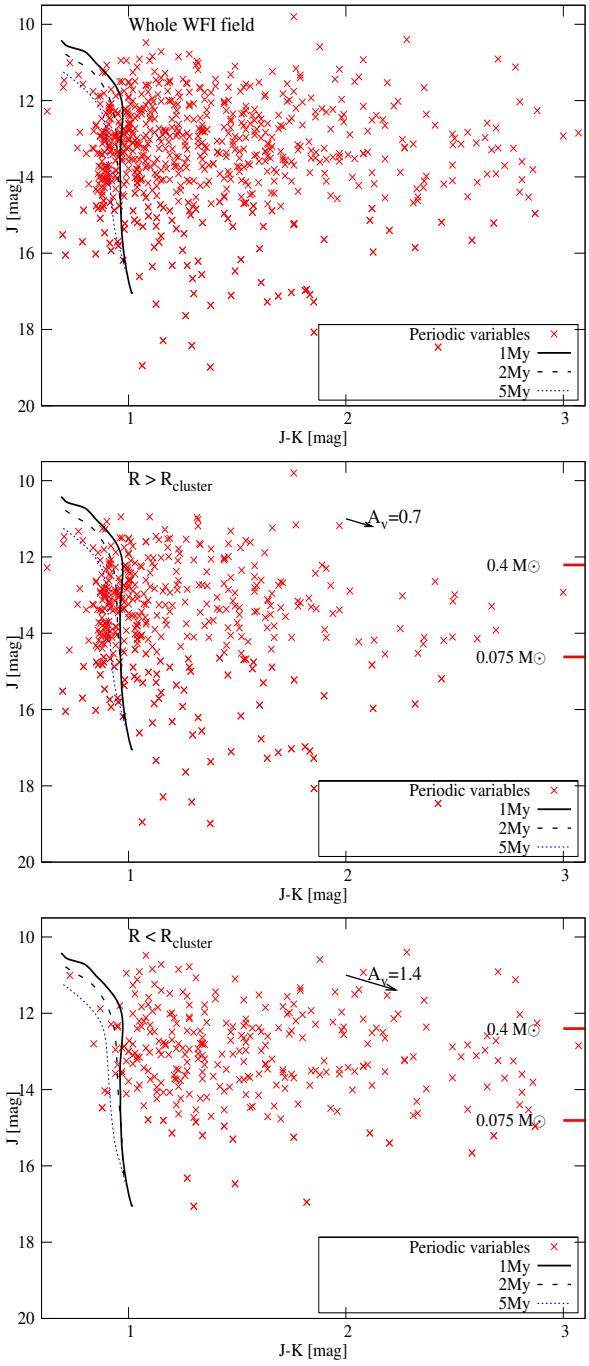

Figure 6.3 J,J-K colour-magnitude diagrams for periodic variables located in the whole WFI field, outside and inside $R_{cluster}$ from top to bottom, respectively. The reddening vector is shown with its corresponding modulus in the two spatial regions. The mass boundaries between the three mass bins are shown with thick red ticks on the right vertical axis and were computed assuming extinction median values and a 1 Myr isochrone from (Baraffe et al. 1998) (see text for details). 1 Myr (solid line), 2 Myrs (dashed line) and 5 Myrs (dotted line) isochrones by (Baraffe et al. 1998) are also shown.

Table 6.1 Number of periodic variables with a near infrared counterpart

	Periodic variables	
	At least one band	All JHK bands
UKIDDS	419	210
VLT	113	113
2MASS	684	409[a]

[a]684 periodic variables in our sample have 2MASS JHK colours, but since UKIDDS and VLT data have higher priority than 2MASS, only for the 409 objects without UKIDDS and VLT data 2MASS colours have been used.

6.3 Mass estimates from J versus J-K colour-magnitude diagram

To estimate masses from evolutionary models it is necessary to know individual extinction values, which requires the knowledge of the spectral type. Since the spectral type of most of our periodic variables is unknown, individual extinction values cannot be determined. For the sake of simplicity a uniform extinction value of A_v=1.4 mag for all stars in the field were assumed for estimating masses based on the I band values. Although spectral types and therefore individual extinction values of our sample remain unknown, it is possible to make use of the near infrared colours to perform additional/independent mass estimates, which are probably more accurate than the estimates based on the I band alone, due to the smaller extinction in the near infrared bands and the smaller variability in this wavelength range.

The J vs J-K colour-magnitude diagram was used for the new mass estimates. In principle H and K bands would be even less affected by extinction than the J band, but in these bands infrared excess due to stellar disks can pretend a much higher stellar flux than is actually present. The median extinction values for inside and outside $R_{cluster}$ were investigated in the literature. First, I computed the median values of the extinction provided by Hillenbrand (1997) in both spatial regions, which resulted in A_v=1.3 mag and A_v=0.7 mag for the inner and outer regions, respectively. Second, I checked extinction maps by Chaisson & Dopita (1977). The latter reveals that there is no strong increase in the extinction towards the inner regions, with median extinction values of about 1 and 1.5 in the inner most parts of the ONC and below 1 in the outer regions. Then, the J vs J-K colour-magnitude diagram was used and average extinctions of $A_v = 1.4$ mag for objects located inside $R_{cluster}$ and 0.7 for objects outside were assumed . Fig. 6.3 shows the resulting colour-magnitude diagrams for the whole ONC field and for outside and inside $R_{cluster}$. The assumed extinction values were

used together with a 1 Myr isochrone by Baraffe et al. (1998) in order to select objects with masses $>0.4\,M_{\odot}$, between 0.075-0.4 $M_{\odot}$, and $<0.075\,M_{\odot}$. In Fig. 6.3 the corresponding J values for the boundaries between the three mass-bins are indicated.

For 99 periodic variables, 81 outside and 18 inside $R_{cluster}$, masses $<0.075\,M_{\odot}$ were derived. This number is smaller than the 124 BDs derived from I-band measurements, which presumably results from lower extinction in J with the possible combination of higher variability in the I band (e.g. due to variable Paschen continuum emission).

It is quite evident from Fig. 6.3 that a large fraction of the periodic variables outside $R_{cluster}$ are concentrated at J-K $\approx$0.8-1.2, while inside $R_{cluster}$ no such concentration is seen at all. In the inner region there is a large spread of objects between J-K $\approx$1-2.5 mag with a somewhat higher concentration at J-K $\approx$1-1.7. The different distributions observed in the J versus J-K diagrams for objects inside and outside $R_{cluster}$ can be due to the following reasons or a combination of them: higher average A_v values and a higher A_v spread inside $R_{cluster}$, smaller age and/or higher disk fraction of objects inside $R_{cluster}$. The determination of individual extinction values will be necessary to find out which effect is most relevant.

6.4 NIR excess determination

6.4.1 Extinction-free indices

The (unknown) extinction of the individual objects and the IR excess from a circumstellar disk can not be easily disentangled in colour-colour diagrams (e.g. Fig. 6.4). Therefore we use an "extinction-free" [1] index Q as defined by Damiani et al. (2006) in order to derive circumstellar NIR excesses. Fig. 6.4 describes in detail the relevant parameters used to defined NIR excess from a circumstellar disk in a J-H versus H-K diagram. As shown in Fig. 6.4 depending on the spectral type and the optical extinction there is a permitted strip of colours on which dwarfs should be located. Since this sample include objects in a broad mass range (i.e. from about 1.5 $M_{\odot}$ to $\sim 20\,M_{jup}$) three limiting values of the index Q_{JHHK} were defined according to the three different mass regimes considered here. The limits were placed at the corresponding Q_{JHHK} values of an M3 ($>0.4\,M_{\odot}$), M6 (0.075 - 0.4 $M_{\odot}$) and M9 ($<0.075\,M_{\odot}$) star (based on colours for main-sequence dwarfs from Bessell & Brett (1988)[2] and extended from M6 to M9 by Kirkpatrick et al. (2000). The extinction-free

[1] To compute those indices an extinction law has to be assumed and therefore they are not completely independent on extinction. In all cases we assumed the Rieke & Lebofsky (1985) extinction law with R=3.1mag.

[2] Transformed into the 2MASS system (Carpenter 2001)

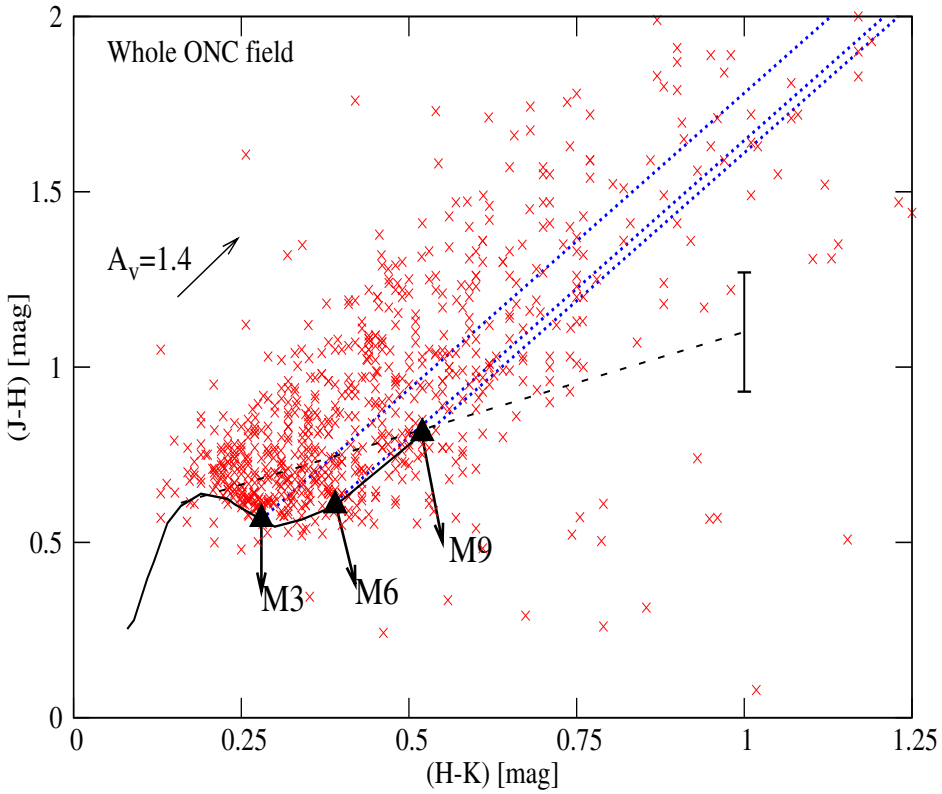

Figure 6.4 J-H versus H-K colour-colour diagram for all the 732 periodic variables in our sample. The three parallel dotted lines define the boundary between objects with and without IR excess (disks) for the three different mass bins considered (see text for details). E.g. an object with a mass $\geq 0.075\,M_{\odot}$ (i.e. spectral type earlier than M6) located to the right of the "M6 line" has an excess in Q_{JHHK}. The full thick line show the intrinsic colours of dwarfs until M6 from Bessell & Brett (1988) and extended to M9 objects according to Kirkpatrick et al. (2000). The classical TTauri locus from Meyer et al. (1997) is shown as dashed lines. The bar shows the typical width of the CTTS locus due to errors in its derivation.

index provides a measurement of the deviation from these permitted strips. I then used the NIR index Q_{JHHK} defined as follows:

$$Q_{JHHK} = (J-H) - (H-K)(E(J-H)/E(H-K)) \tag{6.1}$$

in which the ratio of colour-extinctions E(J-H)/E(H-K) is based on the extinction law of Rieke & Lebofsky (1985).

The Q_{JHHK} index unambiguously indicates the presence of an IR excess which is assumed to result from a circumstellar disk. If I would only take into account objects lying outside the permitted strip for M9 dwarfs I would miss a large fraction of the more massive objects

in our sample since then only objects with very large excesses would be detected. I like to note that the calculated Q_{JHHK} values provide a relatively conservative limit on the presence of an IR excess and therefore the presence of a disk and one should keep in mind that many objects in the permitted strip presumably show such red J-H and/or H-K colours due to a combination of extinction *and* near infrared emission from a circumstellar disk (see Meyer et al. 1997). For many objects located at larger distances from the central Trapezium cluster (where the average extinction is expected to be relatively small) NIR colours redder than those of dwarfs stars are more likely to be due to a circumstellar disk.

According to the Q_{JHHK} index, 162 out of 732 objects with complete JHK data show indications of a circumstellar disk. This number represents $\sim$22% of the objects. These objects are denoted as $Q_{JHHK}+$ in Tables 7.1 and 7.2.

6.4.2 NIR excess from (I-K) colours

In order to have a second independent estimate of the infrared excess an index based on (I-K) colours was used in which I-band fluxes are thought to be dominated by photospheric emission while K-band fluxes can have an additional strong component from the circumstellar disk (Hillenbrand et al. 1998). This approach have the advantage of a longer wavelength base which should in principle result in larger excess than other commonly used indices (e.g. Δ(H-K)). In contrast to the Q_{JHHK} index a NIR excess derived from I-K colours requires the knowledge of individual extinction values and spectral types, both unknown for our objects. In order to get an approximate amount of excess in I-K, average A_v values of 1.4 mag and 0.7 mag for objects inside and outside $R_{\rm cluster}$ were assumed, following the methodology stated above. We are aware that near the ONC center many objects may be more highly extincted than the average, resulting in a sample of objects pretending to have disks which is actually contaminated by highly extincted objects. On the other hand, in the outer regions a certain fraction of objects have lower extinction than the median value considered here and therefore the fraction of objects showing indications of a circumstellar disk may be underestimated in this region. Since I do not have information on individual spectral types, an assumption on the intrinsic photospheric colour $(I-K)_0$ had to be made. Photospheric $(I-K)_0$ colours (Bessell & Brett 1988) of a M3 dwarf for objects in the higher mass bin and of a M6 dwarf for the intermediate and lower mass bin were adopted.

The definition by Hillenbrand et al. (1998) to account for the amount of near infrared

excess from the I-K colour was used:

$$\Delta(I-K) = (I-K)_{measured} - 0.5xA_v - (I-K)_0 \tag{6.2}$$

where $(I-K)_0$ are the intrinsic colours.

A Δ(I-K)=0.3 mag (Hillenbrand et al. 1998) as a lowest value to be regarded as a result from a circumstellar disk. As a result, about 40% of the whole sample show a NIR excess from the Δ(I-K) index.

Due to the various simplifying assumptions made to calculate the Δ(I-K) index it is regarded as a not very accurate disk indicator, and it is used mainly for comparison purposes with the more robust and conservative results given by the Q_{JHHK} index.

Chapter 7

Rotation-disk connection

7.1 Correlation between infrared excess and rotational periods

In the following, I investigate whether there is a correlation between the period distribution of the periodic variables analysed Chapt. 5 and the infrared excess. As described in the introduction such correlation was found for higher mass periodic variables (e.g. H2002; Rebull et al. 2006; Cieza & Baliber 2007). Here, I want to constraint in particular a possible rotation-disk connection in the very low and substellar mass regime, and compare these results with higher mass objects using the same disk indicators.

Fig. 7.1 shows the rotational period as a function of the Q_{JHHK} index for objects in the whole WFI field. Since mass effects may bias any existing correlation between rotation and disks, all following analysis for the periodic variables are performed in the already defined three mass bins. The defined boundary between excess and non-excess objects in each mass regime (i.e. the Q_{JHHK} values of a M3, M6 and M9 dwarf) are shown as vertical solid lines. The horizontal lines in each diagram indicate the median rotational periods for objects with and without IR excess (see Table 7.1). Quite surprisingly, Fig.7.1 only suggests a correlation between NIR excess and rotation for objects with $0.075 < \mathrm{M} < 0.4\,M_{\odot}$. In order to check statistically the significance of this trend, a K-S test was performed, which shows no significant differences in the period distribution of objects with and without disks in the highest and lowest mass bins (85% and 20% probability, respectively), while the period distribution of disks and non-disks holders with masses between 0.075-0.4 $\mathrm{M}_{\odot}$ show a difference at $> 3\,\sigma$ level (i.e. $> 99.9\%$).

Fig. 7.1 also suggests that the amount of NIR excess is mass dependent. Higher mass objects tend to show larger amounts of excess than lower mass objects. This result maybe explained by one or a combination of the following phenomena: lower accretion rates in the

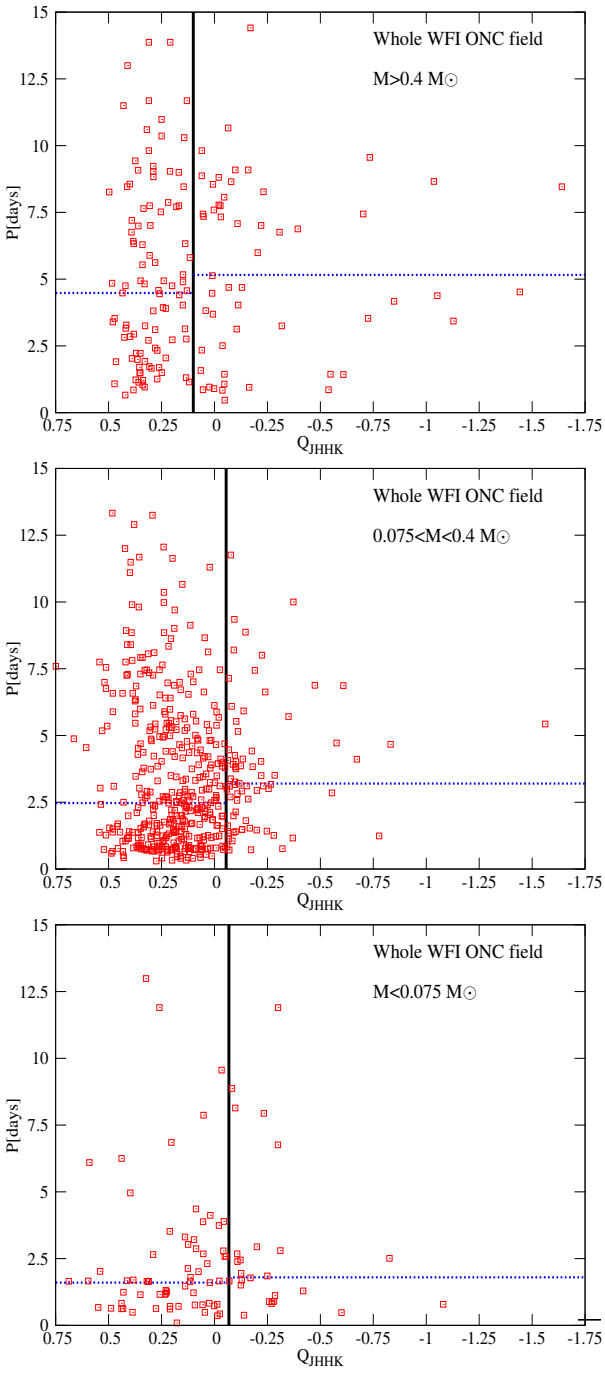

Figure 7.1 Rotational period as a function of the extinction-free index Q_{JHHK} for periodic variables with masses $>0.4\,M_{\odot}$, 0.075-0.4 $M_{\odot}$, and $<0.075\,M_{\odot}$ for the whole WFI field. Vertical solid lines indicate the Q_{JHHK} value of a M3, M6, and M9 dwarf star without IR excess from top to bottom, respectively. Objects located right to this line show an excess in Q_{JHHK}. The median rotational periods for objects with and without an infrared excess are shown as horizontal dotted lines in all three mass regimes.

lower mass objects, larger inner disk holes in lower mass objects, or just a lower contrast between the relatively cool atmosphere and the disk.

The period distribution of the periodic variables with and without disks in the three mass bins are easier to visualise in Fig. 7.2, where the red dotted histograms represent the period distributions of periodic variables with disks and the solid histograms are the correspondent period distributions for objects without disks. Fig. 7.2 shows that the distribution of objects with disks in the higher and intermediate mass bins tend to be flat and in the higher mass bin the distributions of disks and non-disks holders look very similar. In the intermediate mass bin there is a clear difference between objects with and without disks (reflecting the $3\,\sigma$ significance given by the K-S test). In these two mass bins objects with disks rotate on average $\approx$ 1.2-1.3 times slower than objects without disks. In the substellar regime no such difference in the median rotational periods of objects with and without disks were found.

The same trend is found when the Δ(I-K) index is used as diagnosis of a circumstellar disk. High, intermediate, and low mass Δ(I-K)-excess objects in the whole ONC field have a median rotational period of 5.2 days, 4.3 days, and 1.7 days, respectively while those with $\Delta(\text{I-K}) < 0.3$ have a median rotational period of 4.3 days, 2.3 days, and 1.7 days. We found a correlation between rotational periods and Δ(I-K) in the highest mass bin at $> 2\,\sigma$ level of significance (i.e. 97% probability that the two distributions come from different populations) and in the intermediate mass bin at a $>> 3\,\sigma$ level. As was the case for the Q_{JHHK} index no significant differences in the period distribution between objects with and without disks were found for the substellar objects.

In addition to mass effects, age effects may bias the resulting correlations, since older objects tend to rotate faster and also the disk-fraction among an older population should be smaller. Since a possible age spread in the ONC was suggested, with younger objects being located inside R_{cluster}, it would in principle be interesting to do the analysis shown in Fig. 7.2 for inside and outside R_{cluster}. However, due to the reduced number of objects in the two spatial regimes and in particular in the substellar mass regime, no statistically meaningfull analysis could be obtained. We only show the median values of the rotational period distributions in Table 7.1, which may suggest differences between the two spatial regions.

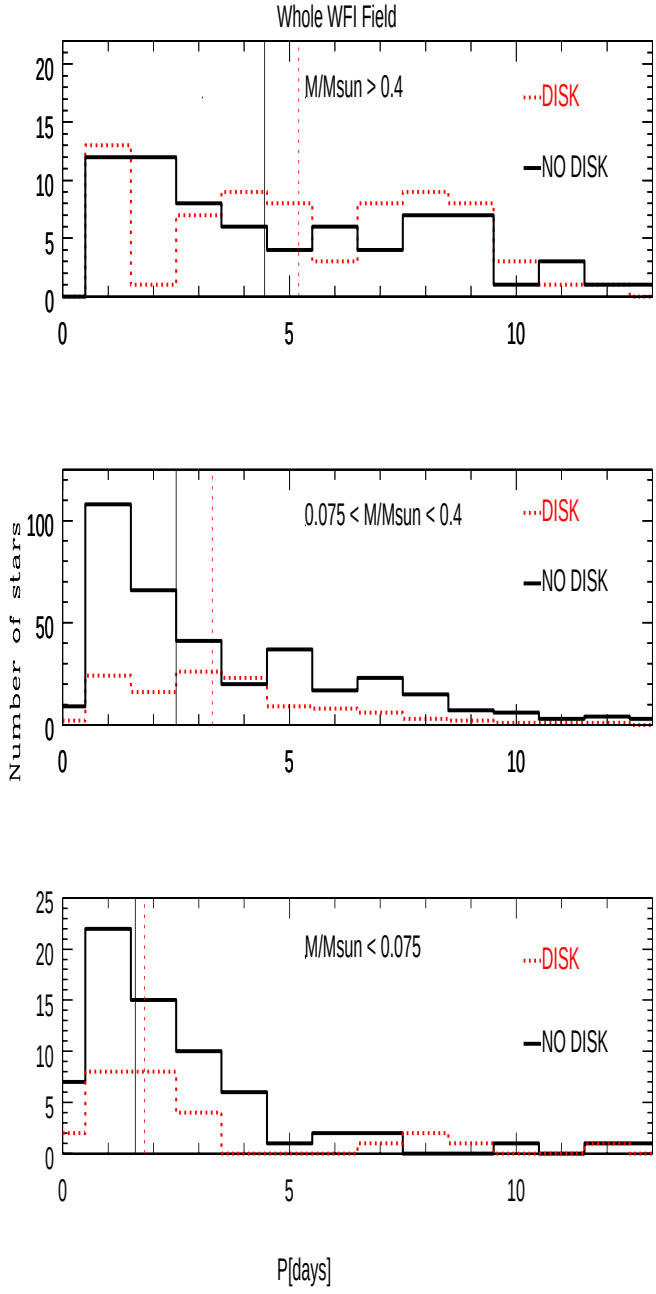

Figure 7.2 Period distribution for objects with and without disks in three different mass bins (see text for details). Solid lines show the period distribution of objects without indications of disks while dotted lines represent the distribution for disk holders. Median rotational periods are shown as vertical lines.

7.2 Correlation between infrared excess and peak-to-peak amplitudes

In the following I analyse if there is a correlation between the peak-to-peak (ptp) amplitude of the periodic variables and NIR excess, i.e. the presence of a circumstellar disk. Since H2002 did not report ptp amplitudes I use here the 487 periodic variables measured in this study. Due to the small number of objects with $M > 0.4\,M_{\odot}$ the ptp-disk correlation was only investigated in the following two mass bins: 0.4-0.075 $M_{\odot}$ and $< 0.075\,M_{\odot}$.

Fig. 7.3 shows the ptp amplitudes as a function of the Q_{JHHK} index for these two mass intervals for the whole WFI field. As for the rotational periods the defined boundary between excess and non-excess objects in each mass regime (i.e. the Q_{JHHK} values of a M6 and M9 dwarf) are shown as vertical solid lines. The horizontal lines in each diagram

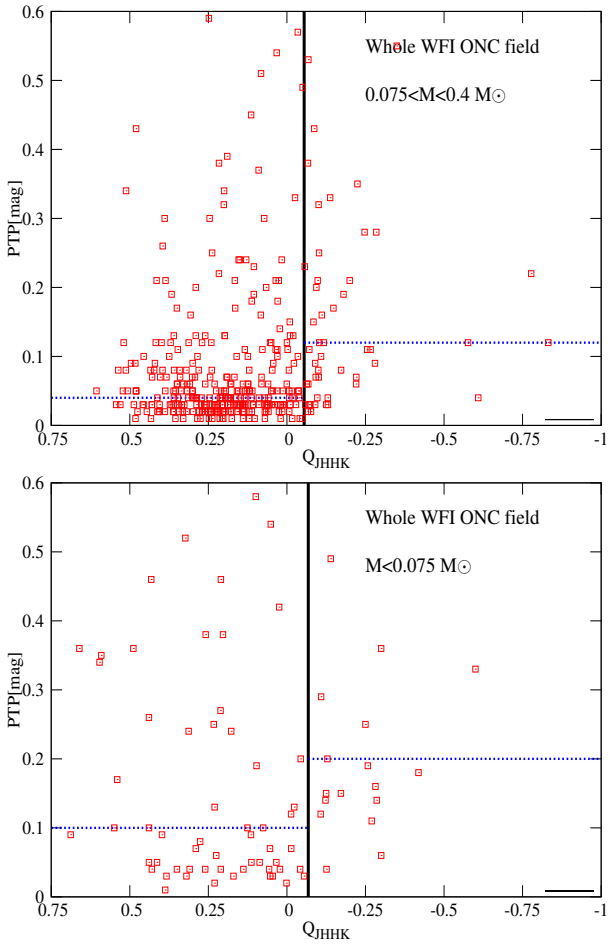

Figure 7.3 The same as Fig. 7.1 but for the peak-to-peak (ptp) amplitude.

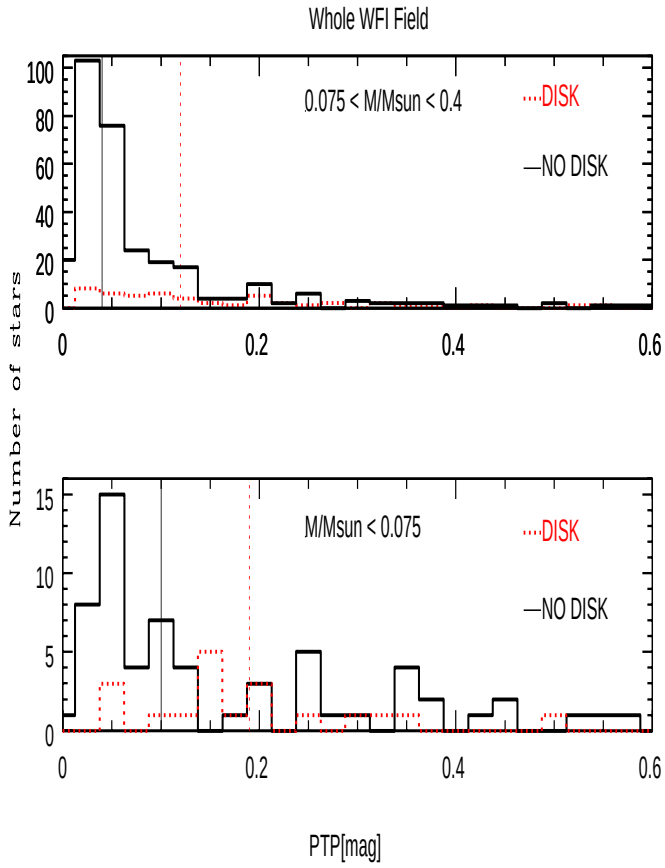

Figure 7.4 Same as Fig. 7.2 but for the ptp amplitude distribution. Only the intermediate and substellar mass bin is shown since we have no information on the ptp amplitudes for most of the highest mass periodic variables which belong to H2002.

indicate the median ptp amplitudes for objects with and without IR excess. A two-sided K-S test gives a $< 10^{-5}$ chance that the distributions of ptp amplitudes of objects showing infrared excess in each mass bin (and also when the whole sample is considered) and the corresponding distributions of non-excess objects belong to the same population. Among the objects with NIR excess there seems to be a trend of increasing ptp amplitude with increasing amount of NIR excess. Fig. 7.4 helps to visualise the ptp distributions of objects with (dotted-histograms) and without (solid-histograms) disks. Median ptp values, which are about a factor 2-3 different between objects with and without disks are also plotted and shown in Table 7.2. The lack of objects with ptp amplitudes below 0.025 mag among the disk-holders is evident from both Fig. 7.3 and Fig. 7.4. We found that $\approx 70\%$ of all periodic variables without disks have ptp amplitudes below 0.1 mag, while the corresponding fraction among the objects with disks is about 30%. These results reveal

a very robust indication of differences in the variability level of objects with and without circumstellar disks, in which objects with disks show on average much larger amplitude variations than objects without disks.

The same trend, median ptp values, and level of significance were found when the Δ(I-K) index was used as diagnosis of a circumstellar disk, providing additional strength for the found correlation.

7.3 Disk frequency

The disk frequency among our sample of 732 periodic variables can be estimated from the number of objects with NIR excess. According to the Q_{JHHK} index 22% of the objects have circumstellar disks. The more optimistic Δ(I-K) index delivered a higher disk frequency of about 40%. It has to be pointed out that this is the fraction among the periodic variables and not among all stars in the ONC, in which case, the disk-frequency is higher, between 50% and 90% (Hillenbrand et al. 1998). These numbers are consistent with the larger fraction of irregular variables (CTTSs) relative to periodic variables (mostly WTTSs) (i.e. the ratio of irregular to periodic variables in our data is ≈ 1.7). Since the disk fraction among the CTTSs will be much larger than among WTTSs, a corresponding increase in the disk fraction of all stars is not surprising. In addition, as will be discussed in latter, the derived fraction may be also smaller than expected since NIR excess is not always an optimum disk indicator.

In order to investigate a possible dependence of the disk fraction on the mass of the periodic variable, the fraction of objects with and without disks were quantified in the three mass bins used before. The disk frequency was found to fall from $\approx 37\%$ to $\approx 16\%$ from the highest to the intermediate mass bin. This trend is also true in the Δ(I-K) index. Hillenbrand et al. (1998) found the same falloff towards masses lower than $\sim 0.4\,M_\odot$ (i.e. lower than $\approx 0.2\,M_\odot$ if the D'Antona & Mazzitelli (1997) models are used). More interesting is the finding that the latter falloff does not seem to extend into the BD regime. Both indices show an increase in the disk fraction among the substellar objects. The Q_{JHHK} index found 1.7 times more brown dwarfs than low mass stars (i.e. in the intermediate mass bin) with disks while the Δ(I-K) index found the same ratio to be 1.3. Table 7.3 summarises the results.

Within each mass regime it was found in addition, that the disk-frequency is always higher inside $R_{cluster}$ than in the presumably older outer region.

Table 7.1 Median values of rotational period for objects with ($Q_{JHHK}+$) and without ($Q_{JHHK}-$) IR excess

	$R<R_{cluster}$						$R>R_{cluster}$						Whole WFI field					
	$Q_{JHHK}+$			$Q_{JHHK}-$			$Q_{JHHK}+$			$Q_{JHHK}-$			$Q_{JHHK}+$			$Q_{JHHK}-$		
Mass bins [a]	A	B	C	A	B	C	A	B	C	A	B	C	A	B	C	A	B	C
N	33	47	10	25	147	8	44	30	17	34	252	64	58	77	27	99	399	72
$< P >$[days]	4.8	3.8	1.7	4.8	3.0	1.4	6.9	4.0	2.0	4.6	2.2	1.7	5.6	3.4	1.8	4.7	2.5	1.6

[a]Mass bins as defined in Chapt. 5: A corresponds to the bright bin containing stars with $M \geq 0.4\ M_{\odot}$, B to the intermediate bin with $0.4< \mathrm{M} < 0.075 M_{\odot}$ and C to the faint bin in which all objects have $M < 0.075\ M_{\odot}$

Table 7.2 Median values of ptp amplitudes for objects with ($Q_{JHHK}+$) and without ($Q_{JHHK}-$) IR excess.

	$R<R_{cluster}$				$R>R_{cluster}$				Whole WFI field			
	$Q_{JHHK}+$		$Q_{JHHK}-$		$Q_{JHHK}+$		$Q_{JHHK}-$		$Q_{JHHK}+$		$Q_{JHHK}-$	
Mass bins [a]	B	C	B	C	B	C	B	C	B	C	B	C
N	42	9	113	7	15	15	199	56	55	24	304	64
$< PTP >$[mag]	0.14	0.3	0.05	0.28	0.11	0.25	0.04	0.09	0.12	0.2	0.04	0.1

[a]Mass bins as defined in Chapt. 5: A is not shown due to the small sample number, B to the intermediate bin with $0.4< \mathrm{M} < 0.075\ M_{\odot}$ and C to the faint bin in which all objects have $M < 0.075\ M_{\odot}$

Table 7.3 Disk fraction found in the whole ONC field by means of the Q_{JHHK} and Δ(I-K) indices.

	Q_{JHHK}			Δ(I-K)		
Mass bins[a]	A	B	C	A	B	C
%	37	16	27	54	34	43

[a]Mass bins as defined in Chapt. 5

7.4 Discussion

According to Fig. 7.1 and Fig. 7.2 there is no correlation between the NIR excess (i.e. the presence of a circumstellar disk) and the rotation rate in the substellar mass regime. The lack of such a correlation is presumably caused by the combination of the following effects:

1. NIR excesses are not good enough accretion disk indicators.

2. There is a certain angular momentum loss in the BD mass regime at the age of ≈ 1 Myr but the following effects strongly weaken any correlation:

   - very large spread in rotational periods.

   - sample has large spread in mass and age.

3. Angular momentum loss rates are indeed significantly lower in BDs than in higher mass objects.

In the following I will discuss in more detail these aspects.

7.4.1 Are NIR excesses good accretion disks indicators?

As outlined in the introduction, theoretical models require ongoing mass accretion from a circumstellar disk onto the star to account for angular momentum losses. To test observationally these theoretical predictions it is necessary to measure mass accretion

rates. Some of the more commonly used mass accretion indicators are: the equivalent width (EW) of Hα or other suitable emission lines (e.g. Ca II triplet), continuum veiling, and UV excess. NIR excesses can only account for the presence of dust in a circumstellar disk which does not imply that gas is being accreted from this disk onto the star. This means it is possible to detect a NIR excess from a pure irradiated circumstellar disk even if the mass accretion rate is zero (see for example Fig. 6 in Hillenbrand et al. (1998)). Nevertheless, impressive correlation between NIR excess and mass accretion indicators such as Hα emission line width has been found (e.g. Sicilia-Aguilar et al. 2005, 2006). This strong correlation allows to use in this study NIR excesses as good accretion disk indicators, since more direct accretion indicators (e.g. Hα emission line fluxes) are not available for our sample.

Near infrared excesses have been widely used as diagnosis of a circumstellar disk, although sometimes ambiguous results have been obtained up to now. As stated by Hillenbrand et al. (1998) NIR excesses miss about 30% of the disks that can be detected at longer wavelengths. Nevertheless, NIR excesses had succeeded in detecting large fraction of very low mass stars and brown dwarfs with circumstellar disks (e.g. Lada et al. 2000; Muench et al. 2001). Muench et al. (2001) found that about 50% of their brown dwarf candidates in the Trapezium region show NIR excesses suggestive of a circumstellar disk. This fraction was similar to the one found by Lada et al. (2000) in very low mass objects, which was increased to about 85% when L-band (3.8 μ) observations were used. A similar increase in the disk fraction among the brown dwarf population studied here is therefore expected.

The amount of NIR excess from a circumstellar disk at a given stellar mass and radius depends on disk properties such as inclination and size of the inner gap. As already stated above it is also closely related with the accretion rate, i.e. an object with a high accretion rate is expected to show a correspondingly larger NIR excess than one with a small mass accretion rate (e.g. Calvet & Hartmann 1992; Meyer et al. 1997; Liu et al. 2003).

The presence or absence of inner gaps is a factor strongly influencing the amount of NIR excess. According to Hillenbrand et al. (1998) for a mass accretion rate of $\dot{M} \approx 10^{-8}\,\mathrm{M}_{\odot}$ and an inner hole of $3\,\mathrm{R}_{\star}$ NIR excess is suppressed in all JHK bands for objects of spectral types later than M2. Even at much higher accretion rates ($\dot{M} \approx 10^{-6}\,\mathrm{M}_{\odot}$) there is no NIR excess at spectral types later than M6 for such an inner gap. Since there is evidence that circumstellar disks around low mass PMS objects have disks which are often truncated in their innermost parts (e.g. Bertout et al. 1988; Kenyon et al. 1996), this effect may play an important role in preventing the detection of circumstellar disks in a certain fraction of the less massive objects in our sample and even for the highest mass objects if they are not strong accretors.

An additional effect in the very low mass and substellar regime is the very low contrast between the star and the disk. Very low mass stars and brown dwarfs are less luminous, the inner regions of their disks are cooler, and therefore excesses in the JHK bands are smaller than in more massive and hotter TTSs. Longer wavelength observations should be more suitable disk indicators since they trace outer regions of the disk. In addition they are less affected by errors due to interstellar extinction and variability. L-band ($3.8\,\mu$) observations were used in several works to detect circumstellar disks in low mass PMS objects (e.g. Lada et al. 2000; Liu et al. 2003). IRAC observations ($3.6\,\mu$m, $5.8\,\mu$m and $8\,\mu$m) have been also used in different clusters and star forming regions (e.g. Rebull et al. 2006; Cieza & Baliber 2007). Rebull et al. (2006) and Cieza & Baliber (2007) analysed the higher mass ($M > 0.4\,M_{\odot}$) periodic variables in the ONC and searched for disk presence and a rotation-disk connection. However, it is very difficult to use Spitzer data in the central region of the ONC, where the nebular background can be extremely high. As stated by Rebull et al. (2006), due to the strong nebular background and source confusion, even relatively bright periodic variables close to the Trapezium are missing IRAC detections. Since our sample of periodic variables is three magnitudes deeper than previous studies and contains many objects in the innermost part of the ONC we had to use NIR data to detect circumstellar disks.

I like to remind the reader that the photometric method used for measuring periodic brightness modulations is more efficient among the WTTSs than for CTTSs, since irregular variations can add a strong noise to the periodic modulation, preventing the detection of the periodic signal. Due to this noise periodic variables are definitely missing among the young highly active CTTSs, which are expected to have larger amounts of NIR excess (i.e. larger mass accretion rates) than the more common WTTSs in our sample of periodic variables. This bias is an additional factor which prevents to find a stronger correlation between rotational periods and the presence of a circumstellar disk.

In summary, NIR excess seems to be a suitable disk indicator in the BD regime, although less favourable than for higher mass stars. Nevertheless, I believe that the used NIR disk indicator is not a major cause for the lack of a disk-rotation correlation in the BD regime.

7.4.2 Correlation destroying/weakening effects

In the following I discuss which effects can weaken or even destroy a correlation between rotation and even an ideal mass accretion indicator.

Large spread of rotational periods

From Fig. 7.1 it is clear that the period distribution of the periodic variables in all three mass bins shows a very large spread. If this spread can weaken or even destroy a correlation between rotation and NIR excess, it should in principle affect all three mass bins. To test whether there is a larger spread in rotational periods in the BD regime than in the intermediate mass regime, in which a highly significant correlation was found, I computed P / P_{median} values and analysed the median and standard deviation (σ) of these new distributions. In addition, a *log-normal* distribution was also fitted and both the geometric medians and the multiplicative σ were compared. The σ values provide the width of the distribution and therefore give information on the spread of the values. The distribution of P / P_{median} in the substellar mass regime was found to be much broader than the corresponding distribution of the intermediate mass objects (i.e. the σ values are a factor ≈ 1.6 larger). In addition, even when the distribution is broader, the number of outliers[1] is much larger in the BD mass regime than in the intermediate mass regime, with 14% and 3% of outliers in each region, respectively.

The observed spread may be a consequence of an initial spread in the period distribution at the birth line, which was suggested by several authors (e.g. Tinker et al. 2002; Landin et al. 2006). Additional effects such as a large range of mass accretion rates and disk life times may contribute to the observed spread in rotational periods as well.

The larger spread in rotational periods among the BDs in our sample may be one of the major reasons for a lack of rotation-disk correlation in the BD regime.

Mass and age effects

The correlation between rotational period and NIR excess can be biased by the strong dependence of rotation with mass. If a sample of periodic variables with a broad mass range is used in order to find a correlation with NIR excess the following effect may mimic a rotation-disk connection: higher mass objects rotate on average slower and show on average larger NIR excesses than lower mass objects, the latter due to the higher contrast between the photosphere and the inner disk emission (e.g. Littlefair et al. 2005). The critical point appears at masses of about $0.4\,M_{\odot}$, according to models by Baraffe et al. (1998). Objects more massive than $0.4\,M_{\odot}$ show a bimodal distribution of rotational periods while lower mass objects do not (H2002; Rodriguez-Ledesma et al. 2009a).

[1]Number of objects with values outside the following range: Q_1-1.5x(Q_3-Q_1) and Q_3+1.5x(Q_3-Q_1), where Q_1 and Q_3 are the first and third quartiles. For our sample, all outliers have values larger than the upper limit, i.e. longer periods.

An age spread may also mimic an intrinsic correlation between rotational periods and disks. In this scenario, if the sample of periodic variables used to search for a rotational-disk correlation is not coeval, the disk frequency is expected to be lower among the older objects, which in turn rotate faster. Therefore, it would be possible to observe a correlation between rotation and NIR excess, which would in reality reflect an age correlation.

A combination of mass and age effects were probably the responsables of the lack of success in finding a rotational-disk correlation in many previous works (e.g. Rebull 2001; Makidon et al. 2004; Littlefair et al. 2005). The mass effect was taken into account in the work of Cieza & Baliber (2007) in which they used rotational period from the literature and IRAC excesses as disk indicators. When analysing only the higher mass objects ($M > 0.4\,M_{\odot}$) in the ONC they found a clear evidence of angular momentum regulation by circumstellar disks. Since they restrict their sample to only objects with known spectral types, no analysis was done for the lower mass objects. Moreover, they also found that when including the rotational data available for the ONC flanking fields (Rebull 2001), the correlation disappears, and attribute this effect to the age difference between the two regions.

The intermediate mass regime has a mass range of about $0.4/0.075 \approx 5$. However, the mass range in the BD regime is most likely much smaller since we have only very few objects below $0.025\,M_{\odot}$, i.e. the mass range is there about 3 (0.075/0.025).

Due to the smaller mass range in the BD regime it cannot be excluded that this effect contributes to the lack of a correlation between disks and rotation rates, but it is regarded as of minor importance.

7.4.3 Are angular momentum loss rates smaller in BDs than in higher mass objects?

Observations of young brown dwarfs reveal that a large fraction of the young substellar population has circumstellar disks (e.g. Muench et al. 2001). Evidence of accretion features have also been observed in substellar objects (e.g. Mohanty & Basri 2003) suggesting that magnetic fields can be as strong as in the very low mass stellar regime. In the following we discuss possible scenarios which can account for smaller angular momentum loss rates in the substellar mass regime compared to higher mass objects.

Low ionisation

All hydro-magnetically driven angular momentum loss mechanisms require a sufficiently high ionisation of the disk and/or wind involved in the angular momentum transport from the star and/or disk to this circumstellar matter. Without a sufficient ionisation the magnetic field would only poorly couple to the circumstellar matter and therefore angular momentum transport would be correspondingly smaller. Since the X ray and UV fluxes of BDs relative to their bolometric fluxes (i.e. L_x/L_{Bol}) are certainly much lower than for higher mass stars it should be theoretically investigated in detail whether the above ionisation considerations could strongly reduce the relative braking (i.e. $\dot{J}/J$) of BDs compared to higher mass objects.

Disk-locking times: τ_{lock} and τ_D

If one assumes that the disk locking scenario explains the rotational data one can consider two extreme cases: case 1; all objects are locked to their disks at their birth, and case 2; they are not locked to their disks and it takes a certain time τ_D until they are locked. In case 1 the amount of angular momentum loss strongly depends on how long this locking is effective (i.e. τ_{lock}).

In the first case, BDs may be efficiently braked for a shorter time than higher mass objects after which they spin up conserving angular momentum or losing angular momentum in a moderate way. This may be caused by lower mass accretion rates in BDs than in low mass stars ($\dot{M} \propto M^2$, Rebull (2001)), with a correspondingly weaker coupling and reduced braking rates, or due to shorter disks life times, although it is difficult to explain why objects showing indications of circumstellar disks are fast rotators.

Concerning case 2, Hartmann (2002) argued that disk-locking is not instantaneous but a certain time τ_D is needed before disk-locking is achieved. Equ. 7.1 (Eq. 8 in Hartmann (2002)) shows that this time is proportional to the mass, the angular velocity, and to the inverse of the accretion rate as follows:

$$\tau_D \gtrapprox 4.5x10^6\, yr\, f\, \frac{M_{0.5}}{\dot{M}^{-8}} \tag{7.1}$$

in which $M_{0.5}$ and $\dot{M}^{-8}$ are the mass and mass accretion rates in units of $0.5\,M_\odot$ and $10^{-8}\,M_\odot yr^{-1}$, respectively and f is the angular velocity in units of the breakup velocity.

Typical values of these quantities for a $0.5\,M_\odot$ star are $\dot{M}$=$10^{-8}\,M_\odot yr^{-1}$ and f = 0.1 (see Herbst et al. 2001) which result in a $\tau_D \approx 0.5$ Myr. A BD is expected to have a smaller $\dot{M}$

(since $\propto M^2$) and a larger f≈ 0.7. If $\dot{M} = 5\text{x}10^{-10}\,M_{\odot}yr^{-1}$ about 10 Myr are needed for a BD to become disk-locked. Since most YSOs have disk life times much smaller than 10 Myr this means that probably all BDs will never get disk locked according to the Hartmann (2002) scenario. If this scenario is correct, it would imply that the average angular momentum loss rate $\dot{J}_{average}$ is much smaller than $\dot{J}_{lock}$, i.e. the one achievable during disk locking.

7.4.4 General discussion

Several effects acting alone or more likely in combination presumably lead to the observed trends particularly in the substellar regime since all these effects are more severe at small masses and small mass accretion rates. It seems that a "moderate" magnetically driving angular momentum loss can more successfully explain the observed rotational periods at the age of the ONC. Moreover, it is likely that the initial rotational conditions are dependent on the mass and on the mass accretion rate. It is still unclear whether objects at the birth line are more likely to be locked to a constant period, or if at this initial stages objects usually lose angular momentum at a moderate rate until effective locking is achieve. In the former scenario, the initial constant period is probably mass dependent, and at a certain time (depending on mass, mass accretion rate, magnetic field strength and/or geometry) objects are released from this effective coupling, lossing angular momentum at a smaller rate or even keeping it constant in some cases. The latter scenario considers an initial moderate angular momentum loss, which last a certain time τ_D until effective breaking is achieve. This achievement time τ_D is highly dependent on mass, namely substellar objects would need larger times to get effectively locked. Even τ_D is probably longer than the disk-life times for most substellar objects and therefore effective braking may probably never occurred for many objects at these small masses.

Further studies, considering larger samples of substellar objects at slightly different ages are needed in order to assess which scenario is more suitable to fit the observations or whether the observed trends are biased due to the method used in both deriving the rotational periods and the presence of disks.

Chapter 8

Summary and outlook

In this chapter I review the work presented in this thesis. I will summarise first, the results obtained in the rotational studies of very low mass stars and brown dwarfs in the ONC and second, the results presented in Chapt. 7 on the search for a rotation-disk connection particularly in the brown dwarf regime. The reader will find the answers to the questions stated in Chapt. 1 in the following summary. Finally, I will introduce some future prospect on the scientific topic of this thesis.

8.1 Rotational periods of low mass stars and BDs.

About 3000 objects in the ONC have been monitored in the I-band over 19 nights. Relative photometry resulted in 2908 objects with good photometric precision ranging from 13 to 21 mag, which means three magnitudes deeper than previous studies in the ONC (H2002).

1. 487 periodic variables in the ONC were found, 377 of which are new detections relative to H2002 and 124 of which are BD candidates on the basis of the I magnitudes and comparison with theoretical models. The combined data-set resulted in 746 periodic variables, 139 of which are BD candidates.

2. 808 irregular variables have been detected (i.e. variable objects for which it was not possible to assign a rotational period) with a 99.9% probability of being variables according to the χ^2 test.

3. The spatial distribution of the variable objects was analysed. Both irregular variables and periodic variables were found to be highly clumped in the inner region of the ONC, however, their locations are not the same. A K-S test resulted in a 99% probability that the distribution of declinations for irregular and periodic variables are different and 43% for the right ascension values. Irregular variables are most likely found south-west of the central Trapezium stars, while most periodic variables are clumped in a region north-west of the same stars.

4. The analysis of the rotational period distributions for different magnitude bins (translated into estimated mass bins), confirms the already known trend to have fast rotators towards lower masses. This trend extends well into the substellar mass regime and was found for the whole ONC field as well as for the regions inside and outside $R_{cluster}$.

5. The analysis of the rotational period distributions for different magnitude bins for objects located inside and outside the $R_{cluster}$, suggests differences between the two regions, where objects inside $R_{cluster}$ tend to rotate on average slower than the outer ones. This trend seems to be true for all mass bins but at different significance levels. It can be interpreted as an age difference between the inner and outer population.

6. In comparing the ONC with the ~ 2 times older cluster NGC 2264 the Lamm et al. (2004) data was used but models of Baraffe et al. (1998) were adopted for mass estimates instead of D'Antona & Mazzitelli (1997). This results in a larger number of low mass objects and even substellar objects than published by Lamm et al. 2004. The period distributions of NGC 2264 were compared, for all mass bins, with the

period distributions of objects located inside and outside $R_{cluster}$ in the ONC. A factor ~ 1.5 faster rotators in NGC 2264 relative to objects located inside $R_{cluster}$ in the ONC was found for every considered mass bin. However, the median values of the period distributions for objects outside $R_{cluster}$ in the ONC are almost identical to the ones in NGC 2264 for all three mass regimes. This finding favours the hypothesis of an age spread in the ONC, in which the older outer population is presumably as old as NGC 2264 according to the median rotational periods found.

7. In order to avoid observational biases due to the higher photometric errors measured in the central part of the ONC due to the strong nebular background, the ptp amplitude distribution of a reduced sample of periodic variables (331 objects) was analysed. Using the whole sample of periodic variables would have biased our results towards smaller ptp variations in the outer region (i.e. outside $R_{cluster}$) with a stronger effect for the faintest objects. No statistically significant differences were found between inside and outside $R_{cluster}$.

8. The period dependence on variability level was investigated in both the ONC and NGC 2264. Low level variables (i.e. ptp amplitudes below 0.1 mag) were found to rotate on average faster than the high level variables in both clusters. This is true for the whole magnitude range studied although in the substellar regime there is a tendency to have mainly fast rotators. Interestingly, very low level variables in the ONC are fast rotators, with periods of about 2 days, quasi-independently of their mass. The higher variable objects in the ONC, as well as the two groups in NGC 2264, show a continuous decrease in the rotational periods towards the lowest masses.

   This intriguing correlation found in the two clusters probably indicates that different magnetic field topologies act on these objects, resulting in large and small amplitude variations for slow and fast rotators, respectively. Complex magnetic field configurations hardly allow magnetic coupling with the circumstellar disk. In addition, they pressumably produce a more uniform surface spot coverage with smaller spot groups resulting in small ptp amplitudes for the fast rotators, while extended dipolar fields allow strong disk coupling and therefore much stronger magnetic braking. The latter will produce big spot groups near the magnetic poles, resulting in large ptp amplitudes for the slow rotators.

9. The best explanation found for the results mentioned in 5 and 6 is an age spread in the ONC region, in which objects located inside $R_{cluster}$ are on average younger than objects outside. This can explain why the younger inner population rotates slower than the somewhat older objects in the outer regions since it has not had enough time to spin up. Moreover, since the comparison with NGC 2264 reveals that the median values of the rotational periods in the outer regions of the ONC are almost

identical to the ones in NGC 2264 for the whole magnitude range, the age of this older population surrounding the ONC can be estimated to be roughly twice the age of the inner region close to the Trapezium cluster.

Age spreads in star forming regions have been discussed in detail by several authors (Huff & Stahler 2006, 2007; Mayne & Naylor 2008). Whether star formation acts in a rapid single episode or slowly, with different star formation rate or in several episodes is still under debate, but we cannot exclude the latter scenario as a possible interpretation of our observed age spread. Particularly in the ONC, an age spread was suggested by several authors (e.g. Hillenbrand et al. 1998; Hillenbrand & Hartmann 1998; Herbst et al. 2000) to account for the correlations found for low mass stars (above $0.4\,\mathrm{M}_{\odot}$) between rotational periods and projected radius and also due to the higher fraction of objects with disks (by means of IR-excess) found in the central region.

8.2 Rotation-disk connection

NIR excess correlations with rotation and variability level of a large sample of VLM stars and BDs in the ONC were investigated. The main results concerning rotation-disk connection are summarised in the following:

1. 732 periodic variables in the ONC from this study and H2002 were analysed with JHK measurements from three different survey/catalogues: UKIDDS, VLT and 2MASS.

2. Masses were estimated from the J versus J-K colour-magnitude diagram and 99 objects with masses in the substellar mass regime were found.

3. The amount of NIR excess from a circumstellar disk were calculated by means of the extinction-free index Q_{JHHK} and, for comparison purposes, also Δ(I-K) indices were computed.

4. All the analysis was perfomed for three mass bins, namely objects with masses $> 0.4\,M_{\odot}$, between 0.4-0.075 $M_{\odot}$, and $< 0.075\,M_{\odot}$. The results in Chapt. 7 show the existence of a significantly rotation-disk correlation for the intermediate mass objects considered in this study, in which objects with NIR excess tend to rotate slower than objects without NIR excess. In the highest mass bin there is a correlation at a $2\,\sigma$ level only if the Δ(I-K) index is used, while from the Q_{JHHK} index the probability that the period distribution of objects with and without disks are different is 85%. Interestingly no correlation was found in the substellar regime.

5. The analysis of the ptp amplitudes and their correlation with NIR excess reveals a robust indication of differences in the variability level for objects with and without circumstellar disks.

6. The disk frequency was estimated between 22% and 40% among the periodic variables in the ONC. This fraction is smaller than the estimated for all objects in the ONC (Hillenbrand et al. 1998), which is as expected since: (*a*) the photometric method used to derived rotational periods is more effective among the WTTs than for the CTTSs, with the latter group having a much higher disk frequency, (*b*) the Q_{JHHK} index is a rather conservative disk indicator which may miss several objects with circumstellar disks.

7. I conclude that disks seem to play a role in the regulation of angular momentum in young very low mass objects, although this effect was not observed in the BD regime. Angular momentum losses seem to be much smaller in the substellar mass regime and consequently no efficient braking seems to ocurred for most objects at these small masses. Several possible reasons for the latter result have been discussed.

8.3 Future prospects

In order to exploit the great scientific potential of this sample, proper mass determinations should be carried on, which require the knowledge of individual spectral types and A_v values. In addition, direct mass accretion indicators such as Hα line widths or other lines in emmision (e.g. Ca II triplet) would highly improve the selection of objects with accretion disks, to better constrain a possible rotation-disk connection. Spectroscopic measurements for this interesting sample of low mass variables are therefore necessary. With this purpose I carried out follow-up multiobject spectroscopy with VIMOS-VLT and HYDRA-CTIO during winter 2008-2009. The follow-up was completed for about 500 variables, with $I \gtrsim 15.5$ mag, most of them periodic variables but also some irregular variables in the original sample analysed in this thesis.

In addition to the spectral type and mass determinations, the analysis of these spectroscopic observations will provide important information on the mass accretion activity of the sample, which, as discussed in this thesis, may strongly influences the rotational braking by magnetically driven outflows resulting from the accretion processes. CTTS spectra not only show $H\alpha$ and other Balmer lines in emission, but they show additional signs of accretion activity, like the rise in metallic emission lines (e.g. CaII-triplet), as well as a pronounced veiling of the absorption line spectrum. Although $H\alpha$ is one of the most

sensitive indicators of accretion, it is also the brightest nebular emission line, and therefore using it as an activity indicator in the central region of our ONC field (with a strong $H\alpha$ nebular background) can not be completely reliable. Mohanty & Basri (2003) show that the CaII triplet emission lines yield a robust estimate of the accretion rate, and therefore these lines can be used as activity indicator in objects surrounded by strong nebular background.

Another insteresting study could be to investigate in detail the X-ray emission data (from CHANDRA) of this unique sample of variables to study the relation between the X-ray activity, rotation and disks. The dependence of the X-ray emission on stellar mass and rotation rate is still a matter of debate, in particular in the fully convective regime (see Reiners & Basri 2007, and references therein). $H\alpha$ and X-ray measurements among M stars show a rough correspondence and $H\alpha$ activity seems to scales with magnetic flux (Reiners & Basri 2007). It is of particular interest, when analysing the X-ray data, to investigate in more detail the previously found rotation-ptp activity correlation (Chapt.5.7) which suggests that different magnetic field topologies are possible present on slow and fast rotators Rodriguez-Ledesma et al. (2009a).

Finally, regarding rotation evolution, should be necessary to study the very low mass and substellar population in slightly older regions. If angular momentum loss occurs in the substellar mass regime it would be interesting to asses which of the two cases presented in Sect. 7.4.3 is the most appropiate to explained the data. Another possibility would be to measure younger objects instead of older ones, to directly observe the "initial" rotational conditions. This would require the used of $v sin i$ measurements since these very young objects (class I objects) are highly embedded and they are expected to be highly variable due to their large mass accretion rates, which would make difficult any period detection by rotational modulation.

Appendix A: Magnitude transformations

A.1.: UKIDDS magnitudes into the 2MASS system.

In order to have an homogeneous data set in J, H, and K, we transform UKIDDS magnitudes into the 2MASS system using the relations described in Hewett et al. (2006).

$$J_{2MASS} = J_{UK} - 0.01 + 0.073(J-H)_{UK}$$
$$H_{2MASS} = H_{UK} - 0.069(H-K)_{UK}$$
$$K_{2MASS} = K_{UK} + 0.073(H-K)_{UK}$$

A.2.: CIT magnitudes into the 2MASS system.

Model by Baraffe et al. (1998) and the CTT locus from Meyer et al. (1997) are given in the CIT system. In order to use them in this thesis both were converted into the 2MASS system using transformation equations given by Carpenter (2001).

$$(J-H)_{2MASS} = (1.076 \pm 0.01)(J-H)_{CIT} + (-0.043 \pm 0.006)$$

$$(H-K)_{2MASS} = (1.026 \pm 0.02)(H-K)_{CIT} + (0.028 \pm 0.005)$$
$$K_{2MASS} = K_{CIT} + (0.000 \pm 0.005)(J-K)_{CIT} + (-0.024 \pm 0.003)$$

A.3.: Bessel and Brett magnitudes into the 2MASS system.

Intrinsic colours of dwarfs until M6 from Bessell & Brett (1988) and extended to M9 objects according to Kirkpatrick et al. (2000) have been used. While the latter are given in the 2MASS system, the Bessel and Brett colours had to be transformed into the 2MASS system using transformation relations by Carpenter (2001).

$$(J-H)_{2MASS} = (0.972 \pm 0.006)(J-H)_{BB} + (-0.011 \pm 0.005)$$
$$(H-K)_{2MASS} = (0.996 \pm 0.019)(H-K)_{BB} + (0.028 \pm 0.005)$$
$$K_{2MASS} = K_{BB} + (0.000 \pm 0.005)(J-K)_{BB} + (-0.044 \pm 0.003)$$

Acknowledgements

I would like to thank all people who, in different ways, helped me during my thesis work. First, I want to thank my supervisor, Reinhard Mundt, for giving me the opportunity to do this PhD thesis, for all the time spent on teaching me, for his suggestions, comments and always fruitful discussions. I would also like to thank him for his help and advice in non-scientific matters.

It is pleasure for me to thank Jochen Eislöffel for his great help during all stages of this work.

I want to thank Mark McCaughrean for providing me the VLT-ISAAC NIR data used for 113 objects in this thesis.

I want to acknowledge the members of my IMPRS committee, Immo Appenzeller, Jochen Eislöffel, and Reinhard Mundt, for all interesting suggestions arising in each committee meeting, which always helped in improving this work.

I acknowledge my Master supervisor Olga Pintado, because she gave me the possibility to get into the world of Astronomy when I was very young. I want to thank her for the interest showed on what I was/am doing, for her teaching and for having always a good piece of advice.

I want to thank some other people who somehow contributed on this work: Jose Luis Borelli for his enormous help on software and computer matters. Steve Boudreault for his always usefull suggestions, for his detailed an instructive emails, and for being my on-

call observational support. Alejo Martinez-Sansigre, for his usefull comments on postdoc-applications writting. Cassie Fallscheer for kindly reading parts of my thesis and for giving me her “native English” comments. My officemates, in particular Frithjof for all the shared moments during the last 3 years. All my friends and colleagues for their support over all these years, for the scientific and non-scientific discussions, and for the good time spent together.

Last but not least, I want to thank my whole family for their support which was strong enough to cross the ocean, and of course I want to particularly thank Jose for his unconditional support and love, and Camila for being the light of my eyes.

Bibliography

Ambartsumian, V. 1947, Erevan, U.S.S.R.

Appenzeller, I., & Mundt, R. 1989, A&A Rev., 1, 291

Attridge, J. M., & Herbst, W. 1992, ApJ, 398, L61

Bailer-Jones, C. A. L., & Mundt, R. 1999, A&A, 348, 800

—. 2001, A&A, 367, 218

Baraffe, I., Chabrier, G., Allard, F., & Hauschildt, P. H. 1998, A&A, 337, 403

Bautista, M. A., Pogge, R. W., & Depoy, D. L. 1995, ApJ, 452, 685

Bertout, C. 1989, ARA&A, 27, 351

Bertout, C., Basri, G., & Bouvier, J. 1988, ApJ, 330, 350

Bessell, M. S., & Brett, J. M. 1988, PASP, 100, 1134

Bodenheimer, P. 1995, ARA&A, 33, 199

Bouvier, J., & Bertout, C. 1989, A&A, 211, 99

Bouvier, J., Cabrit, S., Fernandez, M., Martin, E. L., & Matthews, J. M. 1993, A&A, 272, 176

Burrows, A., Hubbard, W. B., Lunine, J. I., & Liebert, J. 2001, Reviews of Modern Physics, 73, 719

Calvet, N., & Hartmann, L. 1992, ApJ, 386, 239

Camenzind, M. 1990, in Reviews in Modern Astronomy, Vol. 3, Reviews in Modern Astronomy, ed. G. Klare, 234–265

Carpenter, J. M., Hillenbrand, L. A., & Skrutskie, M. F. 2001, AJ, 121, 3160

Carpenter, J. M. 2001, AJ, 121, 2851

Castets, A., Duvert, G., Dutrey, A., Bally, J., Langer, W. D., & Wilson, R. W. 1990, A&A, 234, 469

Chabrier, G., Baraffe, I., Allard, F., & Hauschildt, P. 2000, ApJ, 542, 464

Chaisson, E. J., & Dopita, M. A. 1977, A&A, 56, 385

Choi, P. I., & Herbst, W. 1996, AJ, 111, 283

Cieza, L., & Baliber, N. 2007, ApJ, 671, 605

Damiani, F., Prisinzano, L., Micela, G., & Sciortino, S. 2006, A&A, 459, 477

D'Antona, F., & Mazzitelli, I. 1997, Memorie della Societa Astronomica Italiana, 68, 807

Edwards, S., Strom, S. E., Hartigan, P., Strom, K. M., Hillenbrand, L. A., Herbst, W., Attridge, J., Merrill, K. M., Probst, R., & Gatley, I. 1993, AJ, 106, 372

Eyer, L., & Bartholdi, P. 1999, A&AS, 135, 1

Fallscheer, C., & Herbst, W. 2006, ApJ, 647, L155

Flaccomio, E., Damiani, F., Micela, G., Sciortino, S., Harnden, Jr., F. R., Murray, S. S., & Wolk, S. J. 2003, ApJ, 582, 398

Genzel, R., & Stutzki, J. 1989, ARA&A, 27, 41

Getman, K. V., Feigelson, E. D., Broos, P. S., Micela, G., & Garmire, G. P. 2008a, ApJ, 688, 418

Getman, K. V., Feigelson, E. D., Micela, G., Jardine, M. M., Gregory, S. G., & Garmire, G. P. 2008b, ApJ, 688, 437

Ghosh, P., & Lamb, F. K. 1979, ApJ, 232, 259

Goudis, C., ed. 1982, Astrophysics and Space Science Library, Vol. 90, The Orion complex: A case study of interstellar matter

Grankin, K. N., Bouvier, J., Herbst, W., & Melnikov, S. Y. 2008, A&A, 479, 827

Hartmann, L. 2002, ApJ, 566, L29

Herbst, W., Bailer-Jones, C. A. L., & Mundt, R. 2001, ApJ, 554, L197

Herbst, W., Bailer-Jones, C. A. L., Mundt, R., Meisenheimer, K., & Wackermann, R. 2002, A&A, 396, 513

Herbst, W., Eislöffel, J., Mundt, R., & Scholz, A. 2007, in Protostars and Planets V, ed. B. Reipurth, D. Jewitt, & K. Keil, 297–311

Herbst, W., Herbst, D. K., Grossman, E. J., & Weinstein, D. 1994, AJ, 108, 1906

Herbst, W., Rhode, K. L., Hillenbrand, L. A., & Curran, G. 2000, AJ, 119, 261

Hewett, P. C., Warren, S. J., Leggett, S. K., & Hodgkin, S. T. 2006, MNRAS, 367, 454

Hillenbrand, L. A. 1997, AJ, 113, 1733

Hillenbrand, L. A., & Carpenter, J. M. 2000, ApJ, 540, 236

Hillenbrand, L. A., & Hartmann, L. W. 1998, ApJ, 492, 540

Hillenbrand, L. A., Strom, S. E., Calvet, N., Merrill, K. M., Gatley, I., Makidon, R. B., Meyer, M. R., & Skrutskie, M. F. 1998, AJ, 116, 1816

Hoffmeister, C. 1965, Veroeffentlichungen der Sternwarte Sonneberg, 6, 97

Horne, J. H., & Baliunas, S. L. 1986, ApJ, 302, 757

Huff, E. M., & Stahler, S. W. 2006, ApJ, 644, 355

—. 2007, ApJ, 666, 281

Irwin, J., Hodgkin, S., Aigrain, S., Bouvier, J., Hebb, L., Irwin, M., & Moraux, E. 2008, MNRAS, 384, 675

Jardine, M., Cameron, A. C., Donati, J.-F., Gregory, S. G., & Wood, K. 2006, MNRAS, 367, 917

Jeffries, R. D. 2007, MNRAS, 381, 1169

Joergens, V., Fernández, M., Carpenter, J. M., & Neuhäuser, R. 2003, ApJ, 594, 971

Jones, B. F., & Walker, M. F. 1988, AJ, 95, 1755

Joy, A. H. 1945, ApJ, 102, 168

Kenyon, S. J., Yi, I., & Hartmann, L. 1996, ApJ, 462, 439

Kirkpatrick, J. D., Reid, I. N., Liebert, J., Gizis, J. E., Burgasser, A. J., Monet, D. G., Dahn, C. C., Nelson, B., & Williams, R. J. 2000, AJ, 120, 447

Königl, A. 1991, ApJ, 370, L39

Kürster, M., Schmitt, J. H. M. M., Cutispoto, G., & Dennerl, K. 1997, A&A, 320, 831

Lada, C. J., Muench, A. A., Haisch, Jr., K. E., Lada, E. A., Alves, J. F., Tollestrup, E. V., & Willner, S. P. 2000, AJ, 120, 3162

Lamm, M. H. 2003, PhD thesis, PhD Thesis, Combined Faculties for the Natural Sciences and for Mathematics of the Ruperto-Carola University of Heidelberg, Germany (Naturwissenschaftlich-Mathematische Gesamtfakultät der Universität Heidelberg, Germany). XII + 143 pp. (2003)

Lamm, M. H., Bailer-Jones, C. A. L., Mundt, R., Herbst, W., & Scholz, A. 2004, A&A, 417, 557

Lamm, M. H., Mundt, R., Bailer-Jones, C. A. L., & Herbst, W. 2005, A&A, 430, 1005

Landin, N. R., Ventura, P., D'Antona, F., Mendes, L. T. S., & Vaz, L. P. R. 2006, A&A, 456, 269

Littlefair, S. P., Naylor, T., Burningham, B., & Jeffries, R. D. 2005, MNRAS, 358, 341

Liu, M. C., Najita, J., & Tokunaga, A. T. 2003, ApJ, 585, 372

Lucas, P. W., Roche, P. F., & Tamura, M. 2005, MNRAS, 361, 211

Luhman, K. L., Adame, L., D'Alessio, P., Calvet, N., McLeod, K. K., Bohac, C. J., Forrest, W. J., Hartmann, L., Sargent, B., & Watson, D. M. 2007, ApJ, 666, 1219

Makidon, R. B., Rebull, L. M., Strom, S. E., Adams, M. T., & Patten, B. M. 2004, AJ, 127, 2228

Mandel, G. N., & Herbst, W. 1991, ApJ, 383, L75

Matt, S., & Pudritz, R. E. 2005, MNRAS, 356, 167

McCaughrean, M. J., et al. 2009, in prep.

McCaughrean, M. J., & Stauffer, J. R. 1994, AJ, 108, 1382

Mayne, N. J. & Naylor, T. 2008, MNRAS, 386, 261

Meyer, M. R., Calvet, N., & Hillenbrand, L. A. 1997, AJ, 114, 288

Mohanty, S., & Basri, G. 2003, ApJ, 583, 451

Muench, A., Getman, K., Hillenbrand, L., & Preibisch, T. 2008, Star Formation in the Orion Nebula I: Stellar Content, ed. B. Reipurth, 483–+

Muench, A. A., Alves, J., Lada, C. J., & Lada, E. A. 2001, ApJ, 558, L51

Nguyen, D. C., Jayawardhana, R., van Kerkwijk, M. H., Brandeker, A., Scholz, A., & Damjanov, I. 2009, ApJ, 695, 1648

O'dell, C. R. 2001, ARA&A, 39, 99

Palla, F., Randich, S., Flaccomio, E., & Pallavicini, R. 2005, ApJ, 626, L49

Palla, F., Randich, S., Pavlenko, Y. V., Flaccomio, E., & Pallavicini, R. 2007, ApJ, 659, L41

Parenago, P. P. 1954a, Trudy Gosudarstvennogo Astronomicheskogo Instituta, 25, 1

—. 1954b, Trudy Gosudarstvennogo Astronomicheskogo Instituta, 25, 3

Perez, M. R., The, P. S., & Westerlund, B. E. 1987, PASP, 99, 1050

Preibisch, T., & Feigelson, E. D. 2005, ApJS, 160, 390

Press, W. H., Teukolsky, S. A., Vetterling, W. T., & Flannery, B. P. 1992, Numerical recipes in C. The art of scientific computing, ed. W. H. Press, S. A. Teukolsky, W. T. Vetterling, & B. P. Flannery

Rebull, L. M. 2001, AJ, 121, 1676

Rebull, L. M., Stauffer, J. R., Megeath, S. T., Hora, J. L., & Hartmann, L. 2006, ApJ, 646, 297

Reiners, A., & Basri, G. 2007, ApJ, 656, 1121

Rieke, G. H., & Lebofsky, M. J. 1985, ApJ, 288, 618

Roberts, D. H., Lehar, J., & Dreher, J. W. 1987, AJ, 93, 968

Rodriguez-Ledesma, M. V., Mundt, R., & Eislöffel, J. 2009a, A&A, submitted

Rodriguez-Ledesma, M. V., Mundt, R., & Eislöffel, J. 2009b, in prep.

Rydgren, A. E., & Vrba, F. J. 1983, ApJ, 267, 191

Scargle, J. D. 1982, ApJ, 263, 835

Scholz, A., & Eislöffel, J. 2004, A&A, 419, 249

Shu, F., Najita, J., Ostriker, E., Wilkin, F., Ruden, S., & Lizano, S. 1994, ApJ, 429, 781

Sicilia-Aguilar, A., Hartmann, L. W., Fűrész, G., Henning, T., Dullemond, C., Brandner, W. 2006, AJ, 132, 2135

Sicilia-Aguilar, A., Hartmann, L. W., Szentgyorgyi, A. H., Fabricant, D. G., Fűrész, G., Roll, J., Conroy, M. A., Calvet, N., Tokarz, S., & Hernández, J. 2005, AJ, 129, 363

Spitzer, L. 1978, Physical processes in the interstellar medium, ed. L. Spitzer

Stahler, S. W., & Palla, F. 2005, The Formation of Stars, ed. S. W. Stahler & F. Palla

Stassun, K. G., Mathieu, R. D., Mazeh, T., & Vrba, F. J. 1999, AJ, 117, 2941

Tinker, J., Pinsonneault, M., & Terndrup, D. 2002, ApJ, 564, 877

Vrba, F. J., Rydgren, A. E., Chugainov, P. F., Shakovskaia, N. I., & Weaver, W. B. 1989, AJ, 97, 483

Vrba, F. J., Rydgren, A. E., Chugainov, P. F., Shakovskaia, N. I., & Zak, D. S. 1986, ApJ, 306, 199

Whitworth, A. P., & Stamatellos, D. 2006, A&A, 458, 817